THE FLORIDA STATE UNIVERSITY

COLLEGE OF ARTS AND SCIENCES

STATISTICAL ASSOCIATIONS BETWEEN LARGE SCALE CLIMATE OSCILLATIONS AND MESOSCALE SURFACE METEOROLOGICAL VARIABILITY IN THE APALACHICOLA-CHATTAHOOCHEE-FLINT RIVER BASIN

By

KELLY STEVENS

A Thesis submitted to the
Department of Meteorology
in partial fulfillment of the
requirements for the degree of
Master of Science

Degree Awarded:
Spring Semester, 2008

The members of the Committee approve the thesis of Kelly Stevens defended on November 13th, 2007.

_____

Paul Ruscher

Professor Directing Thesis

_____

Jon E. Ahlquist

Committee Member

_____

Henry Fuelberg

Committee Member

The Office of Graduate Studies has verified and approved the above named committee members.

ACKNOWLEDGEMENTS

The author would like to thank the Statistical Consulting Center at Florida State University for their assistance with interpretation of the canonical correlation analysis results.

TABLE OF CONTENTS

LIST OF TABLES

LIST OF FIGURES

LIST OF ABBREVIATIONS

ACF ..... Apalachicola-Chattahoochee-Flint River Basin
ASOS ..... automated surface observation stations
AMO ..... Atlantic Multidecadal Oscillation
CCA ..... Canonical correlation analysis
CD ..... climate division
COOP ..... Cooperative stations
DEM ..... digital elevation map
DFT ..... discrete Fourier transform
DJF ..... December/January/February
ENSO ..... El Niño/Southern Oscillation
FFT ..... fast Fourier transform
IDL ..... Interactive Data Language
MAM ..... March/April/May
MLR ..... multiple linear regression
MSLP ..... mean sea level pressure
NAO ..... North Atlantic Oscillation
NCDC ..... National Climatic Data Center
NDMC ..... National Drought Mitigation Center
JJA ..... June/July/August
PCA ..... principal component analysis
PDI ..... Palmer Drought Index
PDSI ..... Palmer Drought Severity Index
PDO ..... Pacific Decadal Oscillation
PHDI ..... Palmer Hydrologic Drought Index
PRISM ..... Parameter-elevation Regressions on Independent Slopes Model
SCAS ..... Spatial Climate Analysis Service
SOI ..... Southern Oscillation Index
SON ..... September/October/November
SPI ..... standardized precipitation index
SPI3, SPI6, SPI12, SPI24 ..... SPI of three, six, twelve, and twenty-four month intervals
SPSS ..... Statistical Package for the Social Sciences
SST ..... sea surface temperatures
USACE ..... United States Army Corps of Engineers
WRCC ..... Western Regional Climate Center

ABSTRACT

The "water wars" of the Apalachicola-Chattahoochee-Flint (ACF) River Basin are fueled largely by historic and current droughts in the southeastern United States. In attempts to describe climatological circumstances that could lead to low flows in the ACF, this study examines relationships between some available surface climatological variables connected to evapotranspiration and four climatic oscillations using canonical correlation analysis (CCA).

The surface meteorological variables for the dependent data set include monthly values of maximum and minimum temperature, as well as precipitation, extracted from the National Climatic Data Center (NCDC) and the Parameter-elevation Regressions on Independent Slopes Model (PRISM) data sets for four climate divisions in the ACF. The precipitation data are used to compute standardized precipitation index (SPI) values for three, six, twelve, and twenty-four month periods (SPI3, SPI6, SPI12, SPI24) for 1901-2000. The oscillations chosen based upon their previously researched associations to climate patterns in the southeastern United States include the global scale Atlantic Multidecadal Oscillation (AMO), North Atlantic Oscillation (NAO), Pacific Decadal Oscillation (PDO), and Southern Oscillation Index (SOI). We apply analysis thresholds to the canonical loadings and cross loadings for the canonical roots extracted at the 95% significance level to display the relational results for two separate tests conducted using CCA.

The dependent data set for one test consists of the temperature data and SPI6, while the independent data set consists of all the indices for four seasons, allowing for time-lagged and concurrent relationship discoveries. In this test, the standardized temperature data account for much of the variance explained for the CCA-derived concocted variate, with the strongest canonical relationships occurring during the winter season (DJF). Precipitation appears in the wetter spring (MAM) and summer (JJA) season with an indirect relationship to SOI (spring) and PDO (summer). The climate indices with intra-annual frequencies tend to show inverse relationships with temperature throughout the year. The second test utilizes only the four intervals of SPI values for the dependent variable set to focus on precipitation variability at different time scales for the northernmost and southernmost sub-basin areas. The variations of precipitation in the Apalachicola sub-basin (southernmost) results are most sensitive to the SOI

in the winter and spring seasons, where a significant relationship is found with the standardized precipitation indices with the higher variance (SPI3 and SPI6). Quite differently, the Upper Chattahoochee sub-basin results largely consist of indirect relationships between the climate oscillations with longer frequencies (AMO and PDO) with the longest time averaged SPI variable (SPI24). These findings reveal that weather and climate patterns in the ACF are not heterogeneous, and that multiple scales and multiple indices appear to be required to develop a comprehensive understanding of the nature of drought in this region.

CHAPTER ONE

INTRODUCTION

Recognition of water as a vital and sometimes limited resource has been important in many regions of the world for as long as life has existed. The water wars of the Apalachicola-Chattahoochee-Flint River Basin (ACF) began in the 1980's when a series of droughts in the southeast United States significantly reduced flows in the three named rivers. Water restrictions and allocation became a source of debate among the states of Alabama, Georgia, and Florida, who share the integral resources provided by the waters in the ACF. This meteorologically tied issue motivated the author to investigate the climatological factors possibly involved in the yet to be discovered drought patterns of the ACF.

The Apalachicola-Chattahoochee-Flint River Basin originates in northern Georgia with the Chattahoochee River draining from Lake Lanier, stretching through southern Atlanta with the Flint River southeast of the Chattahoochee River (Figure 1.1). The Chattahoochee River runs north to south along the Alabama and Georgia border, with tributaries and streams existing in far eastern Alabama. The Flint River flows through western and central Georgia and eventually joins with the Chattahoochee River at Lake Seminole at the Georgia/Florida border. The Apalachicola River drains from Lake Seminole down to the Gulf by Apalachicola Bay. The Apalachicola Basin is Florida's largest forested floodplain, creating a sensitive habitat for many endangered wildlife species. The ACF is approximately 619 kilometers (385 miles) long and 80 kilometers (50 miles) wide, covering approximately 50,800 km^2. The majority of the basin lies in Georgia (74%), with the remainder in western Alabama (15%) and the western panhandle of Florida (11%) (USACE 1998).

The waters in the basin are used for a variety of reasons from agriculture and recreation to industry and hydropower production. The growing metropolitan area of Atlanta places concerning demands on several reservoirs in the northern Chattahoochee River. The Flint River runs through a highly agricultural region where water irrigation pulls most of the water from the southeastern section of the basin. The Apalachicola River and floodplain system are regarded as one of the planet's "biodiversity hotspots," providing a habitat for many threatened and

endangered species (Ruhl 2005). The ACF is highly sensitive to the uses and management of the different sections of the basin, as more draw down in Atlanta and more irrigation along the Flint causes lower flows to the Apalachicola Bay.

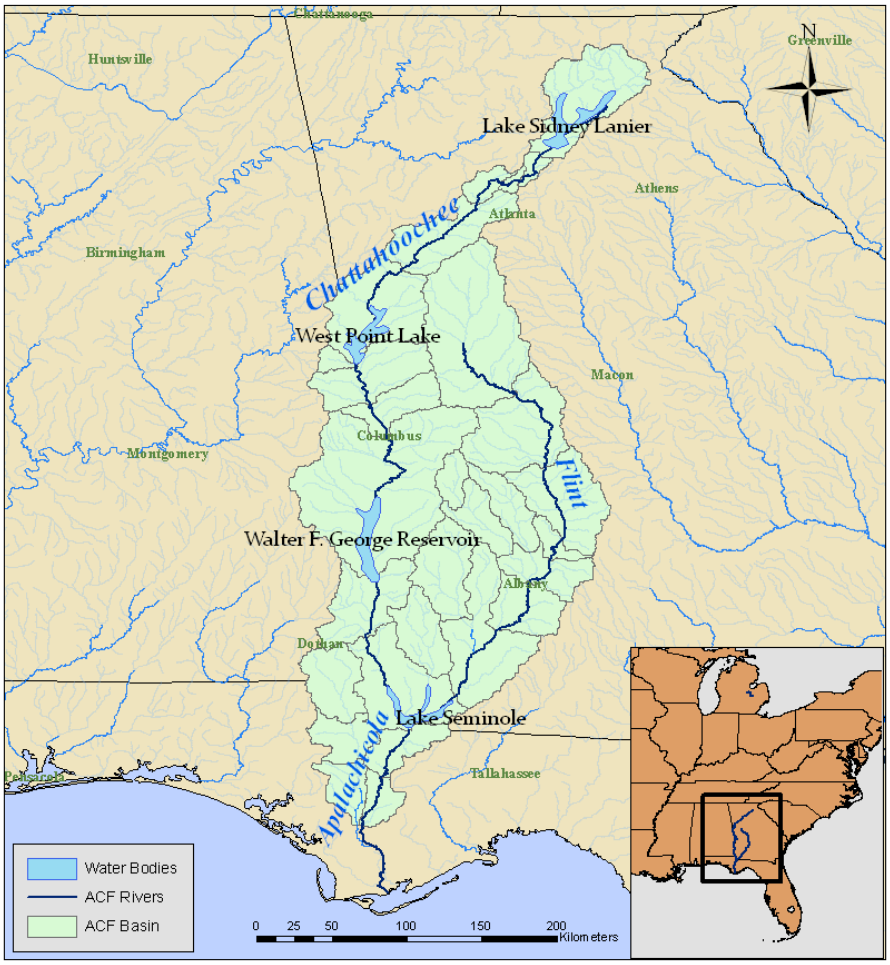

Apalachicola Chattahoochee Flint River Basin

FIG. 1.1: The Apalachicola-Chattahoochee-Flint River Basin and a few of the larger water bodies encompassed in the basin. The shaded green section represents the area with the mapped tributaries', hence, why the bottom of the Apalachicola is not shaded but is included in the basin.

During a series of droughts in the 1980's, hydropower production was reduced, restrictions on water use were placed on municipalities and industries, and navigation on the Apalachicola River was even suspended for several months in 1988 (USACE 1998). This caused increasing request for water reallocations, and in 1990 the United States Army Corps of Engineers (Corps) began studying and approving several of these requests to Georgia municipalities. Alabama then filed suit in a federal court for the Corps to stop granting any reallocations based on several federal environmental laws. Florida eventually became involved, aiming to protect a natural flow hydrograph into the Apalachicola Bay. The litigation was left on hold while the three states became involved in a study of the ACF basin and Apalachicola Bay's physical and socioeconomic conditions, known as the Comprehensive Study. In 1997 the states and federal government entered a compact aimed to develop a fair water allocation formula for the basin, based on protecting "water quality, ecology, and biodiversity" (Ruhl 2005).

In 2000, Georgia began the next round of the "water wars" by filing suit in a federal court stating the Corps was unfairly interfering with Georgia's use of state water by denying any reallocations. Another suit was filed by a group of power distributors arguing the Corps managed waters were created to inflate the price of electricity paid to hydropower producers. The 1997 compact expired in August 2003 leaving the states no closer to an agreement with litigation deadlines looming and the fate of the ACF undetermined (Ruhl 2005). Recently, four ACF litigations, new and reactivated cases, were consolidated into one forum and moved to a U.S. District court in Florida awaiting debate (Gilbert 2007). On 19 October 2007 the Georgia governor filed a lawsuit against the Corps over concerns about current water releases from Lake Lanier, Atlanta's primary water reservoir, during an ongoing drought in Georgia. The Corps has said it must maintain minimum flows of 5,000 cubic feet per second to preserve the habitat for several endangered species in the Apalachicola River, despite the alarming low levels of Lake Lanier (Cusick 2007).

This high interest issue has caused several other studies to be conducted on the ACF or parts of the ACF, particularly concerning streamflow and drought indicators. One such study by Light et al. (2006) focused on the water-level decline in the Apalachicola and the associated effects on the floodplain in the last half century. Another study by Steinemann (2003) used a probabilistic framework to evaluate different drought indicators for the ACF as part of the

developed drought plan between the three feuding states. However, an elaborate study has yet to be conducted for the ACF with a larger meteorological theme investigating the variance and relationships of mesoscale surface meteorological variability with global scale climate oscillations.

This research project is largely a continuation of a previous project conducted by Arrocha and Ruscher in 2005. The title of their project, "Analysis of Precipitation Variability and Meteorological Drought in the Apalachicola-Chattahoochee-Flint River Basin" describes the basic purpose of their study. Their goal was to assess the significant droughts experienced in the ACF and describe precipitation patterns in the last century using annual precipitation data from 50 cooperative and first order stations. The stations are distributed throughout the ACF, with most of the stations located in Georgia.

The data set analyzed consisted of annual precipitation values from cooperative first order automated surface observation stations (ASOS) and the Parameter-elevation Regressions on Independent Slopes Model (PRISM) data for missing station values. The total time period examined is 1885 through 2002. Using a climatological value computed from 1931-1980 data, precipitation anomalies were examined through standard deviation and percentile calculations. Arrocha and Ruscher (2005) defined a meteorological drought as, "three or more consecutive years with precipitation values below normal, and at least one year with precipitation below the 25^{th} percentile." Based on this definition, four periods of prolonged drought affecting more than half of the basin were identified. These periods were 1895-1899, 1949-1952, 1984-1988, and 1998-2001. The research study also found 9 other periods of prolonged drought affecting particular sub-basins (less than 50% of the basin stations). The 1970's and 1990's were determined to be climatologically wetter decades. They also found that extreme dry event years tend to be peaks of a longer drought period; however, there were a few stand alone drought years identified.

The drought analysis found "no obvious pattern" for the return of drought periods. A basic comparison was performed to find a relationship between the precipitation anomalies and one cyclical climate pattern in particular, El Niño Southern Oscillation (ENSO). The cold phase of ENSO, also known as La Niña, occurred during about 30% of the below normal precipitation years. Their study suggests further investigation into the relationship between climate trends

and other multidecadal oscillations such as the Atlantic Multidecadal Oscillation and the Pacific Decadal Oscillation.

The purpose of this study is to extend the previous research, investigating more variables and other possible climate links to drought in the ACF using canonical correlation analysis (CCA). Instead of focusing on precipitation percentiles, we will be looking at the Standardized Precipitation Index (SPI) values of three, six, twelve, and twenty-four month indices. Similar to percentiles, SPI is based only on precipitation; however, SPI uses a probability distribution function based on the long-term record. This then creates an index based on Z-score, with values above 2.00 indicating extremely wet and below -2.00 extremely dry conditions (Hayes et al. 1999). Along with SPI, we also utilize monthly minimum and maximum temperature data for a more complete description of the variance in the mesoscale meteorological variables possibly linked to climate patterns. The temperature data will be provided through cooperative first order ASOS stations and the PRISM data set (Daly et al. 2002). The data are being taken from 24 stations covering 4 different climate divisions in the ACF basin, as seen in Figure 1.2.

FIG 1.2: The ACF basin with main rivers and tributaries. Also located on the map are the 24 COOP stations from which temperature and precipitation data were obtained; dots are color coded by climate division, and labeled with their Cooperative Station Identifier.

The goal of this study is to explain the relationships between the surface meteorological variables in the ACF and several climatic oscillations. Based on previous research, we are exploring the Atlantic Multidecadal Oscillation (AMO), North Atlantic Oscillation (NAO), Pacific Decadal Oscillation (PDO), and El Niño Southern Oscillation (ENSO), all suggested by other authors to have an influence on precipitation patterns in the southeast. While other studies of this nature have been performed on the southeast in general, no study has specifically focused on the ACF and the possible variations throughout the ACF. We will be using a fast Fourier transform (FFT) to explore the oscillatory patterns within these indices, as well as heavily relying on the results from CCA for analysis of the relationships.

Multiple linear regression (MLR) was considered for this research project; however, the nature of the data being considered required a more advanced statistical technique. Variance in the surface meteorological variables and the climate oscillations is difficult to capture using MLR. By using CCA, we can get a broader understanding of the coupled variability of multiple fields. Temperature data, as well as precipitation, are associated with changes in climatic oscillations. Both of these meteorological variables have also been researched to influence streamflow variability by contributing to evapotranspiration (Hornberger et al. 1998). Therefore, precipitation and temperature are both important variables for this project which then requires the more inclusive CCA approach. Previous research (Gershunov and Barnett 1998; Rajagopalan et al. 2000; Sutton et al. 2003; Tootle et al. 2005) has also suggested particular climate oscillations may influence the strength or signal of other climate indices which could possibly be relevant to our results. By using CCA, we can test all four climate oscillations in each statistical analysis run, as well as test four different seasons of the variables at the same time. This is a more inclusive approach available due of the capabilities of CCA.

We did not include streamflow as a variable in our study because the ACF is heavily managed by the Corps through federal reservoirs, dams, and other control structures (Carriker 2000). There is also no streamflow data available prior to 1930 to correspond with our complete data set. The data being used is presented in Chapter 2, the methodologies behind fast Fourier transform and canonical correlation analysis presented in Chapter 3, while the climate oscillations are discussed in more detail in Chapter 4. Finally, the analysis section and conclusions can be found in Chapters 5 and 6, respectively.

CHAPTER TWO

DATA

Climate Indices

The Atlantic Multidecadal Oscillation (AMO) monthly index we used is from the NOAA Earth Systems Laboratory Physical Science Division and is the AMO unsmoothed, long version. This AMO index is computed from the Kaplan Extended SST V2 data set (2002). It is the detrended time series of the area weighted averaged sea surface temperature anomalies of the northern hemispheric Atlantic Ocean from 0° – 70°N latitude. This index can be obtained at: http://www.cdc.noaa.gov/Timeseries/AMO/.

The North Atlantic Oscillation (NAO) index used for this project is the normalized difference in sea level pressure between a station in SW Iceland (Reykjavik) and the Iberian Peninsula at Gibraltar. These are monthly values provided from the website: http://www.cru.uea.ac.uk/cru/data/nao.htm.

The Pacific Decadal Oscillation (PDO) index first developed by Mantua (1997) is the index used for this study. It is defined as the leading principal component of monthly sea surface temperature variability in the North Pacific (poleward of 20° North latitude). The data can be obtained from this website: http://jisao.washington.edu/pdo/.

The Southern Oscillation Index (SOI) was chosen to represent El Niño/Southern Oscillation in this study due to its historical availability. The SOI data set we used follows the methodology in Ropelewski and Jones (1987) and is the monthly normalized sea level pressure difference between Tahiti and Darwin. The data for this index can be found here: http://www.cru.uea.ac.uk/cru/data/soi.htm.

Surface Variables

For the intended climate study, a long and consistent record of monthly precipitation and temperature data was needed. The core of this data was provided by cooperative and first-order stations within the ACF through the National Climatic Data Center (NCDC). Missing and flagged data values were replaced with the Parameter-elevation Regressions on Independent

Slopes Model (PRISM), discussed in more detail later in this chapter. A total of 24 stations were used, 4 of these stations being in Florida and 20 stations in Georgia. A map of the stations and their Cooperative Station Identifiers is located in Figure 2.1. The data used in the canonical correlation analysis covers 100 years from 1901 to 2000.

The NCDC data archives, dating back to 1931, provided the variables used for this study which include monthly maximum and minimum temperature and monthly precipitation. The 24 stations used have all of these variables and a consistent period of record. Table 2.1 summarizes these stations, their data availability, location, and climate division information.

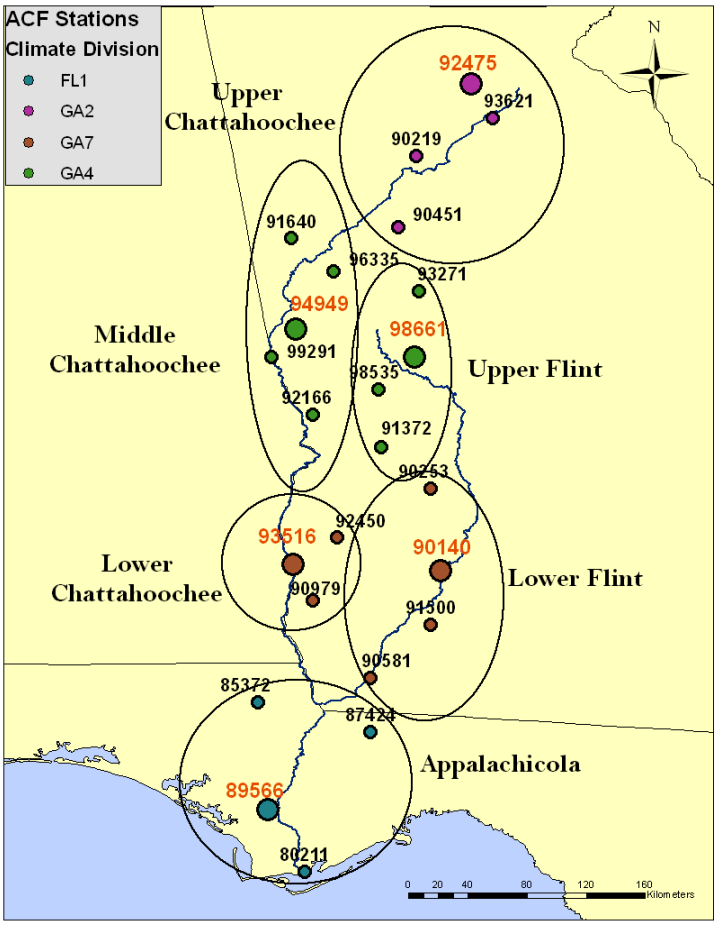

FIG 2.1: ACF and sub-basins as divided up for this study. The larger dots and orange numbering indicate the representative station for each sub basin area. The coloring on the dots indicates which climate division each station belongs to.

TABLE 2.1: Summary of all the stations considered for the CCA, and data missing in NCDC data set. The boldface items are the representative stations for the sub-basins. The color coding indicates the climate division each station corresponds to.

									% Missing NCDC		
St. ID	Location	State	Lat	Lon	CD	Cl. Div	NCDC Data	Years	Min	Max	Precip
80211	Apalachicola WSO City	FL	29.73	-84.98	1	**1** = 5, NW Florida	1948-2004	57	4.3	3.9	4.6
85372	Marianna School for Boys	FL	30.76	-85.26	1		1931-1968	38	7.0	6.7	3.2
87424/9	Quincy Experiment Station	FL	30.58	-84.58	1		1931-2004	74	10.2	9.0	4.0
89566	Wewahitchka	FL	30.11	-85.2	1		1956-2004	48	17.5	13.8	8.8
90140	Albany	GA	31.56	-84.15	7	**7**=7, Southwest	1931-2004	74	2.6	3.0	0.6
90219	Alpharetta 1 NW	GA	34.08	-84.3	2	**2**=4, North Central	1957-1995	38	9.8	10.4	8.3
90253	Americus 1 NE	GA	32.06	-84.21	7		1931-2004	74	7.6	8.3	3.8
90451	Atlanta WSO Airport	GA	33.65	-84.41	2		1950-2004	55	0.0	0.0	0.0
90581	Bainbridge	GA	30.91	-84.58	7		1931-1977	47	0.1	0.1	0.1
90979	Blakely	GA	31.38	-84.93	7		1931-1992	62	10.5	10.8	2.4
91372	Buena Vista	GA	32.31	-84.51	4	**4**=9, West Central	1948-1973,1948-2004	17,57	60.7	60.3	25.5
91500	Camilla	GA	31.23	-84.21	7		1938-2004	67	6.8	4.9	2.6
91640	Carrollton	GA	33.58	-85.06	4		1939-2004	66	12.8	9.8	3.5
92166	Columbus WSO Airport	GA	32.51	-84.93	4		1948-2004	57	0.0	0.4	0.0
92450	Cuthbert	GA	31.76	-84.78	7		1945-2004	60	7.0	5.2	2.7
92475	Dahlonega	GA	34.53	-83.98	2		1931-2000	70	9.6	8.5	5.0
93271	Experiment	GA	33.26	-84.28	4		1934-2004	71	4.5	4.4	2.9
93516	Fort Gaines	GA	31.6	-85.05	7		1931-1984	54	7.7	5.8	2.9
93621	Gainesville	GA	34.31	-83.83	2		1931-2004	74	3.2	2.8	0.7
94949	La Grange 5 W	GA	33.03	-85.03	4		1937-2001,1935-2002	65,68	5.5	3.2	3.3
96335	Newnan	GA	33.38	-84.8	4		1931-2004	74	4.5	4.5	2.7
98535	Talbotton	GA	32.66	-84.53	4		1931-2004	74	10.8	9.0	5.2
98661	Thomaston 2 S	GA	32.86	-84.31	4		1955-2004	50	12.3	9.6	8.5
99291	West Point	GA	32.86	-85.18	4		1931-2004	74	7.3	5.5	2.7

To replace missing station values in the temperature and precipitation data sets from NCDC, we used a comprehensive data set from the PRISM computer model. The Parameter-elevation Regressions on Independent Slopes Model (PRISM) was developed through the Spatial Climate Analysis Service (SCAS) at Oregon State University during the early 1990's to provide a complete gridded data set of temperature and precipitation back to 1895 to aid climate studies. After rigorous testing and implementation of improved methods, the model was approved to release reliable gridded temperature and precipitation maps in 1999 (Daly et al. 1999).

The model was created through use of data from automated surface observation stations (ASOS) and cooperative stations (COOP) which are assimilated and quality control tested for reliability. The quality control involves matching predictions made by a point version of the PRISM model and actual values from stations for large discrepancies (Daly et al. 2004). The data is then applied to collective climate grids for interpolation. Climate grids use geographical data sets with information such as a Digital Elevation Model (DEM), coastal proximity, and effective terrain height (Daly et al. 1999). The Parameter-elevation Regressions on Independent Slopes Model is being used extensively for large spatial and temporal coverage of minimum and

maximum temperatures, precipitation, and dew point on a monthly basis. The data set is reliable and supplements our study with the data needed for missing monthly values. Parameter-elevation regressions on independent slopes model data were created from NCDC data available to Daly et al. (1999) for data back to 1895; unfortunately, these data are no longer available online from NCDC (which restricts data to 1931 for most stations [Griffin, personal communication 2007]).

Studies from other regions throughout the United States have tested the reliability of PRISM data. In addition, we conducted our own test for the purposes of our study. In the previous study by Arrocha and Ruscher (2005), tests for precipitation already validated the use of PRISM for supplementary values. We followed similar procedures to test the temperature values for this study. In Figure 2.2 below, plots for maximum and minimum temperature, as well as precipitation are created covering five sample years (1970-1975). The solid line indicates the PRISM data while the red dashed line represents the NCDC data. As seen below, the PRISM and NCDC data follow closely and PRISM substituted data fit the surface patterns consistently.

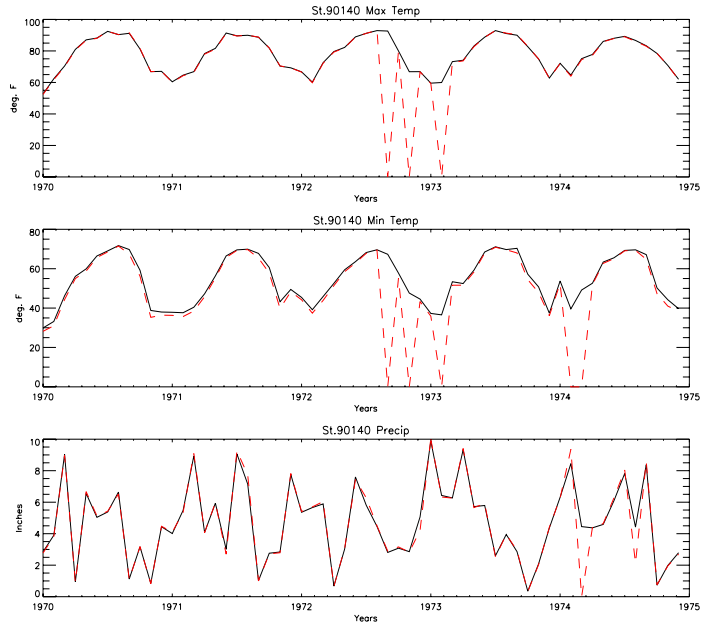

FIG 2.2: A comparison plot for maximum (top) and minimum (middle) temperature and precipitation (bottom) in the lower ACF. The red dashed line indicates NCDC data points, and the black solid line the PRISM data. Missing NCDC points are indicated with a zero value in this figure.

The stations used in this study stretch over four different climate divisions (CD) in Georgia and Florida in the southeast. The annual average precipitation values are discussed in Table 2.2 below for the key stations from each sub-basin. The average monthly precipitation patterns considering mean and median in precipitation (Figure 2.3) and variance in inches squared (Figured 2.4) are also plotted below. The four Florida stations represent CD 1: Northwest Florida. This region experiences hot, humid summers with the peak in precipitation occurring around July. The Florida stations have the highest amount of annual precipitation in the basin around 60 inches/year. The largest amount of the basin falls in Georgia where our stations cover three climate divisions. Climate division 2 is the northernmost division circling Lake Lanier and the upper ACF. Climate division 4 covers the west central part of Georgia, and CD 7 the southwest section of the state and the lower Chattahoochee and Flint River areas. These stations experience annual precipitation amounts between 51 and 54 inches. The Georgia stations generally have a bimodal precipitation pattern, with the largest peak in March for all the divisions except the southwest where peak precipitation occurs in July, transitioning into the Deep South summer convection precipitation pattern.

TABLE 2.2: Annual averages of precipitation for each sub-basin. Precipitation amounts are in inches and based on 1901-2000 values.

Sub-Basin	Climate Division	Precip.
Upper Chattahoochee	GA 2	63.94
Middle Chattahoochee	GA 4	52.21
Upper Flint	GA 4	48.57
Lower Chattahoochee	GA 7	53.12
Lower Flint	GA 7	50.36
Apalachicola	FL 1	65.22

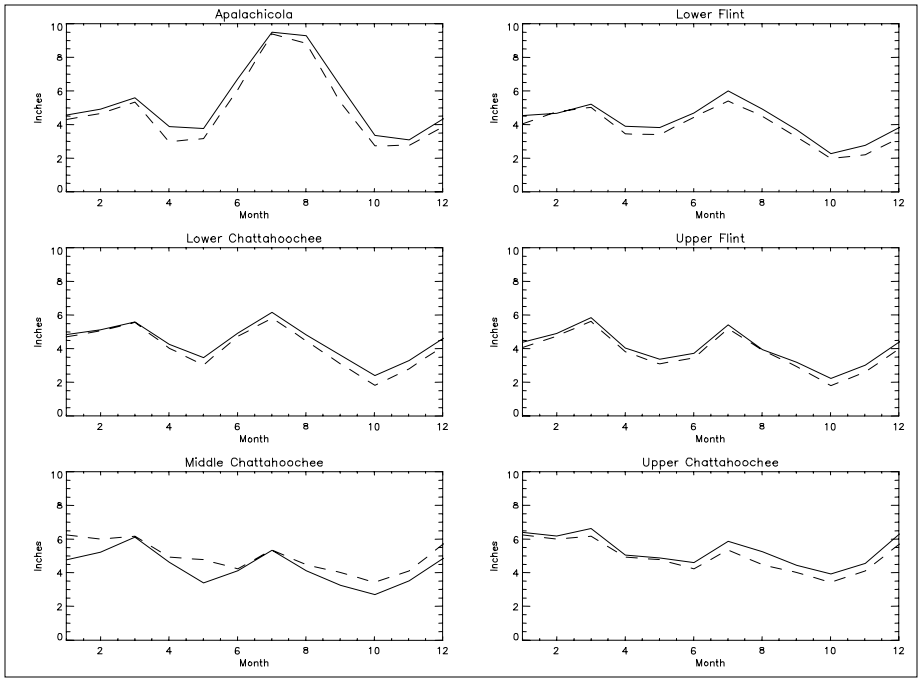

FIG. 2.3: Mean (solid) and median (dashed) monthly precipitation totals for the six representative stations for the sub-basins covering the ACF. Precipitation totals based on 1895-2005 values. Apalachicola shows a single late summer peak in precipitation, while most other stations exhibit a bimodal pattern, with first peak occurring early spring and second peak mid-summer.

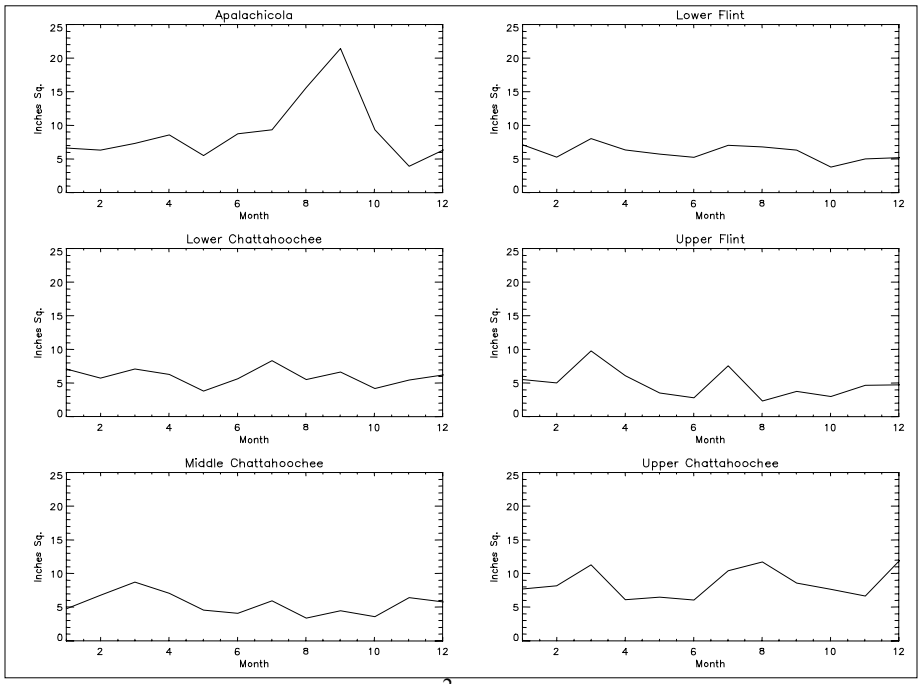

FIG. 2.4: Variance of precipitation in inches^2 for the six stations representing the sub-basins across the ACF. The Apalachicola summer precipitation has the largest amount of variance.

Investigating maximum and minimum surface temperatures could also exhibit information about evapotranspiration and is also included in this study. Average annual maximum and minimum values for the key stations are located in Table 2.3, and plots of average monthly mean and median temperature values are in Figure 2.5. Complete temperature and precipitation statistics tables are located in Appendix B.1 discussing station characteristics such as standard deviation, coefficient of variation, and precipitation percentiles.

TABLE 2.3: Average annual maximum and minimum temperatures for the climate divisions in degrees Fahrenheit based on 1931-1980 values.

Sub-Basin	Climate Division	Max Temp	Min Temp
Upper Chattahoochee	GA 2	69.14	45.88
Middle Chattahoochee	GA 4	74.32	50.14
Upper Flint	GA 4	76.65	50.59
Lower Chattahoochee	GA 7	77.5	54.38
Lower Flint	GA 7	78.21	53.32
Apalachicola	FL 1	79.65	56.03

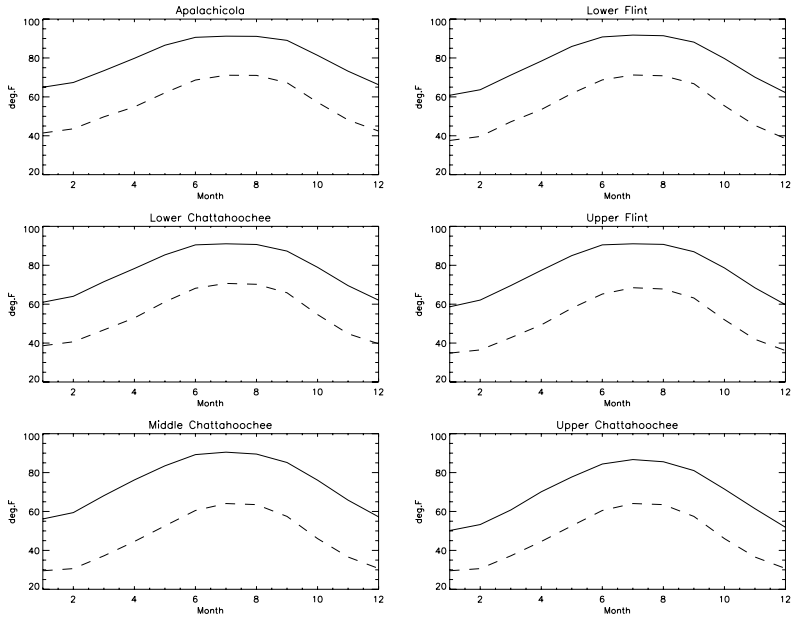

FIG. 2.5: Maximum (solid) and minimum (dashed) average monthly temperature values for key stations in each sub-basin based on 1901-2000 values.

Standardized Precipitation Index

Many different drought indicators have been applied for research and identification of droughts. This study primarily utilizes the Standardized Precipitation Index (SPI), developed by McKee et al. (1993). The SPI ranges from over 2.0 (extremely wet) to less than -2.0 (extremely dry), as indicated in Table 2.4. The SPI uses varying time intervals, typically three, six, nine, and twelve months for its index calculations. Its short-term and long-term drought identification makes the index ideal on both a hydrological and meteorological scale. For example, short-term changes may affect variables such as soil moisture, while long term changes affect streamflow and groundwater supply (Hayes et al. 1999). The SPI was also ideal for this study because it is established from a long-term database (30 or more years) of monthly precipitation.

The SPI is based on standard deviations of precipitation after being normalized and fitted by a probability function. After the long term period of monthly precipitation has been established, a set of averaging periods is selected based on months (*i*-month intervals). In our case, we chose three, six, twelve, and twenty-four month averaging periods. A new value for each month is determined by the average of the previous *i* months. These new data sets are then fitted to a Gamma function to relate precipitation to probability values. The data sets are then fitted to a normally distributed probability density similarly to z-score calculation (1) (McKee et al. 1993). The standardization and use of z-scores allows for wetter and drier climates to be represented in the same way (McKee et al. 1993). The SPI also has the capability to determine an accumulated drought magnitude for comparison and study discussed further below.

$$z = \frac{x - \bar{x}}{s} \qquad (1)$$

z = normalized score

x = precipitation value for a given month

$\bar{x}$ = average value

s = standard deviation of precipitation data set

The SPI is becoming more popular for drought identification and studies over other traditional drought indicators. The National Drought Mitigation Center (NDMC) uses one, three, six, nine, and twelve month SPI intervals for drought identification, and the Western Regional Climate Center (WRCC) advocate use of the SPI over the Palmer Drought Severity Index (PDSI) (Keyantash et al. 2002). The Palmer Drought Index (PDI) and SPI of twelve month interval (SPI12) are related at a correlation value of 0.85 (McKee et al. 1993). The PDSI is a more complicated index, involving over fifty terms for calculation, while the SPI is based purely on precipitation data. The SPI also preserves the rarity of extreme events better than the PDSI (Hayes et al. 1999). In a drought study involving stations across Colorado, the PDSI indicated severe drought more than 10% of the time, while the SPI extreme drought event occurred only 2.3% of the time. The SPI is designed to have consistent frequencies of classifications of extreme events, unlike the PDSI (Hayes et al. 1999).

TABLE 2.4: SPI intervals and their associated classifications considering drought from Hayes et al. 1999.

SPI Values	
2.0+	extremely wet
1.5 to 1.99	very wet
1.0 to 1.49	moderately wet
-.99 to .99	near normal
-1.0 to -1.49	moderately dry
-1.5 to -1.99	severely dry
-2.0 and less	extremely dry

A study by Steinmann (2003) was developed to review the Palmer and SPI drought indices and the nature of their indicators and triggers. The purpose of the study, which took place in the ACF Basin, was to better understand and compare the two indices and how their definitions of drought indicators respond in transitioning, persistence, duration, and frequency over different periods of time. The author evaluated the PDSI and Palmer Hydrologic Drought Index (PHDI), and the SPI3, SPI6, SPI9, and SPI12 month indices, and compared the six indices by transforming the values to percentiles. As expected, considering just the SPI, SPI12 exhibits

less oscillation and more stability than SPI3. The variety and response of the SPI allows for different definitions of drought to be addressed, an advantage over the Palmer indices that consistently respond slowly to short term changes and contain high persistence of drought categories. The study also showed the PHDI was almost four times as likely to remain triggered as a drought category compared to the shorter term SPI3. Although the SPI12 is the longest interval of SPI studied, it was still more responsive than the PHDI, less frequently triggered and less likely to remain invoked than the SPI12. Overall, the author concludes that the Palmer indices may not be sufficient to represent droughts affecting managed water systems adequately. SPI provides multiple indicators based on its different time intervals for short-term and long-term drought identification.

As with any drought index, SPI has limitations and special considerations when being used. Since it is based on precipitation data alone, the SPI is only as good as the long-term monthly precipitation data set used to calculate the index. The use of the normalized distribution means drought frequencies will be the same in all locations over a long period of time, and may not indicate areas that are more "drought prone" (Hayes et al. 1999). Since our study is of a limited area with the purpose of describing the association of drought with other environmental factors, these limitations do not make the SPI an unworthy drought index for this study.

To calculate the SPI, we used a FORTRAN program distributed from the Colorado Climate Center via their website (http://ccc.atmos.colostate.edu/standardizedprecipitation.php). This program inputs a long term record of monthly precipitation for a single location then computes any desired monthly interval SPI values for the selected time period. A sample plot of the SPI at three, six, twelve, and twenty-four month averaging is located in Figure 2.6 for one of our stations used in this study.

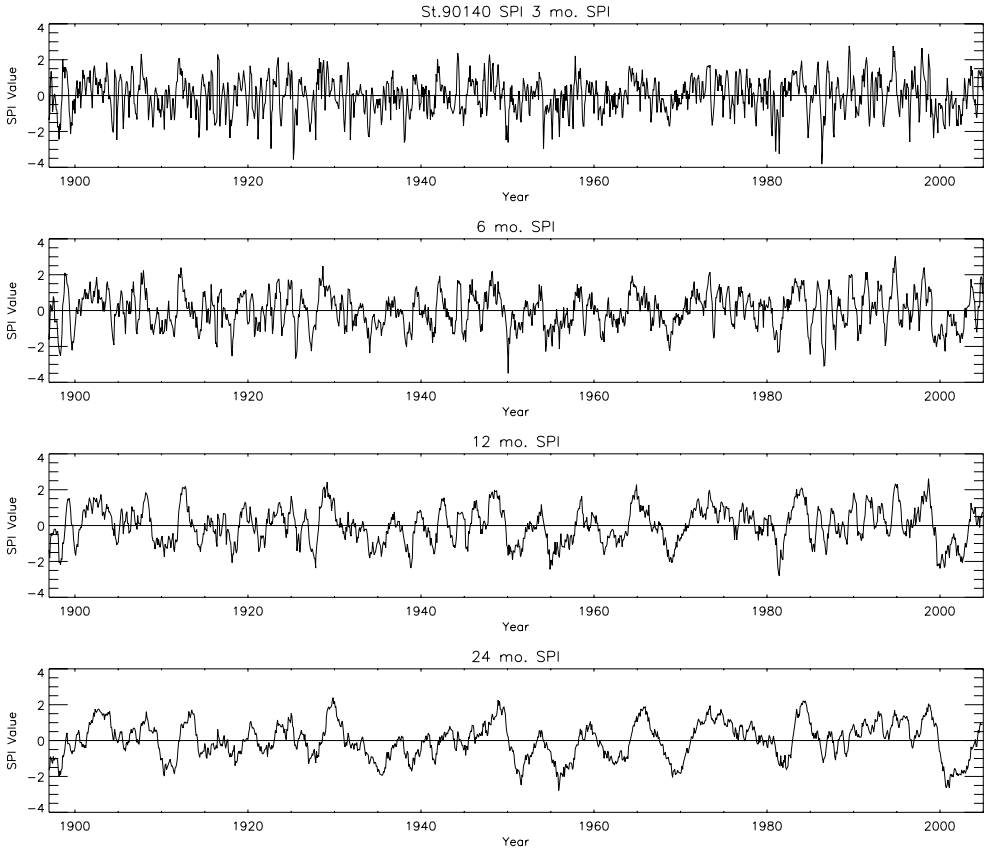

FIG. 2.6: Calculated SPI values for monthly intervals of three (top), six, twelve, and twenty-four months (bottom) from 1897 to 2005 for station COOP ID 90140 (Albany, GA).

CHAPTER THREE

METHODOLOGY

Fast Fourier Transform

The Fourier transform is employed on the climate indices being used in this study to gain a better understanding of their periodicities. The discrete Fourier transform (DFT) transforms the original data series in the time domain to the frequency domain. Specifically, we are employing the fast Fourier transform (FFT) which returns the complex, discrete Fourier transform of the original time series. We are using the Interactive Data Language (IDL) version 6.0 software program to compute the FFT and graph the power spectra with the resulting Fourier coefficients. The power spectrum consists of the squared amplitudes as a function of the frequencies derived by the FFT (Wilks 2006). Specifically, we are using the FFT function in IDL which follows the formula below (3.1) provided by the IDL Reference Guide (RSI, cited 2007). The FFT function returns a complex array with element zero containing the zero frequency component, and element one the smallest, nonzero positive frequency, equal to $1/(N_iT_i)$, where N_i is the number of elements and T_i the sampling frequency. We remove the mean from the indices as a recommended pretreatment of the time series, and then normalize the returned power spectrum before plotting.

$$F(u) = \frac{1}{N}\sum_{x=0}^{N-1} f(x)e^{[-j2\Pi ux/N]} \quad (3.1)$$

Canonical Correlation Analysis

Canonical correlation analysis (CCA), originally developed by Hotelling in 1935, is the main method used for this project to statistically evaluate the interrelationships between the meteorological surface variables and climate oscillation indices. Canonical correlation analysis is a linear multivariate approach to compare two sets of data, independent and dependent, with each set composed of multiple arrays of particular variables (Glahn 1968). Similar to multiple linear regression (MLR), CCA attempts to find relationships between a set of predictor variables

and a set of predictand variables, as opposed to just one predictand in MLR. Canonical correlation analysis is also similar to principal component analysis (PCA), which works to describe the internal variability of a single data set, while CCA describes the shared interrelationships between two data sets (Wilks 2006). Canonical correlation analysis appeared in research mostly in the social sciences in the 1960's (Bretherton et al. 1991). This multivariate approach is increasingly being used in the atmospheric sciences as well, investigating climate data, geophysical fields, and ocean-atmosphere relationships (e.g., Barnston and Ropelewski 1991; Bretherton et al. 1991; Zorita et al. 1991).

There is a fair amount of nomenclature for CCA. Canonical correlation analysis takes two sets of data, $x = (x_1, x_2 \ldots x_n)$ and $y = (y_1, y_2 \ldots y_m)$, categorized as independent (y with m amount variables) and dependent (x with n amount of variables). Arrays, or roots, of canonical variates (U_i, V_i while i equals root number) are created such that the linear combinations of x and y maximize correlations between the concocted variates. The linear combinations represent the weighted sum (a_n = dependent, b_m = independent canonical coefficients) of at least two variables from the respective set, therefore creating two variate arrays (3.2).

$$U_1 = \alpha_1 x_1 + \alpha_2 x_2 + \ldots. \alpha_n x_n$$
$$V_1 = \beta_1 y_1 + \beta_2 y_2 + \ldots. \beta_m x_m \qquad (3.2)$$

The weights are created by solving the coupled eigenproblem with the same eigenvalue (λ^2 = canonical correlation squared) (Zorita et al. 1991). The eigenvalue is the proportion of the shared variance between the two variates, U and V (Hair et al. 1998). The eigenproblem involves solving the autocovariance and cross-covariance matrices as seen in the equation below (3.3). The resulting pair of eigenfunctions (α, β) represents the canonical weights that maximize the correlations between the concocted variates (U, V). The strength of the relationship between the independent and dependent variates is the telling canonical correlation value (Hair et al. 1998).

$$r_c\alpha = \lambda^2\alpha = [S_{xx}]^{-1}[S_{xy}][S_{yy}]^{-1}[S_{yx}]\alpha$$
$$r_c\beta = \lambda^2\beta = [S_{yy}]^{-1}[S_{yx}][S_{xx}]^{-1}[S_{xy}]\beta \quad (3.3)$$

r_c = *canonical correlation*

$[S_{xx}]$ = *variance-covariance matrix of x*

$[S_{yy}]$=*variance-covariance matrix of y*

$[S_{xy}]$=*covariance matrix of x and y*

Equations from Wilkes et al. (2006) and Zorita et al. (1991).

Canonical correlation analysis iterates to find multiple canonical modes, or sets of variates. The first mode is always the strongest with the largest eigenvalue. Each successive mode has the prior canonical roots extracted in order to find an independent mode describing the next largest correlation between a possible set of variates (Hair et al. 1998).

There are many other byproducts from CCA beyond the canonical correlation value and eigenvalues which help to describe the relationships and strength of the statistical analysis. To have a better understanding of the contribution of each variable to the constructed variate, canonical weights are produced. Canonical weights represent each variable's contribution to the respective weighted sum of the variables which produces the respective variate. Canonical weights may be useful for developing predictive models using CCA results; however, the weights can be misleading in interpreting the relationship of each variable to the variate. If two variables are highly correlated, one of the variables will have a large weight while the other will likely have a significantly smaller weight since its variability has already been accounted for by the other variable it shares a high correlation with (Hair et al. 1998). There is also the existence of suppressor variables that have opposite signs in the canonical coefficients and the canonical loadings (correlations). Suppressor variables exist to maximize the correlation between other components in the canonical variates and do not accurately depict the relationship between the variables and the variate, another reason why we do not examine the canonical coefficients for interpretation.

A better way to understand the relationship between the variable and the variate is to analyze the canonical loadings. Canonical loadings, also known as canonical structure

correlations, are the linear correlations between a variable and its respective (independent or dependent) variate. The canonical loadings are considered relatively more valid than canonical weights to interpret the canonical relationships (Hair et al. 1998). Canonical cross loadings are simply the linear correlation between an observed variable of one set (independent, dependent) to the variate from the other set (dependent, independent). Evaluating canonical cross loadings is a preferred method to use to interpret the canonical relationships because they provide a more telling description of the independent to dependent variable relationships. We will examine both types of canonical loadings to aid in the interpretation of our results with more focus on the canonical cross loadings.

Lastly, as used by Zorita et al. (1991), we will examine the percent of variance explained in the dependent set as a whole (surface meteorology variables) by the independent set's variate (climate oscillations of all seasons). This proportion of variance explained is sometimes known as the redundancy coefficient, calculated to measure, in general, the magnitude of the relationships. The redundancy coefficient is calculated by taking the average of the squared canonical loadings of the dependent set and multiplying this value with the squared canonical correlation. This represents the amount of variance in the dependent set explained by the independent variate (Hair et al. 1998). The redundancy coefficient will give us an overall depiction of the effectiveness of the independent canonical variates ability to predict the variance in the original variables of the dependent data set (Garson 2007).

There are a few assumptions that need to be considered before performing CCA. Normality should be examined since it standardizes a distribution to allow for higher correlations among the variables. Standardized precipitation index is already a standardized variable, while precipitation and temperature are not. The variables will have the mean removed and the standard deviation set to 1 before being input to the CCA. Homoscedasticity, caused by variables having very different variances, will be remedied by this normalization as well as provide for better results. Multicollinearity could also interfere with the CCA technique and will be tested by the computation of the covariance matrix intrinsically included in the CCA program being used. We also compute tables of correlation values between all of the data to recognize the already highly correlated variables within a data set as part of the CCA results. The software program Statistical Package for the Social Sciences (SPSS) version 15 is employed for computation of the necessary CCA output for analysis. The methodology involved in the SPSS

calculation of the canonical correlation results fails if any of the above mentioned requirements are not met.

For a more informative study to possibly maximize the correlations, we group the data into seasonal values. We divide up the seasons in the same manner many climate studies use when exploring climate indices, as follows: winter consists of December (previous year), January, and February (DJF, season 1); spring is March, April, and May (MAM, season 2); summer is June, July, and August (JJA, season 3); and autumn consists of September, October, and November (SON, season 4). Oftentimes in the text and figures the numerical representation of the seasons is used as described above (i.e. AMO 2 means the AMO of MAM or season 2).

The methodology we are using concerning the canonical correlation analysis involves multiple steps. Our general purpose is to find a better understanding of how the surface climatological variables collectively relate to the climate oscillations in the ACF. We are looking for a qualitative realization of the spatial and temporal differences in the relationships between the surface climatological variables (dependent data set) and climate indices (independent data set). Focusing on the issue of drought, we will test the basin at a larger scale looking for climate-drought relationship comprehension.

For our first general test, finding relationships between surface meteorological data and climate oscillations in the ACF, we use the surface meteorological variables including standardized precipitation index at the six month interval (SPI6), and minimum and maximum monthly temperature as the dependent data set. We cannot include maximum and minimum temperature with temperature range in one set because it violates the rules of multicollinearity and failed the built-in test in SPSS for such violations. The independent data set for both our statistical tests consists of all four seasons of the climate indices of AMO, NAO, PDO, and SOI. By employing this method, we can also examine if climate indices of other lagged seasons have an affect on the dependent data.

First, we randomly choose one station for each section of the river basin to use in the CCA. A map of the sections is located in Figure 2.1 and the sections are defined as Upper Chattahoochee, Middle Chattahoochee, Lower Chattahoochee, Upper Flint, Lower Flint, and Apalachicola. A sensitivity test was performed to test the variability experienced between two stations of the same climate division in the same section of the basin. The sensitivity test shows

that one station at random will accurately represent any station in the sub-basin area (Appendix C, Table C.1). As seen, the results from the two different stations within the same climate division and sub-basin area do not have largely different results in terms of canonical correlations, canonical cross loadings, and variance explained.

Next we want to choose the data that will best describe the relationships between surface meteorological variables and the climate indices. Through sensitivity tests, SPI6 performed best compared to the SPI3, SPI12, SPI24 and precipitation variables by producing the highest amount of variance in the dependent set explained by the independent set's variate in the redundancy analysis (Appendix C, Table C.2). From our preliminary research, the Palmer Drought Severity Index (PDSI) correlates best to SPI12 (Chapter 2). Since we are looking for a more responsive index than the Palmer indices have been established as (Chapter 2), we choose to use the shorter SPI6. Higher canonical correlations as well as a higher variance explained by the independent variate were found using maximum and minimum temperature as opposed to just temperature range. For these reasons we used maximum and minimum temperature paired with SPI6 for the first test (Appendix C, Table C.3).

The second test focuses on the larger scale drought characteristics of the basin. We compare the four different SPI values (three, six, twelve, and twenty-four month) of the northernmost and southernmost sections of the basin to the four different seasonal values of the climate indices. By doing so, we are looking not only for the differences between the two extreme northern and southern regions, but also the variation in the strength of the climate signal from the climate indices at different time scales.

An example is provided in Tables 3.1-3.3 as an aid for describing the interpretation of the results from the CCA. We begin by analyzing the canonical correlation coefficients and their p-values, located under the section labeled "Canonical Correlations and P-Values". The results from each test are said to be significant with a p-value below 0.05 based on a consensus from previous researchers using CCA (Hair et al. 1998). Any canonical roots that are extracted are immediately disregarded if the p-values are less than 0.05; therefore, every result being examined here is statistically significant at least at the 95% level of confidence. In the example provided of the CCA results for the Lower Flint, the first two roots for the MAM season are

significant with p-values of 0.000 and 0.003 respectively, while the last root is not significant with a p-value of 0.580 and will not be considered in the analysis.

For the first test we will generally only review the first concocted canonical root regardless of the significance of the successively smaller roots. We are employing this method because the first canonical correlations are already fairly small and any smaller roots will not provide additional useful information. We may, however, be analyzing the smaller roots if the redundancy index is higher than the index for the strongest canonical correlation. From the Lower Flint example, the first root for DJF has a squared canonical correlation value (eigenvalue) of 0.326 while the second one is fairly smaller at 0.144 and we will only be evaluating the first root. In MAM the second and significant canonical root has a redundancy index of 0.079 while the first root a value of 0.054. In this case, we will look at the second root with different loadings of the dependent and independent data. This is rare as this is the only case where the second root has a larger proportion of variance explained in all of our results.

For the second test we will be reviewing both canonical roots if both pass the significance test (p-value < 0.05) for more information concerning each sub-basin division. Typically in these tests, each root constructed is made up primarily of a loading from one sub-basin division. By examining both roots, we get a better understanding of how the climate oscillations affect each part of the basin differently. To do so, we chose the stringent criterion that both roots must be significant by passing the p-test (<0.05) and have fairly similar canonical correlation values in order to be included in the analysis.

The canonical correlations will be examined for the measure of the strength between the created linear composites, otherwise known as the canonical variates. The canonical correlations must be considered by the researcher in the scope of the research project because there are no previously created standards these correlations are required to fit to be considered significant. We do not expect large numbers for our canonical correlations since the variance explained by climate oscillations in surface meteorological variables is not generally a large amount. For example, in a study by Katz et al. (2003), correlations between NAO and mean wintertime minimum temperature for stations in the southeast range from 0.382 and 0.604, while correlations for precipitation and NAO under the same conditions range between -0.282 and 0.277. Correlation coefficients for all seasons of all the climate indices with each other are

shown in Table A.2 of the Appendix. For our sample sizes, a critical value of 0.2 is significant at the 99.95% level.

None of the studies researched compare surface meteorological variables such as temperature and precipitation to climate indices using CCA. Although not identical, we can compare similar results from these studies employing CCA. Zorita et al. (1991) compared spatial sea level pressure and sea surface temperature pairs with CCA and found a particular pattern exhibited a canonical correlation value of 0.56 with 19% of the SST variance explained by the SLP variate. In our example, the first canonical correlation value for DJF for the Lower Flint is 0.571 and 17% of the variance in the surface meteorological data set is accounted for in the climate oscillations variate (Table 3.1). This proportion of variance, the redundancy coefficient, measures the overall effectiveness of the CCA. We are only concerned with in the ability of the constructed independent variate to predict the dependent data set. This value is reported as the "Proportion of Variance in Dependent Set Explained by Opp. Can. Var" in the example table 3.2, and will be highly regarded in our analysis.

Next we move on to interpret the canonical variate. This involves analysis of the before mentioned canonical weights, loadings, and cross loadings. In this project, we are not analyzing the canonical weights since they can easily misrepresent the relationships being researched. It is not the intention of this project to create a predictive model with our results, and therefore we focus mostly on analyzing the canonical loadings and cross loadings as opposed to the canonical weights (Table 3.2). It is sometimes difficult to identify significant relationships based on canonical loadings because research lacks precise standards for their interpretation. We can, however, observe the nature of relationships based on the canonical loadings, specifically the cross loadings, and will focus on those properties.

Looking at the DJF values from the Lower Flint example, the first root for the canonical loadings of the dependent data shows SPI6 (spi6LFs1) has a very small contribution to the variate, while maximum and minimum temperatures (maxLFs1, minLFs2) are correlated with the variate at values of 0.765 and 0.998, respectively (Table 3.3). The cross loading values are the correlation between the original surface meteorological variables and the independent data set's variate created from the climate oscillation data. These values are more telling for our overall research scope. The results from this section reveal that DJF maximum and minimum

temperatures have the largest amount of shared variance again, with minimum temperature having the largest cross loading at 0.570.

Continuing with the canonical loadings, we now move to analyze the independent data set (Table 3.3). The canonical loadings for the independent set for DJF from the example show AMO of season 1, season 3, and season 4, as well as the NAO and PDO of season 1 all have the largest structure correlations with values over 0.4. This same pattern holds true in the cross loadings as expected. The cross loadings show the three contributing seasons of AMO are all positively correlated with the dependent variate. The loadings for the surface variables in the variate are negative for SPI6, and positive and larger for maximum and minimum temperature. This would mean AMO of seasons 1, 3, and 4 have a small yet direct relationship with temperature data and a much smaller yet indirect relationship with SPI6 for the DJF season. We perform this type of analysis for each of the four seasons in each of the six sub-basin regions for the two canonical correlation analysis tests previously described. The results presented below provide an example of our analysis of the CCA results for one sub-basin. The complete tables for all sub-sections of the basin for both tests one and two are included in Appendix D.

TABLE 3.1: Example canonical correlation analysis output for Lower Flint, surface meteorology variables with the climate oscillations. The abbreviation s6mLFs1 indicates the SPI6 variable for the Lower Flint season 1 (DJF), with the same being true for maxLFs1 and minLFs1. A few of the correlations are highlighted. The results are split up seasonally and labeled. The significant roots in the canonical correlation results are highlighted in the Canonical Correlations and P-Values section.

Correlations for Lower Flint

DJF

	s6mLFs1	maxLFs1	minLFs1
s6mLFs1	1.000	-0.210	-0.071
maxLFs1	-0.210	1.000	0.797
minLFs1	-0.071	0.797	1.000

MAM

	s6mLFs2	maxLFs2	minLFs2
s6mLFs2	1.000	-0.107	-0.006
maxLFs2	-0.107	1.000	0.882
minLFs2	-0.006	0.882	1.000

JJA

	s6mLFs3	maxLFs3	minLFs3
s6mLFs3	1.000	-0.375	-0.110
maxLFs3	-0.375	1.000	0.405
minLFs3	-0.110	0.405	1.000

SON

	s6mLFs4	maxLFs4	minLFs4
s6mLFs4	1.000	-0.082	0.055
maxLFs4	-0.082	1.000	0.916
minLFs4	0.055	0.916	1.000

Canononical Correlations and P-values

DJF

	Can. Cor	R sq.	Wilk's	DF	Sig.
1	0.571	0.326	0.524	48.000	0.000
2	0.380	0.144	0.778	30.000	0.000
3	0.300	0.090	0.910	14.000	0.017

MAM

	Can. Cor	R sq.	Wilk's	DF	Sig.
1	0.446	0.199	0.661	48.000	0.000
2	0.372	0.138	0.825	30.000	0.003
3	0.204	0.042	0.958	14.000	0.580

JJA

	Can. Cor	R sq.	Wilk's	DF	Sig.
1	0.467	0.218	0.659	48.000	0.000
2	0.323	0.104	0.843	30.000	0.015
3	0.243	0.059	0.941	14.000	0.229

SON

	Can. Cor	R sq.	Wilk's	DF	Sig.
1	0.411	0.169	0.740	48.000	0.000
2	0.301	0.091	0.890	30.000	0.299
3	0.144	0.021	0.979	14.000	0.965

TABLE 3.2: Sample CCA output, the redundancy analysis and the canonical coefficients. Only the significant roots are examined in all cases. The highlighted values in the proportion of variance in dependent set explained by opposite canonical variate section indicate those of the root being examined for each case. In MAM both values are highlighted since in this rare case the second root had a higher proportion of variance explained. The coefficients are not examined and therefore not highlighted. The abbreviations in the independent data represent the climate oscillation and its season being represented as described in the text (i.e. pdos1 = PDO of season 1, DJF).

Redundancy Analysis

Proportion of Variance in Dependent Set Explained by Own Can. Var.

DJF		MAM		JJA		SON	
CV1-1	0.530	CV1-1	0.270	CV1-1	0.501	CV1-1	0.621
CV1-2	0.165	CV1-2	0.568	CV1-2	0.178		
CV1-3	0.305						

Proportion of Variance in Dependent Set Explained by Opp. Can. Var.

DJF		MAM		JJA		SON	
CV2-1	0.173	CV2-1	0.054	CV2-1	0.109	CV2-1	0.105
CV2-2	0.024	CV2-2	0.079	CV2-2	0.018		
CV2-3	0.027						

Proportion of Variance in Independent Set Explained by Own Can. Var.

DJF		MAM		JJA		SON	
CV2-1	0.093	CV2-1	0.090	CV2-1	0.187	CV2-1	0.045
CV2-2	0.121	CV2-2	0.061	CV2-2	0.069		
CV2-3	0.108						

Proportion of Variance in Independent Set Explained by Opp. Can. Var.

DJF		MAM		JJA		SON	
CV1-1	0.031	CV1-1	0.018	CV1-1	0.041	CV1-1	0.008
CV1-2	0.018	CV1-2	0.008	CV1-2	0.007		
CV1-3	0.010						

Standardized Canonical Coefficients Dependent Data

DJF

	1	2	3
s6mLFs1	-0.040	0.028	1.036
maxLFs1	-0.100	-1.641	0.478
minLFs1	1.075	1.261	-0.267

MAM

	1	2
s6mLFs2	-0.946	0.343
maxLFs2	-1.161	-0.927
minLFs2	0.849	0.028

JJA

	1	2
s6mLFs3	-0.028	-0.787
maxLFs3	0.588	-0.949
minLFs3	0.595	0.658

SON

	1
s6mLFs4	0.059
maxLFs4	-0.064
minLFs4	-0.942

Standardized Canonical Coefficients for Independent Data

DJF

	1	2	3
amos1	0.638	0.591	-0.101
naos1	0.492	-0.190	0.460
pdos1	-0.461	0.535	-0.222
sois1	-0.042	-0.405	-0.360
amos2	-0.656	-0.250	0.147
naos2	0.030	0.077	-0.004
pdos2	0.089	-0.331	0.435
sois2	0.105	-0.054	-0.229
amos3	0.457	-0.115	0.273
naos3	0.143	-0.173	-0.152
pdos3	-0.188	0.007	-0.244
sois3	-0.099	0.148	-0.038
amos4	0.298	0.329	-0.503
naos4	-0.031	-0.279	0.075
pdos4	0.133	0.227	0.175
sois4	-0.087	-0.202	-0.343

MAM

	1	2
amos1	0.212	0.358
naos1	0.207	0.150
pdos1	0.104	0.221
sois1	0.663	-0.378
amos2	-0.163	-0.448
naos2	0.154	-0.029
pdos2	-0.197	-0.449
sois2	0.192	-0.138
amos3	-0.311	-0.338
naos3	-0.297	-0.628
pdos3	0.289	0.584
sois3	0.232	-0.033
amos4	0.610	0.150
naos4	0.094	-0.345
pdos4	-0.066	-0.007
sois4	-0.041	0.249

JJA

	1	2
amos1	0.105	-0.193
naos1	0.026	0.445
pdos1	-0.102	0.115
sois1	-0.010	0.618
amos2	0.013	0.169
naos2	-0.138	0.117
pdos2	0.288	0.296
sois2	0.104	0.220
amos3	0.486	-0.354
naos3	0.083	0.096
pdos3	0.171	-0.307
sois3	0.107	0.512
amos4	0.348	0.414
naos4	0.039	0.029
pdos4	-0.108	0.126
sois4	-0.152	-0.385

SON

	1
amos1	-0.326
naos1	0.085
pdos1	-0.372
sois1	-0.003
amos2	0.544
naos2	-0.229
pdos2	0.386
sois2	0.032
amos3	0.598
naos3	0.553
pdos3	-0.429
sois3	0.000
amos4	-0.950
naos4	0.142
pdos4	0.081
sois4	-0.183

TABLE 3.3: Canonical loadings and cross loadings for the Lower Flint. The values highlighted in the canonical loadings meet our analysis threshold of 0.4, and in the cross loadings the threshold of 0.2.

Canonical Loadings for Dependent Data

DJF

	1	2	3
s6mLFs1	-0.095	0.284	0.954
maxLFs1	0.765	-0.642	0.047
minLFs1	0.998	-0.049	0.040

MAM

	1	2
s6mLFs2	-0.827	0.442
maxLFs2	-0.311	-0.939
minLFs2	-0.169	-0.791

JJA

	1	2
s6mLFs3	-0.314	-0.503
maxLFs3	0.840	-0.387
minLFs3	0.836	0.360

SON

	1
s6mLFs4	0.012
maxLFs4	-0.932
minLFs4	-0.997

Cross Loadings for Dependent Data

DJF

	1	2	3
s6mLFs1	-0.054	0.108	0.287
maxLFs1	0.437	-0.244	0.014
minLFs1	0.570	-0.019	0.012

MAM

	1	2
s6mLFs2	-0.369	0.165
maxLFs2	-0.139	-0.350
minLFs2	-0.075	-0.294

JJA

	1	2
s6mLFs3	-0.147	-0.162
maxLFs3	0.392	-0.125
minLFs3	0.390	0.116

SON

	1
s6mLFs4	0.005
maxLFs4	-0.383
minLFs4	-0.410

Canonical Loadings for Independent Data

DJF

	1	2	3
amos1	0.528	0.529	-0.238
naos1	0.487	-0.301	0.438
pdos1	-0.443	0.509	0.162
sois1	0.146	-0.466	-0.548
amos2	0.284	0.477	0.022
naos2	0.022	0.134	0.101
pdos2	-0.231	0.199	0.522
sois2	0.117	-0.225	-0.524
amos3	0.467	0.422	0.007
naos3	0.158	-0.181	-0.075
pdos3	-0.268	0.237	0.292
sois3	0.042	-0.064	-0.383
amos4	0.524	0.524	-0.186
naos4	-0.053	-0.317	0.045
pdos4	-0.139	0.161	0.403
sois4	0.018	-0.293	-0.406

MAM

	1	2
amos1	0.276	-0.175
naos1	0.111	0.067
pdos1	-0.211	0.172
sois1	0.724	-0.344
amos2	0.016	-0.192
naos2	0.033	0.082
pdos2	-0.357	0.034
sois2	0.437	-0.254
amos3	0.110	-0.143
naos3	-0.298	-0.552
pdos3	-0.169	0.450
sois3	0.365	-0.084
amos4	0.325	-0.047
naos4	0.049	-0.338
pdos4	-0.260	0.170
sois4	0.162	0.048

JJA

	1	2
amos1	0.669	-0.024
naos1	0.008	0.435
pdos1	0.210	-0.041
sois1	-0.185	0.625
amos2	0.787	-0.130
naos2	-0.230	-0.012
pdos2	0.397	-0.081
sois2	-0.063	0.413
amos3	0.899	-0.113
naos3	-0.032	0.163
pdos3	0.272	-0.325
sois3	0.079	0.409
amos4	0.858	0.043
naos4	-0.021	-0.021
pdos4	-0.047	-0.094
sois4	-0.053	-0.018

SON

	1
amos1	-0.134
naos1	0.183
pdos1	-0.172
sois1	-0.023
amos2	0.028
naos2	-0.252
pdos2	0.085
sois2	0.043
amos3	-0.060
naos3	0.563
pdos3	-0.221
sois3	-0.026
amos4	-0.377
naos4	0.208
pdos4	0.039
sois4	-0.047

Cross Loadings for Independent Data

DJF

	1	2	3
amos1	0.302	0.201	-0.071
naos1	0.278	-0.115	0.132
pdos1	-0.253	0.194	0.049
sois1	0.084	-0.177	-0.164
amos2	0.162	0.181	0.007
naos2	0.013	0.051	0.030
pdos2	-0.132	0.076	0.157
sois2	0.067	-0.085	-0.157
amos3	0.267	0.161	0.002
naos3	0.090	-0.069	-0.022
pdos3	-0.153	0.090	0.088
sois3	0.024	-0.024	-0.115
amos4	0.299	0.199	-0.056
naos4	-0.030	-0.121	0.014
pdos4	-0.079	0.061	0.121
sois4	0.010	-0.112	-0.122

MAM

	1	2
amos1	0.123	-0.065
naos1	0.050	0.025
pdos1	-0.094	0.064
sois1	0.323	-0.128
amos2	0.007	-0.072
naos2	0.015	0.030
pdos2	-0.159	0.013
sois2	0.195	-0.095
amos3	0.049	-0.053
naos3	-0.133	-0.206
pdos3	-0.075	0.167
sois3	0.163	-0.031
amos4	0.145	-0.017
naos4	0.022	-0.126
pdos4	-0.116	0.063
sois4	0.072	0.018

JJA

	1	2
amos1	0.312	-0.008
naos1	0.004	0.140
pdos1	0.098	-0.013
sois1	-0.086	0.202
amos2	0.367	-0.042
naos2	-0.107	-0.004
pdos2	0.185	-0.026
sois2	-0.030	0.133
amos3	0.420	-0.037
naos3	-0.015	0.053
pdos3	0.127	-0.105
sois3	0.037	0.132
amos4	0.400	0.014
naos4	-0.010	-0.007
pdos4	-0.022	-0.030
sois4	-0.025	-0.006

SON

	1
amos1	-0.055
naos1	0.075
pdos1	-0.071
sois1	-0.010
amos2	0.011
naos2	-0.103
pdos2	0.035
sois2	0.018
amos3	-0.025
naos3	0.231
pdos3	-0.091
sois3	-0.011
amos4	-0.155
naos4	0.085
pdos4	0.016
sois4	-0.019

CHAPTER FOUR

CLIMATIC OSCILLATIONS OVERVIEW

Climatic indices have been related to temporal variability in surface data such as precipitation, temperature and streamflow by many investigators. In a recent study of multidecadal drought frequency across the 344 climate divisions of the United States (1900-1999), 52% of the temporal variability could be attributed to just the Pacific Decadal Oscillation (PDO) and Atlantic Multidecadal Oscillation (AMO) (McCabe et al. 2004). Based on previous research, there are at least four important global scale climatic oscillations that have been considered associated with climatological variability in the ACF. They include the Atlantic Multidecadal Oscillation (AMO), North Atlantic Oscillation (NAO), Pacific Decadal Oscillation (PDO), and El Niño/ Southern Oscillation (ENSO). Some basic characteristics and associations to surface precipitation and temperature patterns are summarized in Table 4.1. These climatic indices can also influence the strength and intensity of other indices which will also be explored. This chapter seeks to identify the important climatic oscillations, understand their annual variability and explain their potential impacts with respect to ACF drought patterns. The data sets were described in Chapter 2 and summarized in Table A.1 in Appendix A.

Atlantic Multidecadal Oscillation

The Atlantic Multidecadal Oscillation (AMO), as termed by Kerr (2000), is a 60-85 year cycle of warming and cooling of sea surface temperatures (SST) in the North Atlantic Ocean. The oscillation of SST is based on the acceleration (warming) and deceleration (cooling) of the Gulf Stream, a byproduct of the changes in the intensity of the Atlantic thermohaline circulation (Enfield et al. 2001). The AMO signal is global in scope, with small effects on the North Pacific SST. It is also highly correlated with precipitation patterns across the contiguous United States. In a recent numerical model simulation study, Sutton and Hodson (2003) showed a mode similar to the AMO as the dominating low-frequency SST oscillation in the Atlantic, affecting climate in the Mid-Atlantic States. The AMO warm phases have been documented from 1860-1880, and 1940-1960. Cool phases occurred from 1905-1925 and 1970-1990 (Enfield et al. 2001). Since

1995, SST have been warming, and we are currently in the developing warm phase with the Gulf Stream expected soon to decelerate, signifying the decline of the latest warm phase.

There is some controversy regarding the signal of AMO in global hurricane trends, as evidenced in recent papers by Trenberth and Shea (2006) and Mann and Emanuel (2006). According to Shea and Trenberth, the AMO signal has a linear warming trend, making it difficult to separate from the warming of SST from global forces. They propose a different AMO index, removing this linear warming trend to focus the signal to variations occurring only in the Atlantic. The AMO index we used is derived from an updated version of the Kaplan extended SST V2 data set (2002) which has the linear trend removed as evidenced in Figure 4.1. A plot of the monthly averaged mean, median, and variance of the AMO index is in Figure 4.2. We did not perform a fast Fourier transform (FFT) on this data set because only two full AMO cycles could be captured in the time period of this data set (1856-2000) which does not provide for reliable FFT results.

Enfield et al. (2001) analyzed the average distributions of 500 hPa geopotential heights for two time periods representing the warm and cool phases of the AMO to gain a synoptic understanding of the effects of the AMO. The analysis showed geopotential heights flattening in the northern United States, while amplifying in the South in the winter time trough-ridge pattern during the warm phase of the AMO. Conversely, the trough-ridge pattern is strengthened only in the North during the cool AMO phase. The study by Sutton and Hodson (2003) suggests this winter pattern of the AMO is similar to that of the winter NAO (2003). Another study by Sutton and Hodson (2005) compared surface temperatures during the AMO warm phase (1931 to 1960) and cool phase (1961 to 1990) during the boreal summer. Results showed temperatures were warmer across the central and southern U.S. during the warm phase which confirmed those of model simulations.

Numerous studies have found a decreased rainfall pattern across the southeast during the AMO warm phase and an increase in rainfall during the cool phase. The strongest correlations between rainfall and the AMO across the United States occurred in the summer rainfall regime (Enfield et al. 2001). From the Enfield et al. study (2001), the ACF basin has mostly negative correlations with summer precipitation and the AMO warm phase, meaning drier seasons are expected in Georgia stations during this time. A weaker and slightly positive correlation between summer rainfall and the AMO cool phase occurs in Northern Florida. We would

therefore expect to see more rainfall in the further inland sections of the basin during the AMO cool phase, and more rainfall in the coastal Apalachicola River stations during the AMO warm phase.

Another study by McCabe et al. (2004) showed weak, but positive correlations between the AMO and drought frequency across much of the contiguous United States. Comparatively, a report from the Southwest Florida Water Management District (Kelly et al. 2004) on the influence of the AMO on Florida river flows showed that northern Florida rivers, including the Apalachicola, have a decreased seasonal peak flow consistently following a warm AMO phase (1940-1969). As expected, an abruptly increased seasonal peak flow occurs during and following the AMO cool phase in northern Florida rivers (1970-1999). As mentioned before, waters in the Apalachicola originate from the two northern rivers of the Chattahoochee and Flint in Georgia and could largely be a reflection of the climate variability from the stations surrounding these rivers.

Similar results were found in a study by Tootle et al. (2005) which focused on streamflow connections in the contiguous U.S. to AMO with the long lead time approach (1 year prior). Their results showed the lower Appalachians/Gulf of Mexico region to have negative correlations with the AMO, indicating decreased streamflow during the warm AMO phase and increased streamflow during the cool phase. The findings also showed a significant number of extreme anomalies in streamflow concurring with the AMO phases as described above. From all of the research, it appears that the ACF lies between two oppositely resulting patterns of precipitation variability associated with the AMO; one in the inland Georgia section of the northern part of the basin, and the other along the Florida coast.

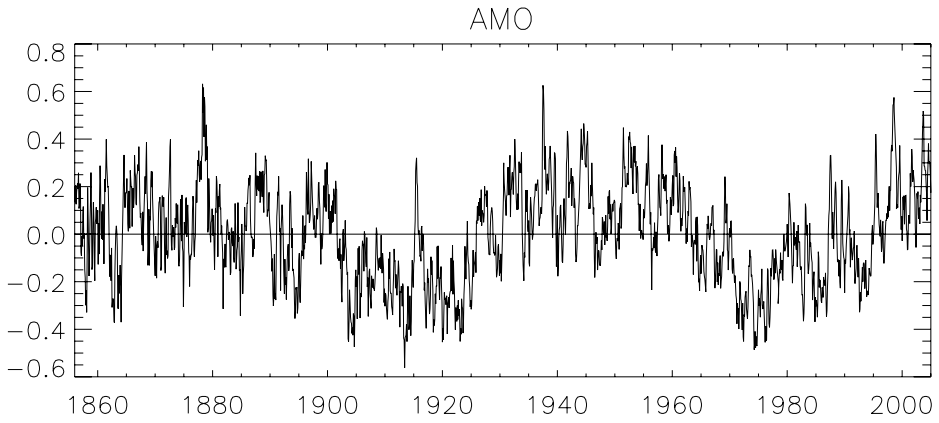

FIG. 4.1: The AMO Index, calculated from Kaplan extended SST V2 (2002) as the detrended time series of the area weighted averaged sea surface temperature anomalies of the northern hemispheric Atlantic Ocean from 0° – 70°N latitude.

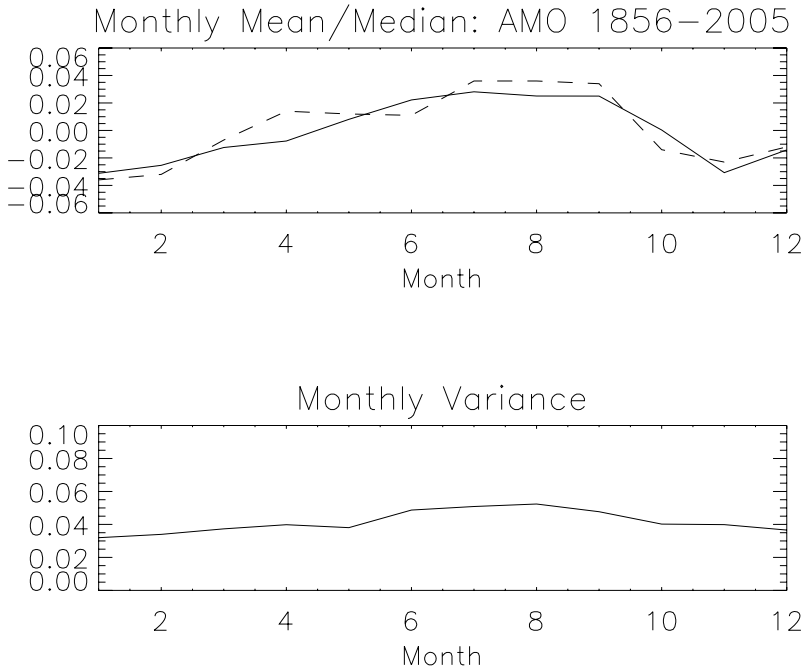

FIG.4.2: The AMO and associated monthly mean and median (solid and dashed lines respectively). The AMO has low monthly variance (standard deviation squared), with a seasonal peak in August, and minimum value in January.

North American Oscillation

The North American Oscillation (NAO) is associated with the seasonal insolation changes and associated variability in mean sea level pressure (MSLP) and geopotential heights over the northern Atlantic Ocean. It is prominent in all months of the year and has a great influence on weather patterns in much of the Northern Hemisphere, including the eastern coast of the United States (Barnston and Livezey 1986). The NAO consists of a north-south dipole of enhanced (positive phase) or diminished (negative phase) Azores High and Icelandic Low over the northern Atlantic (Hurrell et al. 2003). In a positive phase, the NAO has higher than normal surface pressures over the northern central Atlantic (south of 55°N) with anomalously lower pressures occurring throughout the Arctic (Hurrell et al. 2003). This in turn enhances the mid-latitude surface westerlies and also increases the southerly flow over the eastern United States (Hurrell et al. 2003). The NAO varies spatially throughout the year, with the winter northern dipole near Greenland, and southern dipole just west of Portugal. This shifts in the spring with the southern center near the Azores, and in the summer it moves further north and east than the winter pattern, with the fall pattern shifted and oriented southwest to northeast (Hurrell et al. 2003).

The NAO pattern is strongest and exhibits the most influence on surface temperature and precipitation patterns during the northern hemisphere winters. The spring and fall months see smaller sea level pressure anomalies associated with NAO, with minimum values occurring during summer months (June-August) (Hurrell et al. 2003). The NAO index we used is the normalized difference between sea level pressure at a station in SW Iceland (Reykjavik) and Gibraltar (Figure 4.3). A plot of the mean, median, and variance for the monthly averages of the NAO index we used is in Figure 4.4. Since the index is composed of sea level pressure anomalies, the results from our fast Fourier transform include a dominant mode for the NAO at a 6 month time scale featuring the intra-annual frequency, followed by an annual pattern (Figure 4.4). Focusing on the longer-term variability, the third highest peak in the Fourier coefficients occurs near 2.5 years. In our data set, the NAO seems to be more positive during 1930-1940, 1978-1995, with more negative periods occurring 1955-1978 (Figure 4.3). The later positive and negative periods have also been documented by the Climate Prediction Center (CPC) (NOAA 2005).

Precipitation and temperature departures associated with the NAO relationship to MSLP patterns in the Northern Atlantic are notable for the southeast United States. A positive phase of NAO enhances the subtropical Atlantic high-pressure (Azores High) during winter months, which in turn enhances the warm, moist southeasterly flow in the ACF region (Hurrell et al. 2003). In summer months, this enhancement could lead to negative temperature departures in the southeast. A study by the CPC (NOAA 2007) shows a positive correlation in the southeast U.S. between the NAO index and three month surface temperature departures for the winter season (DJF). The summer season (JJA) has a negative correlation, with the positive phase bringing cooler than normal temperatures, as expected.

In a study by Hurrell et al. (2003), typical storm tracks for December through March over the southeast were shown to depart to the north, implying reduced precipitation during the positive NAO phase. The CPC study (NOAA 2005) showed a negative correlation value near -0.40 in the southeast between NAO and precipitation during the March/April/May (MAM) season for a data set covering the years 1950-2000. Focusing on wintertime variability, we will look to confirm these previously found results in our own analysis of a longer period of record with more parameters.

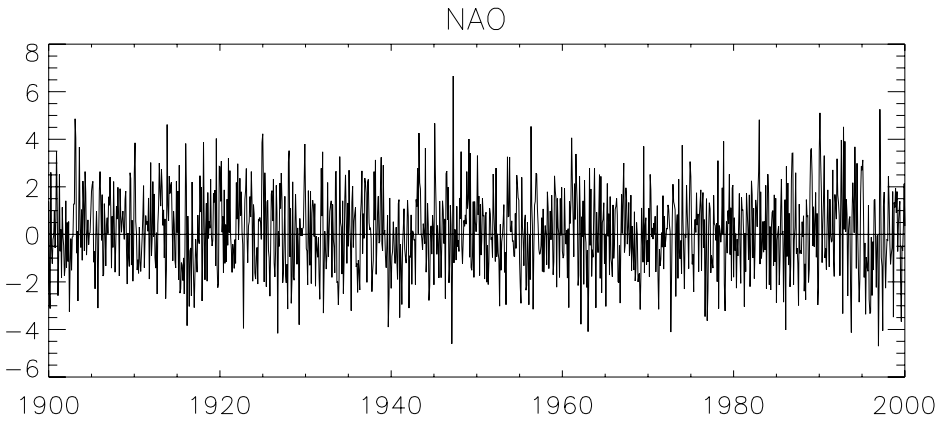

FIG 4.3: The NAO index from the Climate Research Unit defined as the normalized difference in sea level pressure between a station in SW Iceland and the Iberian Peninsula at Gibraltar.

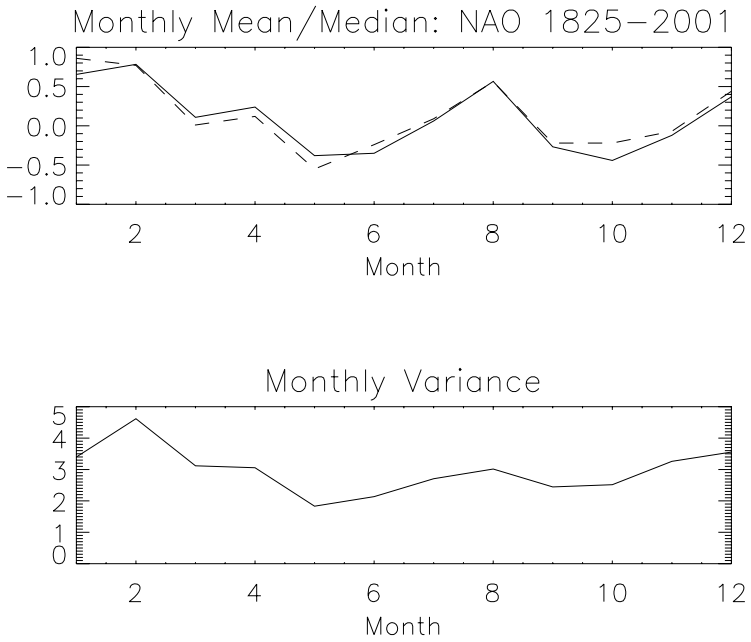

FIG. 4.4: NAO exhibits some bimodal characteristics, with peaks in August and February, seen in the top figure by the mean (solid) and the median (dashed) lines. The NAO index has a high variability with the peak in variance occurring in February around 4.8 units.

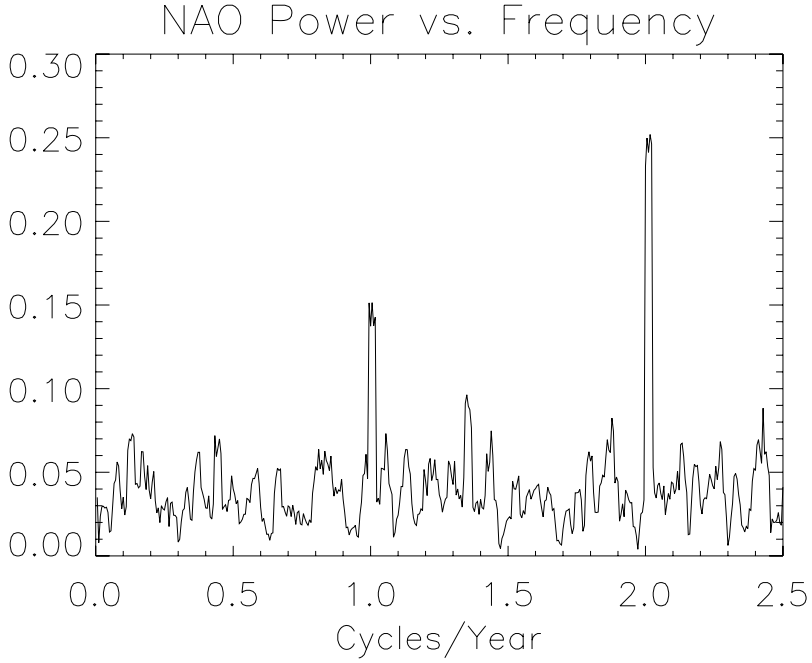

FIG. 4.5: The normalized power spectrum of NAO, with mean removed and boxcar average for smoothing (window size 5). The three largest peaks occur near 6 months, 12 months, with a few peaks near 2.5 years. The expected interdecadal peak appears at 7.6 years (0.131 cycles/year).

Pacific Decadal Oscillation

The Pacific Decadal Oscillation (PDO) is another index included in this study for its possible affects on the ACF. The PDO is associated with the ENSO pattern due to similar characteristic pressure, wind, temperature and precipitation patterns. The PDO, however, varies spatially and temporally from ENSO. The PDO signal is largest in the northern Pacific Ocean as opposed to the tropical Pacific like ENSO. The PDO index we used consists of the leading principal component of monthly sea surface temperature variability in the North Pacific (Figure 4.6), and monthly averaged mean, median, and variance for the PDO index used are plotted in Figure 4.7. While ENSO generally acts on 3-6 year time scales, the PDO is generally a 20-30 year oscillation (Mantua 2002) that has been associated with weather and climate patterns in the southeastern United States. One study by Minobe (2000) found a very energetic periodicity for the 20th century PDO of 50-70 years. Unfortunately our record is not long enough to accurately depict a frequency larger than 50 years in the FFT analysis. Consistent with other results, however, our fast Fourier transform results show a dominant peak near 26 years (Figure 4.8).

The phases of the PDO are defined by associated SST and SLP anomalies in the North Pacific. A positive (negative) phase has SST in the interior North Pacific anomalously cooler (warmer) with warmer (cooler) SST along the coast of North America. North Pacific SLP anomalies have a wave-like pattern with a stronger (weaker) than average Aleutian low and anomalously high (low) pressure in the Northwestern U.S. during the positive (negative) phase (Manuta 2002). The PDO index we are using (Chapter 2) also has an annual cycle since it is based on MSLP changes in the Northern Pacific which changes with the seasonal insolation variations, much like the NAO. The PDO signal, minus this annual cycle, is most apparent in the winter and spring indices (October-March) (Mantua 2002). Studying the PDO indices shows a well documented two-cycle occurrence in the past century, with warm phase taking place from 1925-1946, and 1977 through late 1990's. The cool phases occurred from 1900-1924, and 1947-1976. Interestingly, within these phases, short sign reversals have existed, such as the sudden

three year warm phase in 1959-1961, and a cool phase from 1989-1991 (Figure 4.6) (Mantua 2002).

The study by Mantua (2002) defines connections to the PDO and temperatures and precipitation patterns in the United States similar to that of ENSO. His study shows cooler than average temperatures across the southeast United States and slightly wetter than average conditions in the PDO warm phase during October - March, consistent with the warm phase of ENSO. Conversely, conditions in the southeast are typically warmer and dryer during the negative PDO phase, typical of the La Niña signature in wintertime precipitation and temperature patterns as well. For summertime patterns, a study by Barlow and Berbery (2000) depicted the PDO as a significant mode in Pacific decadal variability and examined its links to precipitation, drought, and streamflow in the United States. Their results are from a regression against principal components of the extracted modes for the summer months of June, July, and August. The PDO has a slightly negative correlation (-0.2) to PDSI in the southeast, meaning decreased precipitation occurs during a PDO positive phase, with that sign reversing to positive further south into Florida. Streamflow in the ACF region also has a negative correlation with PDO during summer according to this study.

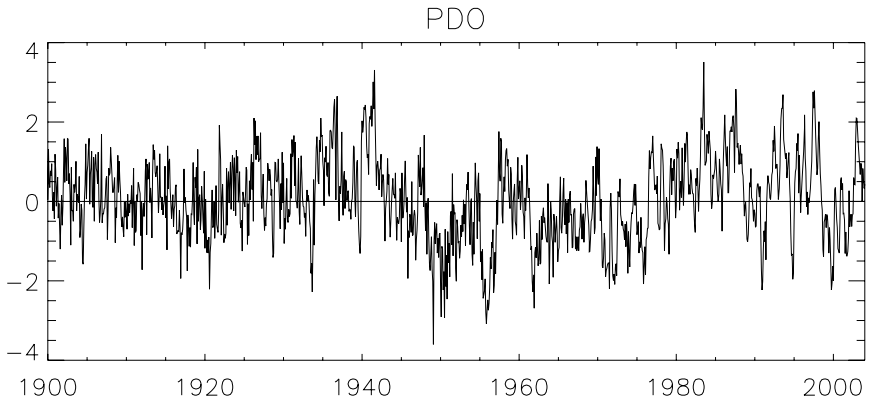

FIG 4.6: The PDO index from Mantua (1997) consisting of the leading principal component of monthly sea surface temperature variability in the North Pacific.

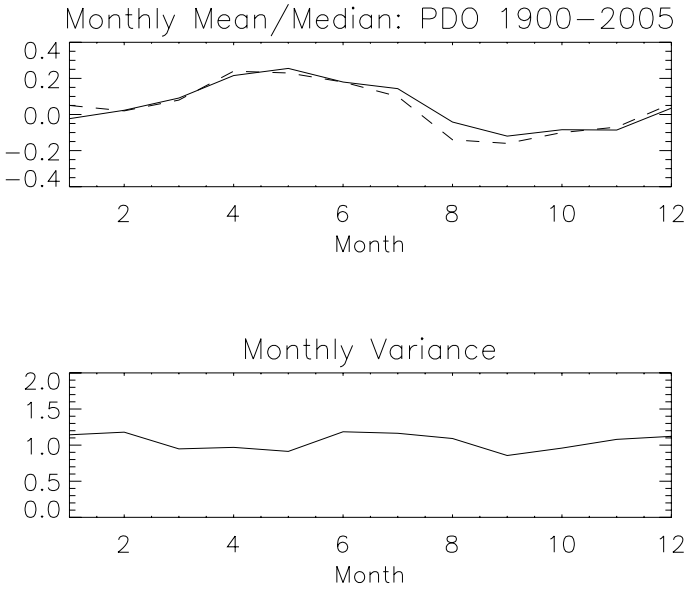

FIG 4.7: Monthly normals for the PDO, showing a seasonal cycle with a peak in late spring (May) and low point late summer/early fall (September). Variance occurs most during the transition periods of winter and summer.

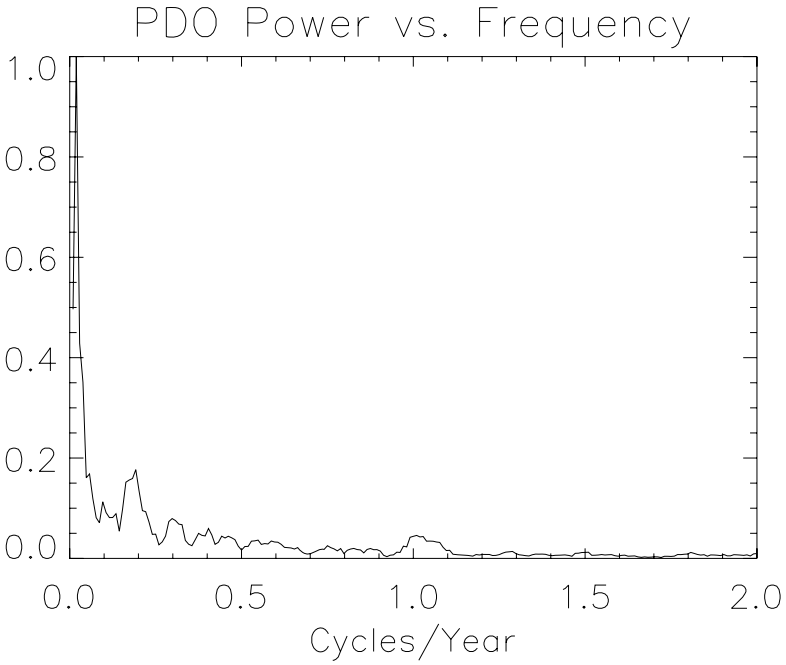

FIG. 4.8: The normalized power spectrum of the PDO with boxcar averaging applied for smoothing. The largest peak occurs around 26 years (0.038 cycles/year), with a smaller peak around 5 years (0.190).

El Niño/Southern Oscillation

One of the most studied climatic influences is the El Niño/Southern Oscillation (ENSO). The index used in this study to measure ENSO is the Southern Oscillation Index (SOI) chosen for its historical availability. The positive phase of SOI is associated with La Niña (cold) events, while the negative phase indicates El Niño (warm) events. The ENSO phenomenon occurs on the seasonal to interannual timescale, and is more predictable than most climatic oscillations (Gershunov et al. 1997). El Niño involves the relaxing of Easterly trade winds and anomalous warming of equatorial Pacific waters, changing sea level pressures and surface patterns in variables such as temperature and precipitation (Green et al.1997). The Southern Oscillation is the other associated aspect of ENSO involving a dipole of anomalous sea level pressures at Darwin and Easter Island (Ropelewski and Halpert 1986). A plot of the SOI used is in Figure 4.9, with the average monthly mean, median, and variance plotted in Figure 4.10. A plot of the FFT results on the SOI are in Figure 4.11 displaying the semiannual, annual, and 3-6 year frequencies involved with the SOI.

The affects of ENSO on the U.S. precipitation and temperature patterns have been widely studied with essentially consistent results. Generally, the associated surface climate patterns are strongest in winter in the southeast. One of the founding studies on North American precipitation and temperature patterns associated with ENSO comes from Ropelewski and Halpert (1986). In the southeast they found increased precipitation during the warm phase from October of the onset year to March of the following year. They also concluded temperatures were generally cooler during El Niño events during this “season”. The spatial area mostly borders the Gulf, with greater than median precipitation occurring in 18 of the 22 warm ENSO events studied.

Gershunov and Barnett (1998) performed a similar temperature and precipitation study, however focused more on the extreme events occurring in the tails of probability density functions. Their study of wintertime (DJF) warm and cold phase events show an increase in the frequency of heavy rainfall events in the southeast enhanced by 15%-30% along the southeastern seaboard during warm phases. La Niña events were associated with decreased heavy rainfall

frequencies in much of the southern United States, as strong as 30%-50% near Northern Florida. Concerning temperature, there is an increased frequency of cold outbreaks in winter El Niño events, with fewer cold outbreaks during La Niña. Central tendency of temperatures shift in the negative direction during warm events, reflecting overall colder temperatures in the southeast for the warm phase.

A conclusive study by the Center for Ocean-Atmospheric Prediction Studies (COAPS) looked at year round changes in temperature and precipitation in association with ENSO. Focusing on the southeast, a warm event typically involves wetter than normal fall, winter, and spring seasons, with decreased temperatures during winter. A cold event begins with a warm and wetter than normal fall, warm and dry winter and spring, leading into a wet and cold summer (Green et al. 1997). Another study from COAPS confirms these findings with evidence of an increase in precipitation along the Gulf, from 2-3 cm in the DJF composite of warm phase events. The cold phase experiences a 1-2 cm dry departure in the southeast, with both results considered mostly predictable based on root mean square differences (Smith et al. 1998).

The possible physical explanations for the winter precipitation changes related to ENSO have also been explored. Smith et al. (1998) looked at anomalies and their robustness in low level winds, sea level pressure, convergence, jet stream locations, and vorticity advection as potential conduits for enhanced precipitation. Their study resulted in possible physical explanations for both phases of ENSO. The warm phase is set up with a weak Pacific High, a stronger than normal Aleutian low and a more easterly location of the Bermuda high from neutral times. The changes in the Bermuda high are more variable, with the Pacific pressure systems typically more predictable. This set up provides mostly southwesterly flow into the entire Gulf, providing low level moisture for increased precipitation. The southwesterly flow is 90% statistically robust during warm phase events. Also occurring during the ENSO warm phase is a southwest to northeast jet at 300 hPa over the southeastern United States. The orientation of this jet allows for more lift connected to the equatorward entrance region of the jet over the southeast, assisting with a wetter than normal season.

In contrast, the cold event has mostly opposite features of the warm event, beginning with the set up of surface pressures. The cold phase exemplifies a stronger than normal Pacific High, weaker Aleutian Low and westward expanding Bermuda High. The westward movement of the Bermuda high sets up an anticyclone off the coast of Cape Hatteras, influencing stronger than

normal easterly winds over the south and Gulf. Low level flow is mostly southeasterly, allowing for low level moisture in the western Gulf and drier air in the eastern Gulf. The 300 hPa eastern jet is more zonally oriented, with the conducive area for lift relocated northwest over the lower and middle Mississippi Valley. Therefore, the southeast experiences less precipitation in cold phases and enhanced precipitation in warm phases.

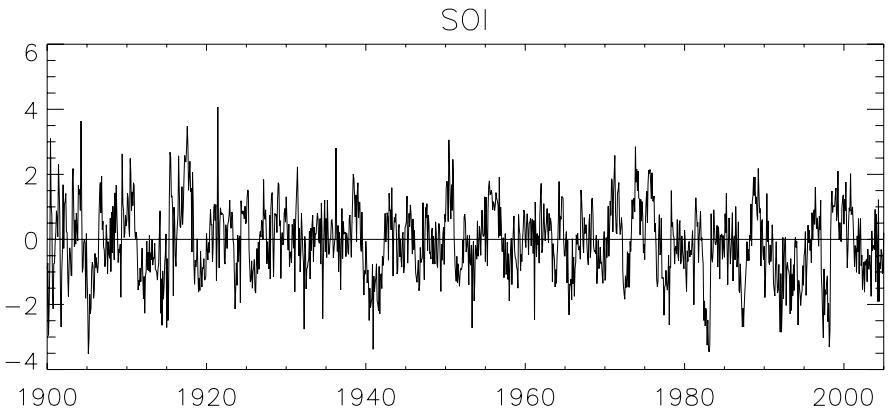

FIG. 4.9: The SOI index from the Climatic Research Unit composed of monthly normalized sea level pressure difference between Tahiti and Darwin.

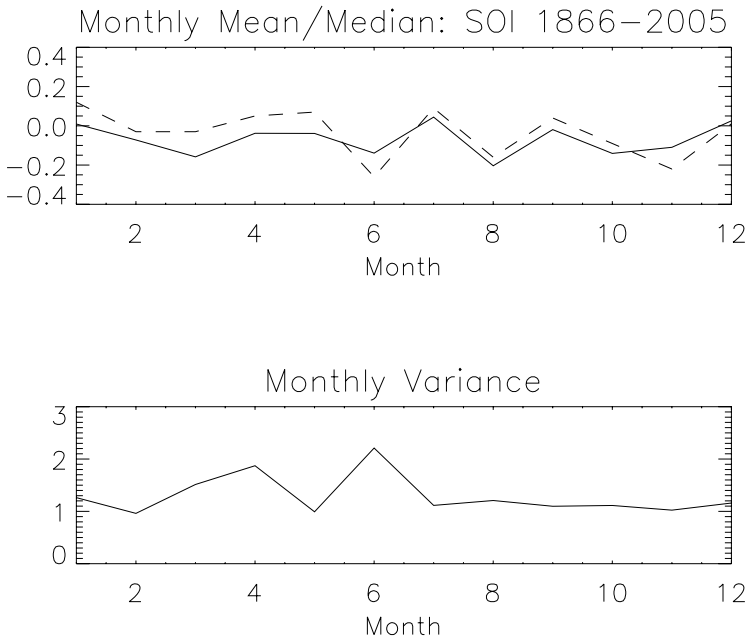

FIG. 4.10: (Top) The mean (solid) and median (dashed) monthly averages of SOI show several fluxes throughout the year. The monthly variance (bottom) peaks in June and March.

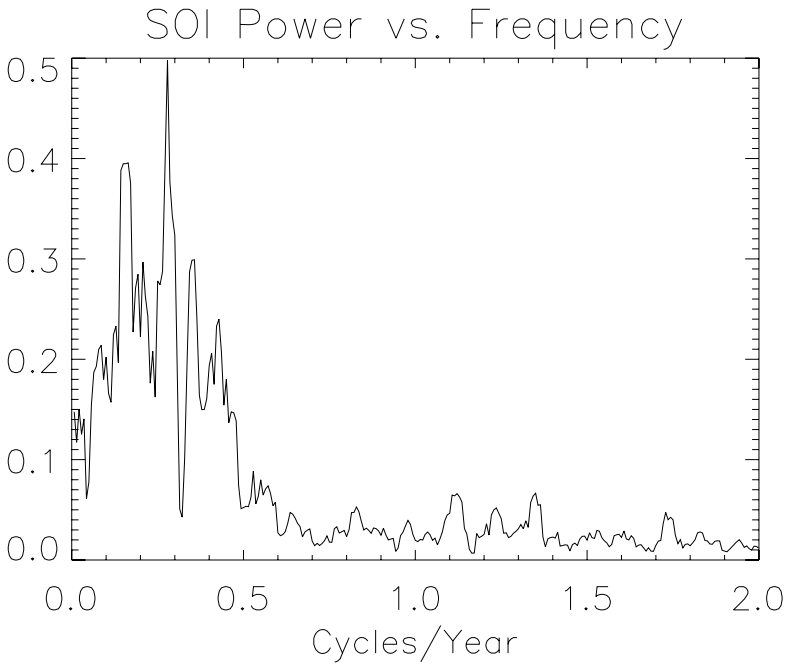

FIG. 4.11: The normalized power spectrum of SOI in cycles/year with boxcar averaging applied for smoothing. The most dominant peaks occur between 2 and 6.5 years (0.5 and 0.15 cycles/year). Interannual variability is also present in the 1.1-1.4 cycles/year range.

TABLE 4.1: A summary of the four climatic indices and their associated characteristics and relationships to the surface climatological variables in the ACF from previous research.

		Significant Historical Phases			Affect on ACF		
Name	Region and Substance	Length of phases	Positive Phases	Negative Phases	Seasonality	Temperature	Precipitation
Atlantic Multidecadal Oscillation AMO	North Atlantic Ocean SSTs	60-85 years	1860-1880, 1930-1960	1905-1925, 1970-1990	Summer strongest	Pos: summer warmer Neg: summer cooler	Pos: summer decreased precip Neg: summer increased precip
North Atlantic Oscillation NAO	Northern Atlantic MSLP dipole	Interannual, multidecadal	1978-1995	1955-1978	Winter strongest Prominent all months of year	Pos: winter warmer, summer cooler Neg: winter cooler, summer warmer	Pos: decreased precip, esp late spring Neg: increased precip
Pacific Decadal Oscillation PDO	Northern Pacific SSTA, MSLP difference	20-30 years 50-70 yr secondary peak	1925-1946, 1977-1998	1900-1924, 1947-1976	Winter and spring strongest	Pos: Oct-Mar cooler Neg: Oct-Mar warmer	Pos: Oct-Mar wet, summer dry Neg: Oct-Mar dry, summer wet
Southern Oscillation Index SOI	Equatorial Pacific SLP Diff.Darwin & Tahiti	Interannual, 3-4 years	1945-1949, 54-56, 70-71 *Cold ENSO Phases	1951,57,65,76,82,86-87,91,98 *Warm ENSO Phases	Winter strongest	Pos/cold: Oct-Mar warmer, cooler summer Neg/warm: Oct-Mar cooler, esp. winter	Pos/cold: Fall wet, dry winter, wet summer Neg/warm: Oct-Mar increased precip.

Coupling

Climatic oscillations and their associated effects have been known to vary in strength of signal from cycle to cycle. A possible explanation for this is the modulation of one oscillation by the cycle of another. Preliminary research has indicated a few potential coupling relationships with the climatic oscillations being used for this study, and we will explore for evidence of these in our results.

One of the most studied coupling effects is that of the ENSO and PDO relationship. As noted earlier, ENSO and PDO have spatially similar patterns occurring in the North Pacific/Equatorial Pacific concerning sea level pressure and sea surface temperature. Gershunov and Barnett (1998) showed that during the constructive phases of ENSO and PDO (high phase PDO, warm phase ENSO), the ENSO signal is enhanced with stronger associated sea level pressure anomalies. In turn, destructive phases (high phase PDO, cold phase ENSO) masks or deteriorates the ENSO signal in the North Pacific. According to a study by Rajagopalan et al. (2000), precipitation effects from ENSO are enhanced by the PDO only in winter regimes and do not change the summer season PDSI values. Another study by Tootle et al. (2005) showed no PDO affect on ENSO streamflow influences in the United States at the 95% significance level.

Interestingly enough, the destructive phases of ENSO and PDO seem to enhance the NAO signal in the North Atlantic (Figure 4.12). Wintertime destructive ENSO/PDO (warm/negative) is associated with a more significant negative NAO phase (Gershunov and

Barnett 1998). In theory, an enhanced El Niño signal (by high PDO phase) would further increase positive rainfall anomalies in the southeastern United States. Looking at destructive wintertime warm El Niño patterns, an enhanced NAO signal should be prevalent and therefore drier than normal conditions in the ACF Basin could be exacerbated by the stronger NAO.

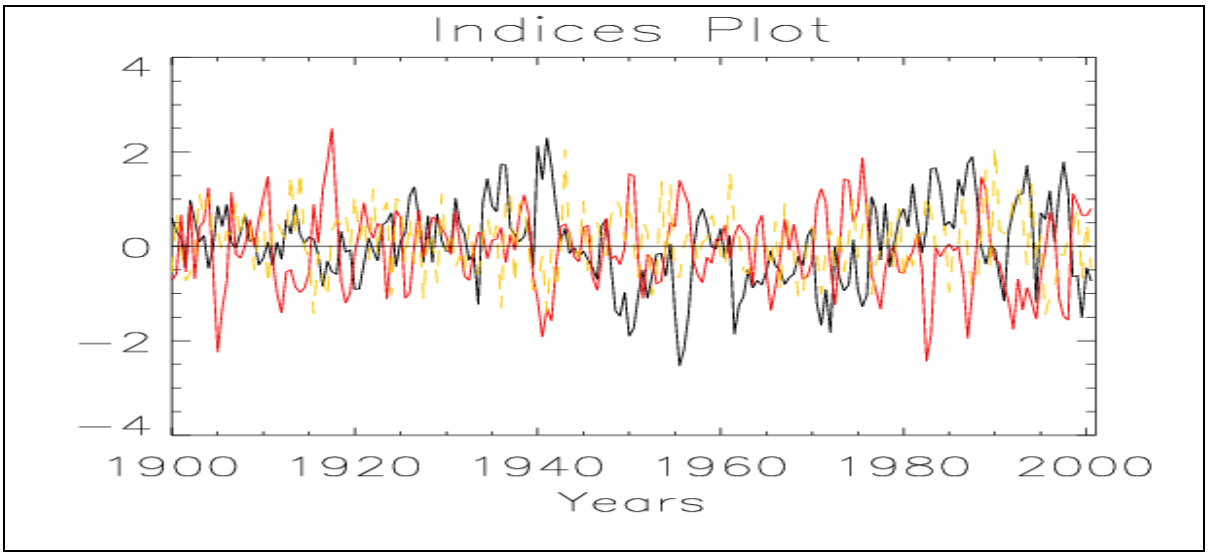

FIG. 4.12: PDO (black), SOI (red), and NAO (yellow dashed). SOI negative representative of warm ENSO phase, therefore enhanced SOI during opposite PDO phase (warm phase ENSO, positive PDO, e.g., 1940). During years of destructive alignment (PDO negative, SOI negative) a stronger opposite sign NAO results (e.g., positive NAO, 1943).

A study by Tootle et al. (2005) proved the coupling of AMO and ENSO and their affects on streamflow in the southeast to be statistically significant. Again, the cold phase of ENSO and warm phase of AMO result in decreased streamflow in the southeast. Therefore, a La Niña event during the warm phase of AMO generally results in more severe droughts in the southeast, and an El Niño during the cool phase of AMO could result in higher precipitation across the ACF. In comparison, the AMO has the largest affect on streamflow with destructive streamflow coupling of ENSO still resulting in the AMO overall influence. For example, a warm phase of ENSO coupled with a warm phase of AMO is more likely to result in drought rather than a flooding

event based on this research. We will be looking at these coupled capabilities to draw conclusions on their influence in the ACF.

Previous studies by others reviewed here have indicated certain climatic oscillations are associated with influencing the southeast in terms of temperature, precipitation, and streamflow. As temperature and precipitation are important ingredients for calculating evapotranspiration, a better understanding of the fluctuations of these variables may lead to a better prediction of drought in the ACF with the changing oscillations.

To summarize from the literature, the negative phase of the AMO during summer, NAO during winter, and SOI from October-March and the positive phase of PDO from October-March are all associated with positive rainfall anomalies and cooler temperatures in the southeastern United States. In turn, the positive phases of the AMO, NAO, SOI, and the negative phase of the PDO are generally associated with decreased rainfall and warmer conditions during the above mentioned seasons for each climate oscillation.

Coupling of constructive phases of the ENSO and PDO can lead to an enhanced increase in precipitation (positive phases) during the winter season, or a stronger decrease in precipitation (negative phases). A destructive combination of these may be associated with a heightened NAO signal, influencing rainfall as respectively discussed above. The coupled AMO and ENSO, with a warm phase AMO and cold phase ENSO may be associated with more severe droughts than when only one of these signals acts alone. The nature of this problem suggests a new multivariate approach be used to examine these interrelationships, such as canonical correlation analysis (CCA), which will confirm some of these findings for our extended data set, and develop new ideas.

CHAPTER FIVE

ANALYSIS

The results from the multiple canonical correlation analyses are summarized in several tables and figures for the two tests conducted for this study, as previously described in Chapter 3. In most studies utilizing CCA, interpretation of the results is left largely to the researcher as there have been no generally accepted guidelines for suitable results for CCA among researchers (Hair et al. 1998). As with most statistical tests, the results should be interpreted with care to the research being performed and may not be suitable for guidelines anyhow. For these reasons, we create and apply analysis thresholds based on our familiarity with the data being used and the nature of this study.

The first type of summary table includes which climate signals appeared most dominant in the cross loadings by applying an analysis threshold of 0.2 to be considered in our terms "significant" (Table 5.1 and 5.3). As mentioned in Chapter 3, all roots that are being examined are statistically significant at the 95% confidence level. The numbers following the climate indices indicate which season they represent, with 1 for DJF, 2 for MAM, 3 for JJA, and 4 indicating SON. Although lagged seasons often appear with "significant" relationships, we will not compare these results to previous research because it is outside the scope of this project. However, we will present them as they often do appear in the results. The dominant surface characteristics must pass our analysis threshold of having a canonical loading larger than 0.4. This case, any variable must share at least 16% of the variance with the respective variate. These thresholds are based in part on CCA work by others and their own interpretation in geophysical data analysis, and could be considered somewhat arbitrary. However, the analysis done here reveals some fairly consistent patterns when applied to independent data, and therefore, we believe them to be appropriate choices.

The signs of the loadings and the signs of the cross loadings determine the kind of relationship between the "significant" variables in the results. For example, in the DJF results for test one (Table 3.3), the Lower Flint maximum and minimum temperatures both have a positive loading, while the NAO 1 cross loading is also positive, indicating a direct relationship between the NAO 1 and maximum and minimum temperature. A direct relationship implies that

as the NAO index increases, maximum and minimum temperatures during DJF season also increases in the Lower Flint sub-basin region. We then compare our findings with previous research in this area (Chapter 4) to look for consistent results.

In some cases, previous research may not describe the same surface meteorology patterns found here, in association with a certain climate index for the particular season. Other studies have applied different seasons than ours, in which case we indicate which season the previous research has described the relationship for, as seen in the case of Apalachicola MAM with SOI 2 "winter yes" (Table 5.1). One study, by Ropelewski and Halpert (1986) analyzed October – March ENSO affects, while another study by Gershunov and Barnett (1997) focused more on December-February results. When the seasons and researched affects are similar, we generalize the seasons into winter, spring, summer, and fall. Since spring and fall are the transition seasons, their results are often times the least studied, and in these cases we relate what we know from the more dominant seasons of summer and winter. We will see that results in terms of predictor-predictand relationships are clearly much different for DJF than they are for JJA.

While coupling between climate oscillations is an important factor to consider, it is difficult to display in the CCA results. We will not heavily focus on coupling in the analysis; it is mentioned to quantify why we chose the CCA approach. For example, prior research has focused on the role of ENSO in understanding precipitation variability in the southeastern United States (and other regions). Our research suggests that a multivariate approach to predictors might lead to more robust findings and relationships, and possibly better forecast model approaches than those that just consider relationships to ENSO phases.

Test One Results

In this section we will describe the results from test one consistent with the methodology described in Chapter 3. The goal of this test is to collectively describe the relationships between the climatological surface variables and climate oscillations for a potential multivariate approach to understanding drought in the ACF. A summary table of these results can be seen in Table 5.1, and the full CCA results for each section of the basin are located in Appendix D. Table 5.2 summarizes the overall strength of the canonical tests and correlations for each sub-basin area for each season.

TABLE 5.1: A focus on the loadings, cross loadings, and therefore relationships between the dependent and independent variables from the CCA results for test one.

	DJF-1				MAM-2				JJA-3				SON-4			
Section	Dominant Climate	Dominant Surface	Relationship	Consistent with Research	Dominant Climate	Dominant Surface	Relationship	Consistent with Research	Dominant Climate	Dominant Surface	Relationship	Consistent with Research	Dominant Climate	Dominant Surface	Relationship	Consistent with Research
Apalachicola	NAO 1	max & min temp	direct	yes	SOI 1	precip	indirect	NS	AMO 3	max temp	direct	yes	NAO 3	max & min temp	indirect	NS
	PDO 1		indirect	yes	SOI 2		indirect	winter yes	AMO 2		direct	NS				
									AMO 4		direct	NS				
									AMO 1		direct	NS				
Lower Flint	AMO 1	max & min temp	direct	NS	NAO 3	max & min temp	direct	NS	AMO 3	max & min temp	direct	yes	NAO 3	max & min temp	indirect	NS
	AMO 4		direct	NS		precip	indirect	NS	AMO 4	max & min temp	direct	NS				
	NAO 1		direct	yes	*This is the second root from the canonical correlation				AMO 2	max & min temp	direct	NS				
	AMO 3		direct	NS	since it had a larger proportion of variance explained				AMO 1	max & min temp	direct	NS				
	PDO 1		indirect	yes												
Lower Chattahoochee	NAO 1	max & min temp	direct	yes	SOI 1	precip	indirect	NS	AMO 3	max & min temp	direct	yes	NAO 3	max & min temp	indirect	NS
	PDO 1		indirect	yes		max & min temp	indirect	NS	AMO 4		direct	NS				
					NAO 3	precip	direct	NS								
						max & min temp	direct	NS								
Upper Flint	NAO 1	max & min temp	direct	yes	NAO 3	max & min temp	direct	NS	PDO 2	min temp	direct	NS	NAO 3	max & min temp	indirect	NS
	PDO 1		indirect	yes		precip	direct	NS		precip	indirect	NS				
Middle Chattahoochee	NAO 1	max & min temp	direct	yes	NAO 3	max & min temp	direct	NS	PDO 2	max & min temp	direct	NS	NAO 3	max & min temp	indirect	NS
	PDO 1		indirect	yes		precip	direct	NS		precip	indirect	NS				
									PDO 3	max & min temp	direct	NS				
										precip	indirect	yes				
Upper Chattahoochee	NAO 1	max & min temp	direct	yes	NAO 3	max & min temp	direct	NS	AMO 4	max & min temp	direct	NS	AMO 4	max & min temp	direct	NS
	PDO 1		indirect	yes		precip	direct	NS		precip	indirect	NS		precip	indirect	summer yes
	AMO 4		direct	NS					AMO 3	max & min temp	direct	yes				
	AMO 3		direct	NS						precip	indirect	yes				
	AMO 1		direct	NS					AMO 2	max & min temp	direct	NS				
										precip	indirect	NS				
									PDO 2	max & min temp	direct	NS				
										precip	indirect	NS				

NS indicates "Not Sure". Either research does not define the relationship for this season, or it's a lagged relationship which was not previously researched for this project, but is presented.

TABLE 5.2: The strength of the CCA results from test one for each sub-basin area during each season.

	DJF				MAM				JJA				SON			
	Canonical Correlation	Proportion of Variance	Correlation Max and Min Temp	Correlation Max Temp with SPI6	Canonical Correlation	Proportion of Variance	Correlation Max and Min Temp	Correlation Max Temp with SPI6	Canonical Correlation	Proportion of Variance	Correlation Max and Min Temp	Correlation Max Temp with SPI6	Canonical Correlation	Proportion of Variance	Correlation Max and Min Temp	Correlation Max Temp with SPI6
Apalachiocola	0.507	0.160	0.846	-0.170	0.492	0.084	0.900	-0.090	0.406	0.042	0.190	-0.328	0.397	0.102	0.940	-0.042
Lower Flint	0.571	0.173	0.797	-0.210	0.372*	0.079*	0.882	-0.107	0.467	0.109	0.405	-0.375	0.411	0.105	0.916	-0.082
Lower Chattahoochee	0.522	0.162	0.818	-0.112	0.433	0.080	0.923	-0.130	0.366	0.042	0.244	-0.452	0.412	0.095	0.924	-0.095
Upper Flint	0.516	0.148	0.768	-0.067	0.417	0.086	0.928	-0.076	0.420	0.067	0.336	-0.334	0.399	0.102	0.934	-0.078
Middle Chattahoochee	0.528	0.166	0.801	0.003	0.407	0.080	0.924	-0.071	0.422	0.085	0.482	-0.342	0.439	0.104	0.930	-0.071
Upper Chattahoochee	0.553	0.170	0.808	0.056	0.406	0.080	0.933	-0.096	0.405	0.087	0.543	-0.376	0.434	0.098	0.908	-0.056

The winter season (DJF) consistently has the strongest canonical correlation values and proportion of variance explained (Table 5.2). The canonical correlation values range from 0.50 to 0.57, meaning 25% to 32% of the variance is explained by the canonical variates. The proportion of variance explained in the dependent set by the opposite canonical variate ranges from 14.8% to 17.3%. These results were not surprising as wintertime variability is often the strongest when the atmosphere is most dynamically active (Hurrell et al. 2003).

For all of the stations during DJF, maximum and minimum temperatures are the only dominant surface variables. The winter NAO and PDO appear in every basin as an influencing climate oscillation, with the AMO of seasons 1, 3, and 4 appearing in the Lower Flint and Upper Chattahoochee regions (Figure 5.1). The NAO and PDO are strongest in the winter, a likely reason why the winter seasons all share some variability with these indices. In every case, the NAO shares a direct relationship with the maximum and minimum temperatures while the PDO has an indirect relationship, implying surface temperatures increase in a positive NAO phase and negative PDO phase, which is consistent with our research (Hurrell et al. 2003; Mantua 2002). When AMO 1 is present in the DJF results, it shares a direct relationship with temperature, also consistent with previous studies for summertime affects (Sutton et al. 2005).

The spring season (MAM) exhibits stronger correlations between maximum and minimum temperature than in the winter season (DJF), and continued weak correlations between temperature and SPI6. The proportion of variance explained is around 8.2% throughout the basin. March typically contains the second highest monthly precipitation peak in all regions of the basin (Figure 2.3). This explains why precipitation appears as a contributing surface component to the dependent variate in all the sub-basins. Maximum and minimum temperatures are contributing components as well, except in Apalachicola in which the only important variable appears to be SPI6.

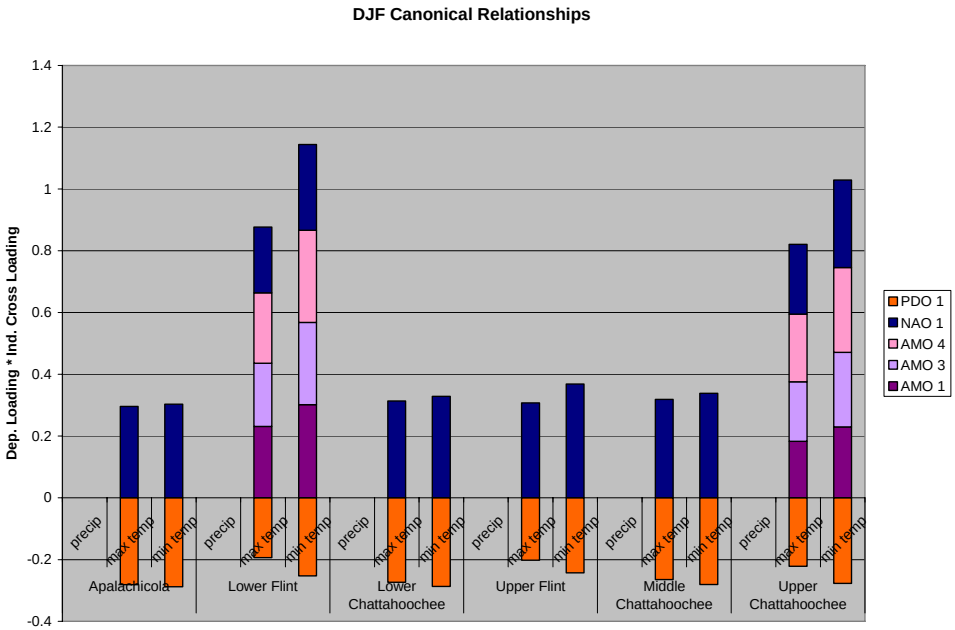

FIG. 5.1: A graphical depiction of the CCA results for DJF for test one. The y-axis represents the dependent loading multiplied by the independent cross loading to gain an idea of the sizes of the loadings. The sub-basins with several contributing climate oscillations do not necessarily have stronger relationships, they have more "significant" relationships to graph. The positive (negative) values indicate a direct (indirect) relationship.

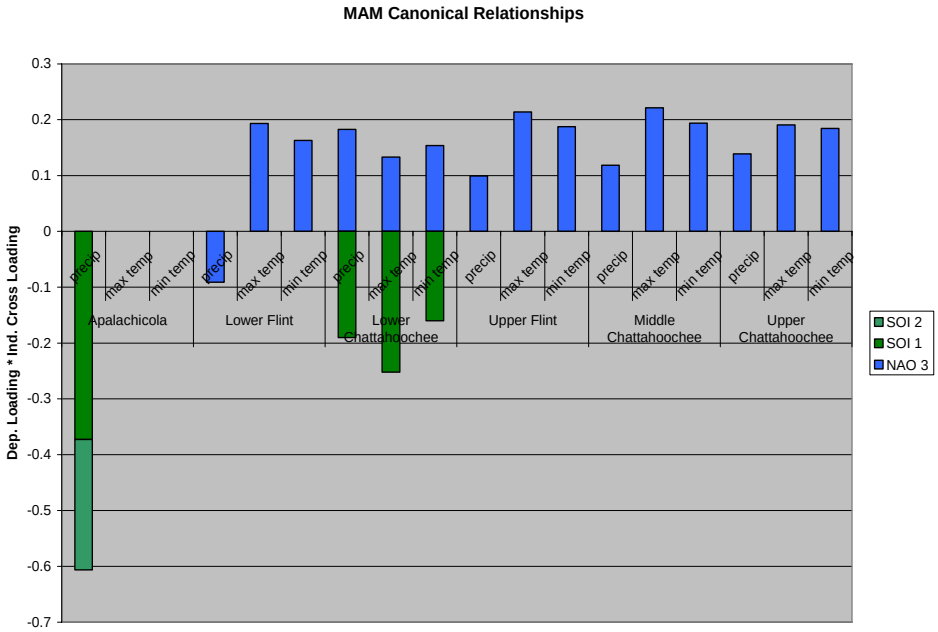

FIG. 5.2: Same as figure 5.1, but for MAM.

The two main climate oscillation components are SOI 1 and NAO 3 (Figure 5.2). Since NAO is typically strongest in winter and summer, it is not surprising NAO 2 or 4 never show up as dominant climate oscillations in our results. The NAO is generally prominent throughout the year, and perhaps is why it appears consistently in the transition seasons (MAM, SON) while other climate oscillations are minimized. Except for the Lower Flint, NAO 3 has a direct relationship with precipitation and in all cases a direct relationship with maximum and minimum temperature. Previous research has found an indirect relationship between concurrent seasons of NAO and precipitation during the spring; however, this indirect lagged relationship was not a consistent finding in our results (Hurrell et al. 2003; NOAA 2005). The study by Hurrell et al. (2003) also suggests the warm, moist southeasterly flow is enhanced during NAO positive phase in winter months, which could explain the largely direct relationship in MAM between NAO and precipitation.

The El Niño/Southern Oscillation has been extensively researched for its impact on precipitation in the United States. Perhaps SOI appears consistently in MAM because precipitation becomes a more contributing component to the variate. Previous research has stated SOI affects on the southeast are strongest in the wintertime, which is why SOI 1 appears more frequently than any other seasonal SOI value (Ropelewski and Halpert 1986). In Apalachicola MAM results, precipitation is the only component to pass our analysis threshold and SOI 2 also comes up in the results as an influencing factor. This may be due to the isolation of precipitation as the only surface component.

The summer season (JJA) generally has the lowest proportion of variance explained, ranging from 4.2% to 10.9%. This result is not surprising in that statistically, summer precipitation has the lowest forecast skill of any season (Cartwright 2004). Precipitation usually experiences its largest monthly peak in July and occurs frequently as a dominant surface component for the JJA season in the CCA results. At least one of the temperature variables is a surface component in every sub-basin area. This is the only season where the correlation between maximum temperature and SPI6 is noticeable, ranging from -0.334 to -0.452. Conversely, the correlations between maximum and minimum temperature are their weakest in this season, around 0.4 departing from their typical 0.8-0.9 values in the other seasons.

The dominant climate oscillations are several seasons of AMO, particularly in the southern regions of the basin, and the PDO 2 in the more northern regions (Figure 5.3). The

AMO affects on precipitation appear largest on the summertime rainfall regime, suggesting why this is the first appearance of an AMO and precipitation relationship in the CCA results (Enfield et al. 2001). The summer value of AMO has the largest cross loading in the results for all three of the southern basins (Apalachicola, Lower Flint, Lower Chattahoochee). In each case, AMO has a direct relationship with maximum and minimum temperatures, while an indirect relationship with precipitation occurs in the Upper Chattahoochee region. As follows with research, the positive phase of AMO causes anomalously warm and dry summers and can be a large influence on drought and streamflow. The Enfield et al. (2001) study did show a slight positive correlation in the Northern Florida region between AMO and precipitation that is not apparent in our results. The AMO may exhibit more of an influence on the southern part of the ACF because it is closer to the Gulf of Mexico, however, the only precipitation signature revealed in our research is in the Upper Chattahoochee sub-basin.

The PDO signal is strongest in the winter and springtime (Mantua 2002), which is why PDO of the MAM season appears consistently in the summertime results where there is a PDO relationship. In each case, PDO has a direct relationship with maximum and minimum temperatures and an indirect relationship with SPI6. In the Middle Chattahoochee results with a PDO 3 component, the indirect relationship between precipitation and PDO is consistent with previous research. Therefore, a positive phase of PDO is associated with a drier summer, particularly in the northern section of the basin.

Fall (SON) is typically the dry season with rainfall values at their lowest during October throughout the basin. Correlations are strongest between maximum and minimum temperature and weakest between maximum temperature and SPI6 during this season, as expected. Precipitation only appears in the Upper Chattahoochee dependent canonical variate, as transitory mid-latitude systems move across that part of the basin in fall, more so than the rest of the region studied.

Similar to the other transition season, MAM, NAO 3 appears as a dominant climate oscillation in the cross loadings (Figure 5.4). In five of the six regions, NAO 3 and maximum and minimum temperatures are the only dominant climate and surface variable components, respectively. Again, NAO is the only climate oscillation prominent in all months of the year in the Northern Atlantic which could explain how it is the most frequently occurring oscillation in the SON results. In every case, NAO 3 has an indirect relationship with temperature, consistent

with non-time-lagged summertime effects found in previous research (e.g. NOAA 2007; Hurrell et al. 2003).

In the Upper Chattahoochee region, all three of the surface meteorological variables meet our analysis thresholds, while the only "significant" climate oscillation is AMO 4. The inclusion of precipitation in the dependent variate may explain why the AMO appears only in this region during SON. In these results, precipitation has an indirect relationship with AMO 4, consistent with researched summertime AMO affects (Enfield et al. 2001).

Overall, maximum and minimum temperatures generally share the largest portion of variance explained in the dependent canonical variate, implying temperature has more variance associated with climate oscillations throughout the year. The MAM and JJA are the only seasons where SPI6 is considered a "significant" component in our terms in more than one sub-basin. These are the wetter seasons throughout the basin.

Several seasons of AMO appear as dominant components during DJF and JJA throughout the basin, but particularly in the southern sub-basins and the Upper Chattahoochee sub-basin. During DJF and JJA, AMO has a direct relationship with maximum and minimum temperatures, and an indirect relationship with precipitation in JJA, consistent with previous studies.

The NAO is prominent during the DJF, MAM, and SON seasons. It is the only climate oscillation to appear in SON across the basin, and one of the few in MAM. The NAO is seasonally strongest in winter, then summer, possibly explaining why the variance from JJA appears in MAM and SON results. From our results, NAO of JJA has a direct relationship with precipitation in MAM in 4 of the 5 basins it appears in. The DJF NAO has a direct relationship with maximum and minimum temperatures in DJF, while NAO 3 also has a direct relationship with temperatures during MAM but an indirect relationship in SON.

The PDO influence occurs mainly in DJF and JJA, when the oscillation is at its strongest peaks of variability (Figure 4.7). The DJF PDO appears in the DJF results with an indirect relationship to maximum and minimum temperatures, consistent with previous research. Conversely, PDO 2 has a direct relationship with temperatures during JJA. In JJA, PDO 3 and 2 appear to have an indirect relationship with precipitation, implying drier summers under a positive PDO influence.

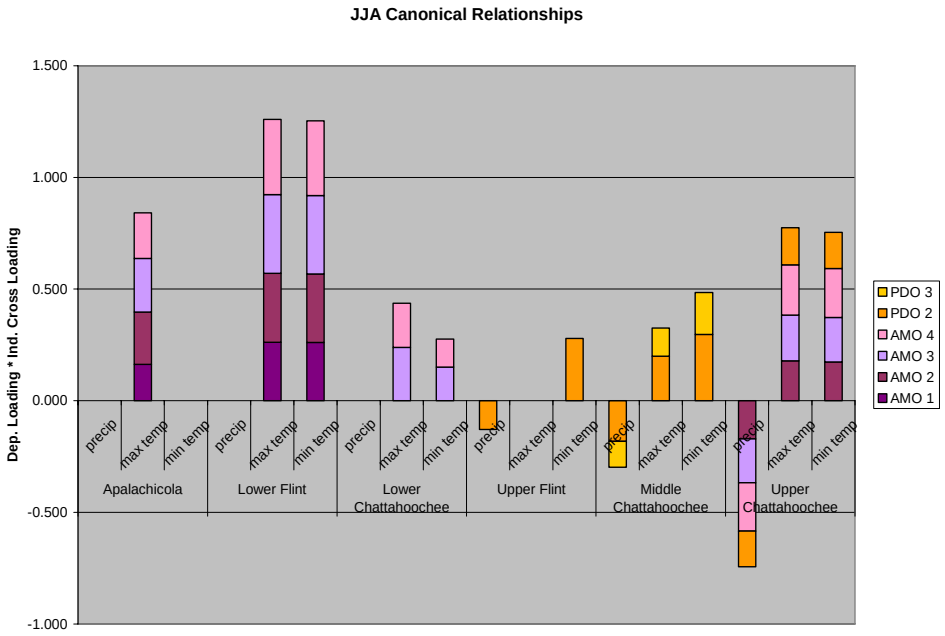

FIG. 5.3: Same as Figure 5.1, but for JJA.

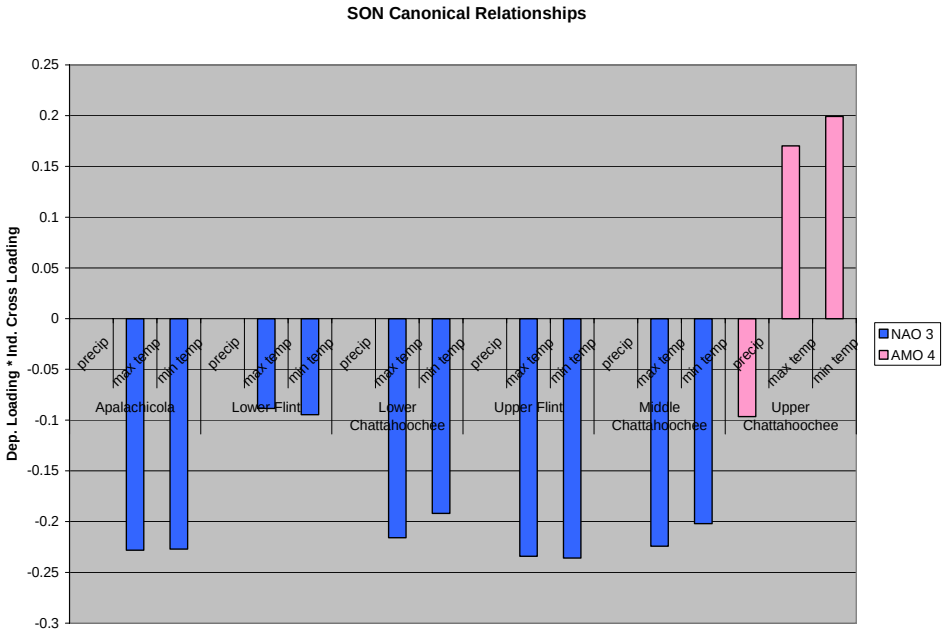

FIG. 5.4: Same as figure 5.1, but for SON.

The more extensively researched SOI appears only during MAM in our results for test one as a "significant" climate contributor, and only in the southern sections of the basin. During MAM, precipitation becomes a larger component to the variate, and possibly SOI has a larger influence on precipitation than temperature, particularly during spring. The DJF value of SOI appears in the Apalachicola and Lower Chattahoochee sub-basins in MAM. The MAM value of SOI also appears in the Apalachicola region. In all cases, SOI has an indirect relationship with precipitation. Previous research has found SOI to have this indirect affect during wintertime precipitation patterns. The SOI associations to surface climate patterns are strongest during winter and could explain why this is the more dominant SOI season in our results (Ropelewski and Halpert 1986). The SOI is shown to have a direct relationship with maximum and minimum temperatures during MAM. Previous research has shown positive SOI (cold ENSO events) to experience warmer October through March temperatures in the southeast making our results consistent with previous findings. A breakdown of the results by basin is presented in more detail in Appendix E.

Test Two Results

The goal of the second test is to focus on the precipitation variables in the two extreme northern and southern regions of the basin for a larger scale understanding of climate influence on precipitation in the ACF. As described in Chapter 3, this test uses the four different SPI values (three, six, twelve, and twenty-four month) for the Apalachicola and Upper Chattahoochee sub-basin regions. This test is necessary since so much of the variance in test one is accounted for by the temperature values and precipitation does not always make our results. Since there are only two sub-basin areas, two roots will be extracted from the CCA. In this test, the dependent canonical variate for each root is made up mostly from one sub-basin; therefore, we will examine all significant roots (p-value < 0.05) for a more focused understanding of each region's tie to climate oscillations concerning only SPI. We are using the four different time averaging intervals of SPI to examine how the variance of the different climate indices with their own associated frequencies can be captured by the different monthly SPI values.

Similar to test 1, we apply an analysis threshold of 0.2 for the independent cross loadings and 0.4 for the dependent loadings. Since temperatures accounted for much of the variability in

test one, there are several cases in test two where no "significant" climate oscillations appeared. In SPI3 SON results, neither canonical root passed the p-test.

The canonical correlation values throughout test two are generally consistent from each version of SPI and in each season, ranging around 0.30 to 0.45 (Table 5.3). The proportion of variance is lower than those found in test one since temperatures are not included in this test, and generally range around 4% to 12%. The correlations between the SPI values from the basins range near 0.27 to 0.42. The canonical correlations and proportion of variance is always the strongest in the SPI24 roots compared to the other SPI roots for all seasons, possibly due to an increased influence of multiple seasons of AMO and PDO which experience longer frequencies.

The SPI value with the highest amount of variance, SPI3, contains a relationship with SOI in every significant season (all except SON) (Figure 5.5). The first root for DJF and MAM largely represents the Apalachicola station. In the Apalachicola canonical roots, SOI 1 appears dominant in DJF while SOI 1 and 2 appear in MAM. In every case where the SOI value appears in the same season being studied (i.e. SOI 1 during DJF), the relationships are consistent with previous research (Ropelewski and Halpert 1986; Gershunov and Barnett 1997; Green et al. 1997). In DJF and MAM, SOI 1 and 2 have an indirect relationship with precipitation. In JJA, the Upper Chattahoochee region makes up the majority of the loading, and SOI 3 appears with a direct relationship to precipitation, also consistent with research.

The PDO appears in two of the three seasons of the SPI3 results with roots from the Upper Chattahoochee region only. In MAM and JJA, PDO 2 and PDO 3 have an indirect relationship with SPI3, respectively. These results are consistent with studied summertime effects of PDO on precipitation in the southeast. The SOI and PDO have been known to have intra-annual variability, thus explaining why they are included in the SPI3 results.

The next SPI value, SPI6, has significant climate contributors only during MAM and JJA (Figure 5.6). In each case, Apalachicola shows a relationship with SOI as does the Upper Chattahoochee with PDO. In MAM and JJA, the Apalachicola SPI6 has an indirect relationship with SOI 1 and SOI 2, consistent with winter time SOI affects. The Upper Chattahoochee has an indirect relationship with PDO during MAM and JJA, consistent with summertime affects.

TABLE 5.3: Summary of the results similar to Table 5.1 except for test two results. Blank boxes indicate no significant roots found.

	DJF				MAM				JJA				SON			
	Dominant Surface	Dominant Climate	Relationship	Consistent with Research	Dominant Surface	Dominant Climate	Relationship	Consistent with Research	Dominant Surface	Dominant Climate	Relationship	Consistent with Research	Dominant Surface	Dominant Climate	Relationship	Consistent with Research
SPI3 rt.1	Apalachicola	SOI 1	indirect	yes	Apalachicola	SOI 1 SOI 2	indirect indirect	NS winter yes	Up. Chatt.	SOI 3 PDO 3	direct indirect	yes yes	failed sig.			
SPI3 rt.2	Up. Chat.	NAO 4	indirect	NS	Up. Chatt.	PDO 2	indirect	summer yes								
SPI6 rt.1	Up. Chat.	none			Apalachicola Up. Chatt.	SOI 1 SOI 2	indirect indirect	NS winter yes	Up. Chatt.	PDO 2 PDO 3	indirect indirect	NS yes	Up. Chatt Apalachicola	none		
SPI6 rt.2					Up. Chatt.	PDO 2	indirect	summer yes	Apalachicola	SOI 1 SOI 2	indirect indirect	NS NS				
SPI12 rt.1	Up. Chat.	AMO 3 AMO 4 AMO 2	indirect indirect indirect	NS NS NS	Up. Chatt.	none			Up. Chatt.	SOI 3	direct	yes	Apalachicola Up. Chatt	SOI 1	indirect indirect	NS
SPI12 rt.2					Apalachicola	SOI 1	indirect	NS					Up. Chatt Apalachicola	none		
SPI24 rt.1	Up. Chat.	AMO 1 AMO 2 AMO 3 AMO 4	indirect	NS winter NS NS NS	Up. Chatt.	AMO 3 AMO 2 AMO 4 AMO 1 PDO 1	indirect indirect indirect indirect indirect	NS NS winter NS NS NS	Up. Chatt.	AMO 3 AMO 2 AMO 4 PDO 3 SOI 3 PDO 1 AMO 1 PDO 2	indirect indirect indirect indirect direct indirect indirect indirect	yes NS NS yes yes NS NS NS	Up. Chatt	AMO 4 AMO 3 AMO 2 PDO 3 SOI 3 PDO 1 PDO 2	indirect indirect indirect indirect direct indirect indirect	summer yes NS NS NS NS NS NS
SPI24 rt.2																

NS indicates "Not Sure". Either research does not define the relationship for this season, or it's a lagged relationship which was not previously researched for this project, but is presented.

TABLE 5.4: The strength of the CCA results similar to Table 5.2, except for test two results.

	DJF			MAM			JJA			SON		
	Canonical Correlation	Proportion of Variance	Correlation Between Basins	Canonical Correlation	Proportion of Variance	Correlation Between Basins	Canonical Correlation	Proportion of Variance	Correlation Between Basins	Canonical Correlation	Proportion of Variance	Correlation Between Basins
SPI3 rt. 1	0.403	0.072	0.336	0.424	0.084	0.342	0.359	0.064	0.430	Not Sig.	Not Sig.	0.401
SPI3 rt. 2	0.345	0.066		0.304	0.049		Not. Sig	Not. Sig		Not Sig.	Not Sig.	
SPI6 rt. 1	0.371	0.054	0.271	0.483	0.135	0.410	0.374	0.077	0.408	0.040	0.065	0.391
SPI6 rt. 2	Not Sig.			0.302	0.038		0.320	0.046		Not Sig.	Not Sig.	
SPI12 rt. 1	0.377	0.075	0.288	0.349	0.055	0.280	0.381	0.080	0.334	0.431	0.129	0.411
SPI12 rt. 2	Not Sig.			0.293	0.047		Not. Sig	Not. Sig		0.318	0.031	
SPI24 rt. 1	0.489	0.129	0.309	0.442	0.105	0.265	0.478	0.122	0.294	0.455	0.107	0.364
SPI24 rt. 2	Not Sig.			Not Sig.	Not Sig.		Not. Sig	Not. Sig		Not Sig.	Not Sig.	

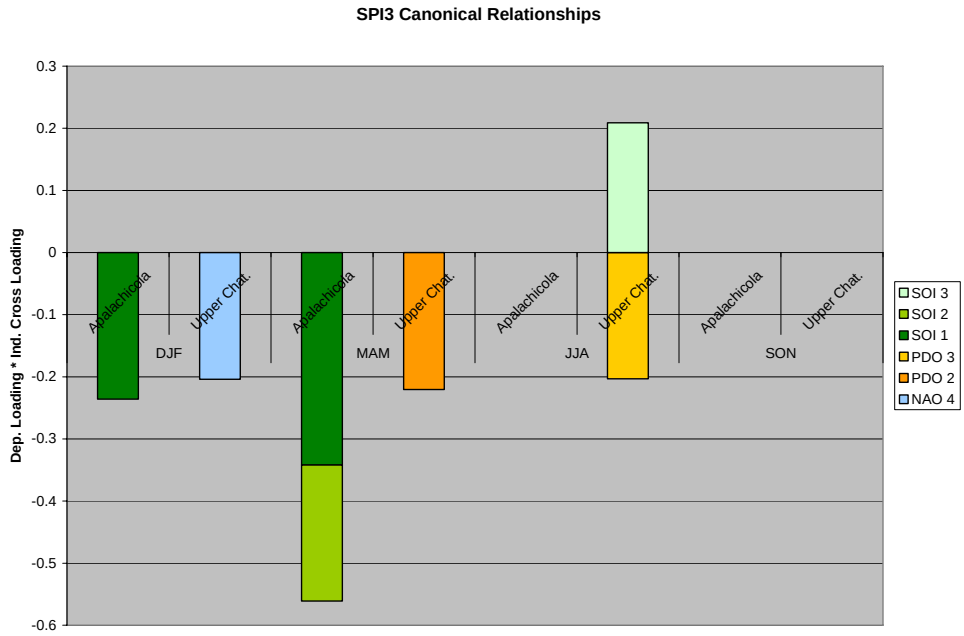

FIG. 5.5: SPI3 results for test two following the same methodology described above and in Figure 5.1, however broken down by season with the two sub-sections representing each of the sub-basins.

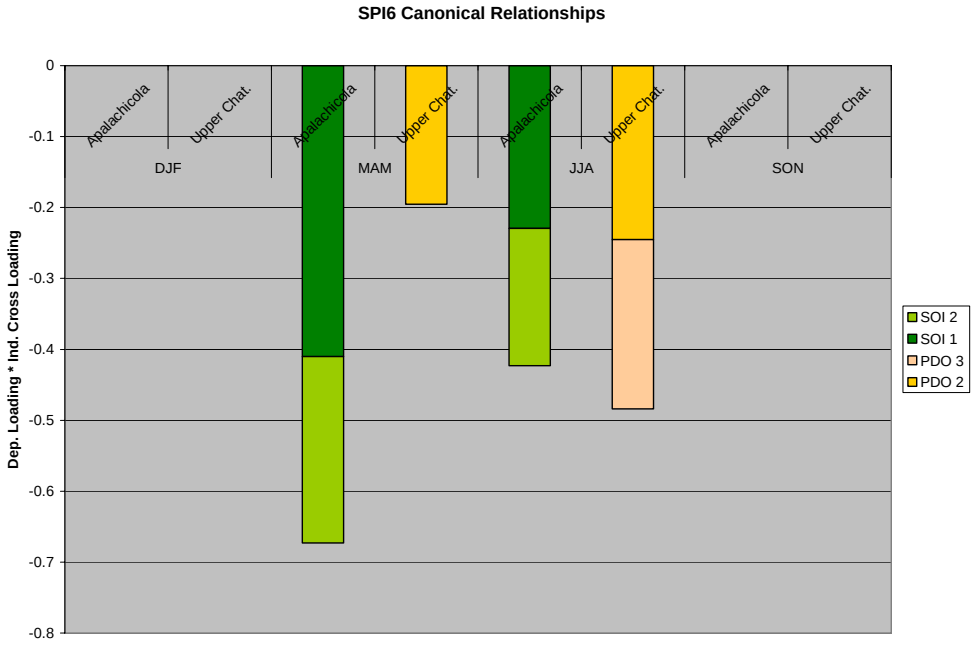

FIG. 5.6: Same as that of Figure 5.5, except for SPI6.

The twelve month SPI value contains AMO and SOI as the only climate contributors (Figure 5.7). The AMO of seasons 2, 3, and 4 appear in the DJF Upper Chattahoochee root, with an indirect relationship to precipitation. The MAM and SON seasons in the Apalachicola station show an indirect relationship to SOI 1. The Upper Chattahoochee shows a direct relationship with SOI 3 in JJA and an indirect relationship to SOI 1 in SON.

The SPI value in this study with the longest averaging time at 24 months only contains "significant" loadings from the Upper Chattahoochee in all four seasons (Figure 5.8). As mentioned before, the results from SPI24 contain the highest canonical correlation values and proportion of variance explained. The AMO of seasons 1 through 4 appears in every seasonal result for Upper Chattahoochee, except SON which has AMO of seasons 2, 3, and 4. The AMO is known to vary on a longer time scale, which could explain why its variance is only captured in the SPI24 results. In every case, the AMO has an indirect relationship to precipitation, which is consistent with research where the seasons are concurrent.

The PDO is the next most contributing climate oscillation in SPI24 results. The PDO of seasons 1 and 3 appear in JJA and SON with an indirect relationship to precipitation, consistent with previous research of summertime precipitation (Figure 5.8). The PDO 2 is also included in the SON results. We expect PDO 1 and 3 to be more dominant than 2 and 4, as 1 and 3 represent the winter and summer seasons respectively, when PDO variability is at its largest. The PDO frequency also operates on a longer time scale, similar to AMO, which could be why it appears in SPI24 results frequently.

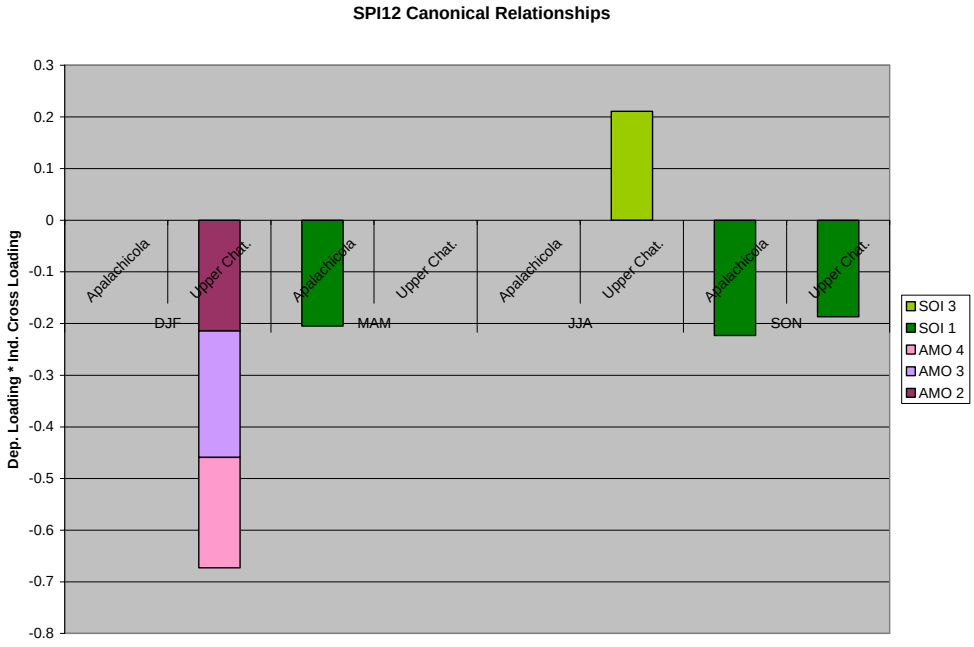

FIG. 5.7: Same as that of Figure 5.5, except for SPI12.

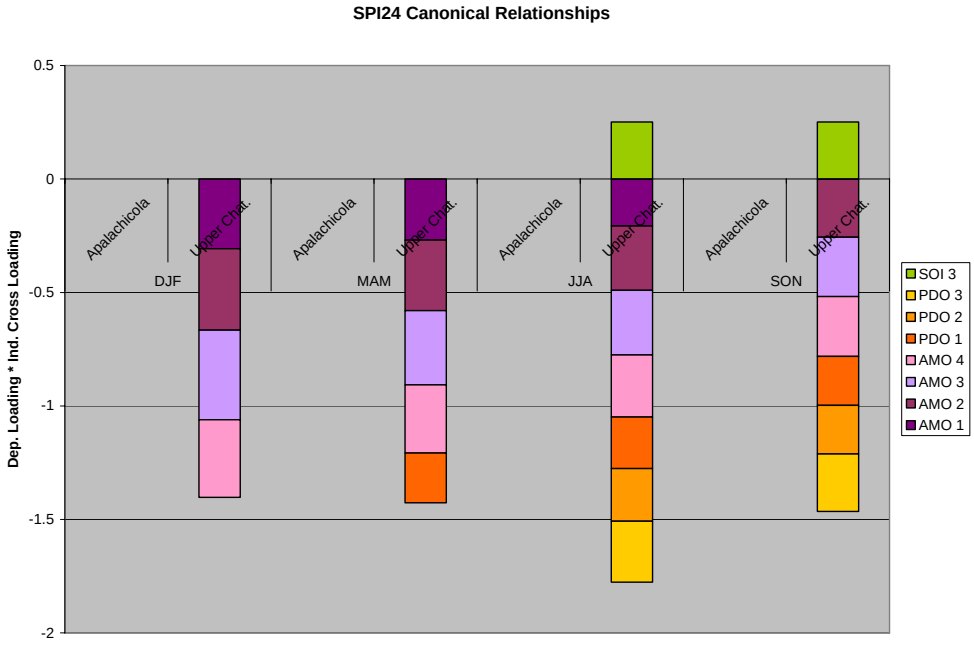

FIG. 5.8: Same as that of Figure 5.5, except for SPI24.

The summertime SOI (JJA) makes an appearance in the JJA and SON SPI24 results. In each case, it has a direct relationship with precipitation, consistent with summertime research results and results from other SPI values. The SOI operates on a 3 to 7 year time scale, which could explain why some of its variance is included in the SPI24 results.

The NAO hardly appears as a "significant" climate oscillation in test two results. We hypothesize from this finding that the NAO has a larger affect on temperatures and less to do with precipitation than the other climate oscillations, which is why it is commonly extracted in test one findings but not test two findings. Additional research would be needed for a more solid conclusion on this. The SOI appears most frequently in the Apalachicola roots (Figure 5.9), while the PDO and AMO occur in the Upper Chattahoochee roots (Figure 5.10). As seen in test one, the SOI of seasons 1 and 2 have an indirect relationship with precipitation in DJF and MAM. In JJA and SON the SOI of season 3 (SOI 3) reverses to a direct relationship in most cases. The PDO appears in every season except DJF, and has an indirect relationship with precipitation in every case. The climate index with the longest frequency, the AMO, appears only in SPI24 results, but in every season with an indirect relationship to precipitation.

From these results we can conclude the precipitation patterns in the southern section of the ACF are mostly associated to SOI of seasons 1 and 2, particularly in MAM, with an indirect relationship to precipitation. The upper section of the basin is largely influenced by the AMO and PDO throughout the year with an indirect relationship to precipitation. The Upper Chattahoochee precipitation also experiences a direct relationship with SOI of season 3 in JJA and SON. Climate influences of AMO and PDO are best seen in the longer SPI values of 12 and 24 months, while SOI appears in every SPI value used in this study, but particularly in the smaller time averaged values of SPI3 and SPI6.

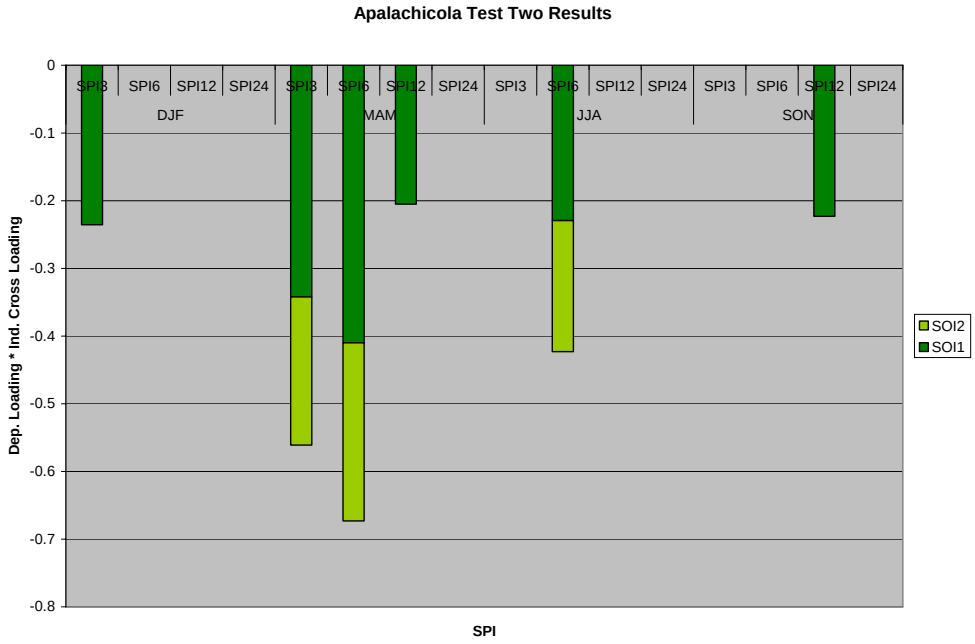

FIG. 5.9: Results from test two as described in Figure 5.5, except broken down by basin and including all four time intervals of SPI. This figure represents the Apalachicola (southernmost) sub-basin.

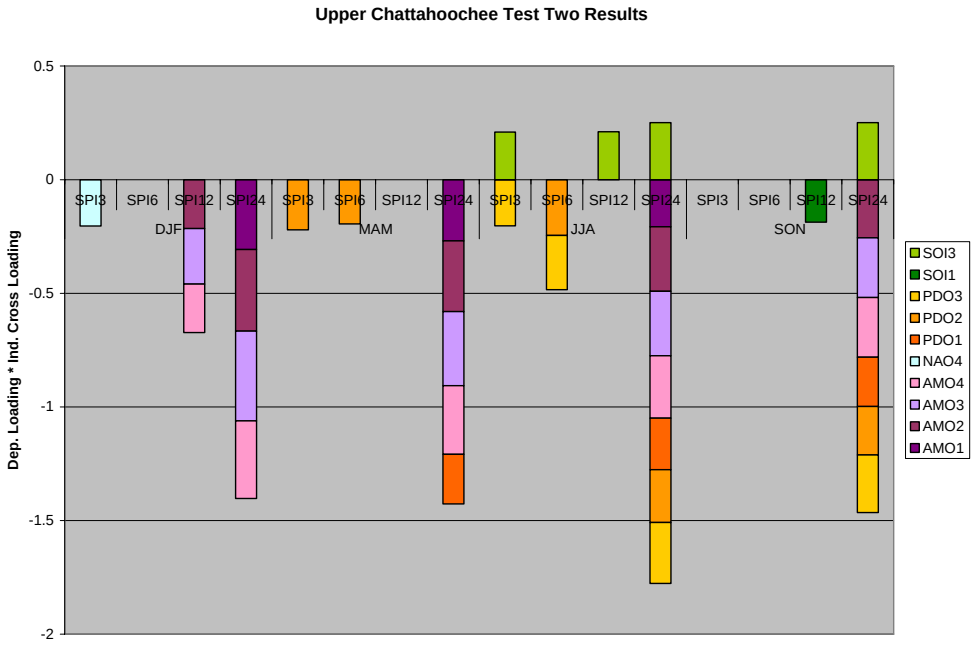

FIG. 5.10: Same as that described in Figure 5.9, except for the Upper Chattahoochee sub-basin.

CHAPTER SIX

SUMMARY AND CONCLUSIONS

The ongoing controversy surrounding water allocation disagreements in the Apalachicola-Chattahoochee-Flint River Basin provides motivation for a better understanding of the climatic circumstances that could lead to low flow scenarios in the ACF. The goal of this study is to investigate the relationships between surface meteorological variables to four influencing climate oscillations with ties to the southeast United States using canonical correlation analysis. Temperature and precipitation are two of several important variables to affect streamflow and evapotranspiration and represent the surface meteorological variables being used in this study. The climate oscillations investigated are the Atlantic Multidecadal Oscillation, North Atlantic Oscillation, Pacific Decadal Oscillation, and the Southern Oscillation Index, all having been previously researched and demonstrated to have some effects on the weather and climate of the southeastern United States.

The Parameter-elevation Regressions on Independent Slopes Model (PRISM) is employed to fill in gaps in the monthly maximum and minimum temperature and precipitation data for the time period of 1901-2000. The Standardized Precipitation Index (SPI) is calculated for three, six, twelve, and twenty-four month intervals from the precipitation data used in place of precipitation for the statistical analysis. We use the fast Fourier transform (FFT) to identify frequencies in the climatic oscillations for our data periods. The AMO and PDO generally operate on longer time scales, with the AMO around 60-85 years and PDO 20-30 and 50-70 years (Enfield et al. 2001; Mantua 1997). The NAO and SOI exhibit interannual and multidecadal variability (Hurrell et al. 2003; Gershunov et al. 1997).

Canonical correlation analysis (CCA) is utilized to develop a complex, multivariate approach to analyze the climate oscillation and surface climatology relationships in the basin. Canonical correlation analysis uses two sets of variables, dependent (surface climatological variables) and independent (climate oscillations), to create canonical variates for each set of data that maximize the correlations between the variates. Two tests are developed using CCA for the analysis. Test one examines the potential multidimensional aspects of drought by analyzing the relationships between SPI6 and maximum and minimum temperature to all four seasons of the

four climatic oscillations across the ACF basin. This test could ultimately be used to understand the interplay between temperature and precipitation variance on the manifestations of drought. Test two focuses purely on precipitation at various time scales by employing the four intervals of SPI in the northernmost and southernmost sub-basins as the dependent variable set, and the four seasons of the four climatic oscillations for the independent set. In both tests, only the statistically significant canonical roots with a p-value of less than 0.05 are examined. The canonical loadings and cross loadings are used to understand the relationships, while the canonical correlation values and proportion of variance explained in the dependent variables by the independent variate are used to examine the overall strength of each analysis. We apply analysis thresholds to simplify the interpretation of our results, although again, everything being examined is a statistically significant result.

Test one reveals the strongest canonical relationships occur in the winter seasons (DJF) when only the temperature variables contribute to the variate make up in all six sub-basins. The proportion of variance explained in the surface meteorological variables ranges from 14%-17% in DJF, around 8% in MAM, 4%-10% in JJA, and around 10% in SON. The temperature variables generally have the largest loadings and higher values of variance explained by the climate oscillations. Precipitation becomes more of a factor in the wetter spring and summer seasons throughout the basin when precipitation variance tends to peak (Figure 2.4).

The two climate oscillations closest to the basin's multivariates are the AMO and NAO, with the AMO consisting of sea surface temperature anomalies and the NAO measured by sea level pressure changes, both in the Northern Atlantic. The AMO of several seasons at a time generally appears in the results during DJF and JJA with a direct relationship to temperature and an indirect relationship to summer and fall precipitation in the northernmost sub-basin. This implies a positive phase of the AMO is associated with warmer temperatures particularly in winter and summer throughout the basin, and drier conditions in summer and fall in the northern section. The NAO appears consistently in the transition seasons of MAM and SON with a generally direct relationship to temperature and precipitation in MAM which reverses to an indirect relationship to temperature in SON. The NAO is the only climate oscillation in the North Atlantic that is generally prominent throughout the year, possibly explaining its appearance during the less dynamically active transition seasons of spring and fall.

Previous research (Gershunov and Barnett 1998; Rajagopalan et al. 2002) suggests an association between the PDO and SOI oscillations, both of which occur in sea level pressure patterns in the Pacific Ocean. Interestingly, the two oscillations do not appear simultaneously anywhere in our results for test one. The PDO appears in the temperature results in DJF with an indirect relationship, which reverses to a direct relationship in summer. The PDO also has an inverse relationship to precipitation in two northern sub-basins for DJF which is consistent with previous research (Barlow et al. 2002). The SOI only appears in the spring results with an indirect relationship to precipitation and temperature in two of the southern sub-basins, also consistent with research (Green et al. 1997).

Test two was designed to focus on precipitation by including only the four intervals of SPI in the dependent set of variables, again interpreting just the statistically sound canonical roots at the 95% significance level. Generally these tests have consistently similar results from season to season considering canonical correlation values and proportion of variance explained in the dependent set. However, in every case the least varying SPI24 has the largest of these values, indicating more robust results. We believe this is attributed to the influence of the longer frequencies in the climatic oscillations such as AMO and PDO, where several seasons of each oscillation generally appear at a time in the SPI24 results.

The variance in precipitation in the southern part of the basin is only attributed to seasons 1 and 2 of SOI. Throughout the year, SOI has an indirect relationship with SPI3, SPI6, and SPI12. This implies El Niño (negatively correlated with SOI) is associated with wetter conditions in the southern part of the basin. This is especially apparent in spring when three of the four SPI values exhibit this inverse relationship. It seems appropriate the beginning season of ENSO evolution (DJF) appears most frequently in our results.

The cross loadings in the results for the northern part of the basin have several climatic oscillations with the most prevalent ones being several seasons of AMO and PDO. The least varying SPI24 has AMO of just about every season in the results throughout the year with an indirect relationship to precipitation. The PDO also appears in SPI24 for MAM, JJA, and SON with an indirect relationship to precipitation. The only direct relationship to precipitation exists in summer and fall seasons through SOI 3. This relationship is also consistent with prior ENSO research (Green et al. 1997). Previous research on coupling between SOI and PDO suggests their relationships to surface precipitation patterns are manifested while the two are in opposite

phases (as SOI is negatively correlated with ENSO) during winter (Gershunov and Barnett 1998). The opposite relationships of SOI and PDO to the SPI values in our results may suggest (but cannot prove) that coupling enhancement is apparent in summer and fall precipitation patterns in the northern section of the basin.

In all of our results from tests one and two where the results for each season include an oscillation from that same season (i.e. JJA including SOI 3 in its results), our findings are consistent with previous research, however, this is the first time a test of this type has been developed for the smaller scale changes across the ACF basin only. Future work would include a more detailed literature investigation into time-lagged relationships to compare with our results. We could also examine results for different intervals of SPI, perhaps considering longer values that may capture more of the variance in the climate oscillations. There are other variables tied to evapotranspiration and drought that could be included in this study in future work, such as relative humidity, solar radiation, wind speed, and soil moisture. We could also try to use the canonical coefficients derived from our results to create a model for the surface meteorological variables in the ACF. A different statistical evaluation could be performed on the variables for a more informative look into the results of coupling effects on the basin perhaps using quantile regression.

Overall, our research was designed to provide a better understanding of the climate link to surface meteorological variables that may contribute to streamflow fluctuations in the ACF (Light et al. 2006). Our results give a comprehensive, statistically significant depiction of the relationships between all of the seasons of the climate oscillations and maximum and minimum temperature, as well as four intervals of SPI. This information could be interpreted in a way to aid water resource management practices in the fight over water rights in the Apalachicola-Chattahoochee-Flint River Basin.

APPENDIX A

CLIMATE OSCILLATION DATA

TABLE A.1: Summary of the climatic indices used for this study.

Name / Abbrev.	Region and Substance	Resource	Formula	Data Availability	Length of phases	Phase (2007)	Positive Phases	Negative Phases	Used by
Atlantic Multidecadal Oscillation AMO	North Atlantic Ocean SST	NOAA Earth System Research Lib. Physical Sciences Division	detrended time series of the area weighted averaged SSTA over AO from 0º – 70ºN latitude	1856-2005 monthly	60-85 years	Positive	1860-1880 1930-1960	1905-1925 1970-1990	Kerr (2000), Enfield et al. (2001) Kaplan SST, with global mean removed (Trenberth and Shea, 2005)
North Atlantic Oscillation NAO	Northern Atlantic MSLP dipole	Climatic Research Unit	$NAO = \overline{SLP_{Gilbraltar} - SLP_{Reykjavik}}$	1825-2000 monthly	Interannual multidecadal	Positive 2006/07 DJFM	1978-1995	1955-1978	Jones et al. 1997
Pacific Decadal Oscillation PDO	Northern Pacific SSTA	Nathan Mantua	leading principal component of SST variability in North Pacific poleward of 20º N latitude	1900-2004 monthly	20-30 years	Positive	1925-1946 1977-1998	1900-1924 1947-1976	Mantua (1997)
Southern Oscillation Index SOI	Equatorial Pacific SLP Diff.Darwin & Tahiti	Climatic Research Unit	$SOI = \overline{SLP_{Tahiti} - SLP_{Darwin}}$	1866-2005 monthly	Interannual 3-4 Years	Positive (late summer early fall)	1945-1949 1954-1956, 1970-197 *Cold ENSO Phases	1951,57,65,76, 82,86-87,91,98 *Warm ENSO Phases	Ropelewski and Jones (1987)

TABLE A.2: Pearson correlation coefficients for the four seasons of the four climatic indices. Highlighted numbers indicate a significant correlation at the 99.5% level (any correlation coefficient above 0.20 for 298 degrees of freedom). The blue numbers indicate correlations between different seasons of the same climatic oscillation, while the red for those significant correlations between different climatic oscillations. The number at the end of the climate oscillation label indicates the season of the climate oscillation, as described in Chapter 2.

	amos1	naos1	pdos1	sois1	amos2	naos2	pdos2	sois2	amos3	naos3	pdos3	sois3	amos4	naos4	pdos4	sois4
amos1	1.000	-0.122	-0.007	-0.030	0.785	-0.049	-0.037	0.058	0.636	-0.019	-0.118	0.131	0.662	0.040	-0.233	0.026
naos1	-0.122	1.000	-0.043	-0.012	-0.081	-0.029	0.015	-0.042	-0.009	0.143	-0.035	0.041	-0.015	-0.047	-0.033	0.094
pdos1	-0.007	-0.043	1.000	-0.297	0.121	-0.054	0.602	-0.146	0.137	0.032	0.381	-0.127	0.083	-0.036	0.223	-0.129
sois1	-0.030	-0.012	-0.297	1.000	-0.249	-0.118	-0.368	0.341	-0.166	0.004	-0.298	0.125	-0.100	-0.006	-0.159	0.059
amos2	0.785	-0.081	0.121	-0.249	1.000	-0.101	0.176	-0.126	0.781	-0.083	0.038	0.064	0.722	-0.017	-0.154	0.002
naos2	-0.049	-0.029	-0.054	-0.118	-0.101	1.000	-0.047	-0.090	-0.084	-0.061	-0.034	-0.086	-0.077	-0.043	-0.014	-0.125
pdos2	-0.037	0.015	0.602	-0.368	0.176	-0.047	1.000	-0.269	0.193	-0.010	0.589	-0.220	0.119	0.013	0.428	-0.159
sois2	0.058	-0.042	-0.146	0.341	-0.126	-0.090	-0.269	1.000	-0.112	0.039	-0.279	0.360	-0.111	0.120	-0.181	0.278
amos3	0.636	-0.009	0.137	-0.166	0.781	-0.084	0.193	-0.112	1.000	-0.151	0.086	0.086	0.808	-0.044	-0.117	0.060
naos3	-0.019	0.143	0.032	0.004	-0.083	-0.061	-0.010	0.039	-0.151	1.000	-0.029	-0.050	-0.115	-0.030	0.034	-0.044
pdos3	-0.118	-0.035	0.381	-0.298	0.038	-0.034	0.589	-0.279	0.086	-0.029	1.000	-0.308	0.057	-0.057	0.546	-0.259
sois3	0.131	0.041	-0.127	0.125	0.064	-0.086	-0.220	0.360	0.086	-0.050	-0.308	1.000	0.054	0.068	-0.341	0.554
amos4	0.662	-0.015	0.083	-0.100	0.722	-0.077	0.119	-0.111	0.808	-0.115	0.057	0.054	1.000	-0.110	-0.126	0.010
naos4	0.040	-0.047	-0.036	-0.006	-0.017	-0.043	0.013	0.120	-0.044	-0.030	-0.057	0.068	-0.110	1.000	0.011	0.148
pdos4	-0.233	-0.033	0.223	-0.159	-0.154	-0.014	0.428	-0.181	-0.117	0.034	0.546	-0.341	-0.126	0.011	1.000	-0.290
sois4	0.026	0.094	-0.129	0.059	0.002	-0.125	-0.159	0.278	0.060	-0.044	-0.259	0.554	0.010	0.148	-0.290	1.000

APPENDIX B

STATION STATISTICS

TABLE B.1: Temperature statistics for all of the stations representing a sub-basin.

					Maximum Temperature in°F							
					Climatology	Data Set	Extremes				Standard	Coeff. Of
St. ID	Location	State	CD	Month	1951-2000	1895-2004	Max	Year	Min	Year	Deviation	Variation
89566	Wewahitchka	FL	1	Jan	64.23	64.95	76.70	1974	54.81	1940	4.57	7.12
				Feb	67.56	67.38	77.83	1932	55.76	1895	3.99	5.91
				Mar	73.43	73.46	81.10	1945	66.80	1969	3.10	4.23
				Apr	80.18	79.82	85.96	1981	72.93	1901	2.52	3.14
				May	86.75	86.55	92.90	1962	82.36	1923	2.06	2.37
				Jun	90.74	90.60	96.90	1998	86.04	1903	2.18	2.41
				Jul	91.66	91.21	95.85	1932	87.80	1984	1.62	1.77
				Aug	91.48	91.12	96.03	1954	87.30	1994	1.75	1.91
				Sep	88.58	89.04	96.60	1925	85.10	2003	1.90	2.15
				Oct	81.27	81.34	89.47	1919	75.90	1964	2.32	2.85
				Nov	73.30	73.20	79.30	1909	66.70	1976	2.76	3.76
				Dec	66.57	66.24	75.31	1931	58.30	1989	3.50	5.26
90140	Albany	GA	7	Jan	60.32	60.83	73.50	1950	47.80	1940	4.71	7.82
				Feb	64.39	63.66	74.50	1962	51.78	1895	4.49	6.97
				Mar	71.32	71.18	81.40	1945	62.06	1926	3.47	4.86
				Apr	78.91	78.39	83.70	1967	71.13	1901	2.53	3.21
				May	85.85	85.92	95.50	1962	79.40	1976	2.72	3.16
				Jun	90.60	90.80	96.20	1952	84.70	1997	2.60	2.87
				Jul	92.52	91.78	97.10	1980	84.60	1975	2.61	2.82
				Aug	92.23	91.44	96.90	1954	85.28	1898	2.61	2.83
				Sep	88.32	88.13	97.18	1925	82.83	1901	2.67	3.02
				Oct	80.10	79.69	87.06	1919	73.10	1976	2.53	3.16
				Nov	70.95	70.10	77.00	2001	62.56	1976	3.22	4.53
				Dec	63.01	62.19	72.10	1931	53.00	1935	3.91	6.21
92475	Dahlonega	GA	2	Jan	49.09	50.21	60.49	1907	38.30	1977	4.15	8.46
				Feb	53.32	53.27	61.57	1976	42.15	1895	4.18	7.85
				Mar	60.66	60.75	71.10	1945	47.00	1960	4.03	6.65
				Apr	70.56	70.12	78.70	1942	62.56	1907	3.26	4.62
				May	77.62	77.72	86.40	1962	70.48	1895	2.94	3.78
				Jun	83.47	84.41	92.50	1952	75.42	1900	2.95	3.53
				Jul	86.53	86.69	95.30	1952	81.10	1967	2.81	3.25
				Aug	85.34	85.56	91.70	1951	80.30	1992	2.76	3.23
				Sep	79.56	81.03	93.34	1925	74.50	1967	2.86	3.60
				Oct	70.64	71.50	78.30	1897	64.50	1957	2.78	3.94
				Nov	60.95	61.44	68.52	1909	55.31	1976	3.58	5.88
				Dec	51.95	51.88	61.50	1984	43.11	2000	3.74	7.21

TABLE B.1 Continued

					Maximum Temperature in°F							
					Climatology	Data Set	Extremes				Standard	Coeff. Of
St. ID	Location	State	CD	Month	1951-2000	1895-2004	Max	Year	Min	Year	Deviation	Variation
93516	Fort Gaines	GA	7	Jan	60.28	61.00	74.10	1950	48.80	1940	4.30	7.14
				Feb	64.58	64.06	74.80	1962	51.64	1895	4.14	6.41
				Mar	71.63	71.56	80.90	1938	62.70	1947	3.46	4.82
				Apr	78.77	78.32	83.90	1981	70.34	1901	2.45	3.11
				May	85.26	85.35	91.60	1962	80.00	1976	2.40	2.81
				Jun	89.79	90.49	97.00	1952	83.84	1997	2.82	3.14
				Jul	91.21	91.05	96.98	1986	86.30	1975	2.46	2.70
				Aug	90.95	90.70	99.20	1954	86.00	1898	2.78	3.06
				Sep	86.91	87.29	97.41	1925	82.50	1967	2.44	2.81
				Oct	78.67	78.97	87.58	1919	71.53	1906	2.52	3.21
				Nov	69.46	69.55	78.10	1931	61.40	1976	3.07	4.42
				Dec	62.50	62.06	72.10	1933	54.10	2000	3.50	5.60
94949	La Grange 5 W	GA	4	Jan	55.68	56.16	68.70	1950	42.90	1977	4.50	8.08
				Feb	60.52	59.43	70.20	1976	45.63	1895	4.16	6.87
				Mar	68.44	68.13	78.80	1907	58.70	1960	3.74	5.47
				Apr	76.90	76.21	83.50	1977	69.17	1901	2.77	3.60
				May	83.17	83.46	90.70	1962	77.90	1976	2.67	3.21
				Jun	88.39	89.23	95.36	1931	81.80	1997	2.75	3.11
				Jul	90.48	90.50	96.58	1952	85.70	1994	2.48	2.74
				Aug	89.39	89.51	95.50	1954	83.68	1898	2.20	2.46
				Sep	84.21	85.17	97.25	1925	79.30	1924	2.42	2.88
				Oct	75.38	76.10	84.87	1919	69.28	1898	2.63	3.49
				Nov	66.30	65.81	74.46	2001	57.90	1947	2.98	4.50
				Dec	57.99	57.23	67.50	1956	48.97	1935	3.88	6.69
98661	Thomaston 2 S	GA	4	Jan	58.12	58.63	68.72	1950	46.09	1940	4.22	7.25
				Feb	63.00	62.10	72.60	1976	49.23	1895	3.84	6.10
				Mar	70.00	69.57	78.40	1997	59.80	1960	3.64	5.20
				Apr	78.12	77.39	84.10	1967	70.00	1901	2.85	3.65
				May	84.52	84.98	92.40	1962	79.40	1997	2.75	3.26
				Jun	89.92	90.49	96.55	1911	81.20	1997	3.00	3.34
				Jul	91.50	91.05	98.20	1980	85.10	1994	2.83	3.09
				Aug	91.11	90.74	96.55	1954	83.71	1898	2.66	2.92
				Sep	86.46	86.96	99.10	1925	81.19	1967	2.62	3.03
				Oct	78.42	78.62	86.11	1919	73.20	1988	2.58	3.29
				Nov	69.12	68.41	76.40	1978	61.23	1947	3.08	4.46
				Dec	60.51	59.74	70.30	1984	47.80	2000	4.19	6.93

TABLE B.2: Precipitation statistics calculated for the six representative sub-basins.

				Annual Precipitation (in)														
				Data Set	Climatology	Percentiles (in/year)									Standard	Coeff. Of	Extremes (in/year)			
St. ID	Location	State	CD	1895-2004	1951-2000	10th	20th	30th	40th	50th	60th	70th	80th	90th	Deviation	Variation	Max	Yr	Min	Yr
89566	Wewahitchka	FL	1	65.22	66.44	49.62	55.76	57.77	60.10	62.17	64.35	75.36	78.43	85.02	15.27	22.93	112.41	1966	41.26	2000
90140	Albany	GA	7	50.36	50.77	40.07	43.13	46.01	46.76	49.42	51.98	57.21	59.64	63.00	9.50	18.61	72.57	1994	31.73	1954
90219	Alpharetta 1 NW	GA	2	51.32	51.47	41.66	44.11	46.72	48.59	50.53	51.64	56.13	58.72	63.61	8.21	15.93	74.99	1929	34.73	1904
92475	Dahlonega	GA	2	63.94	63.40	49.98	53.42	57.29	60.70	63.86	68.16	70.03	72.52	76.06	9.88	15.53	93.71	1929	42.60	1904
93516	Fort Gaines	GA	7	53.12	52.04	38.69	44.72	48.53	50.43	52.10	53.85	56.34	60.03	65.03	9.44	18.08	88.95	1948	32.25	1954
94949	La Grange 5 W	GA	4	52.21	53.10	42.04	45.70	49.28	50.60	51.68	53.38	58.10	61.48	66.24	9.48	17.80	75.64	1929	28.99	1954
98661	Thomaston 2 S	GA	4	48.57	49.50	39.82	41.71	45.58	46.89	49.00	51.01	54.60	57.74	60.03	8.32	16.74	71.71	1929	28.78	1954

APPENDIX C

SENSITIVITY TEST RESULTS

TABLE C.1: Complete results from the sensitivity test comparing CCA results for two stations in the same climate division. For this test, stations 92475 and 90219 from the Upper Chattahoochee section are used for the season DJF. UC represents station 92475 and UC2 station 90219. The abbreviations s6mUCs1 indicates SPI6 of season 1 for station 92475, as similar to maxUCs1 and minUCs1 represent maximum and minimum temperature, respectively. Highlighted numbers are all the significant roots in the canonical results, values above 0.4 in the canonical loadings, and values above 0.2 in the canonical cross loadings, following the methodology described in Chapter 3.

Canononical Correlations and P-values

DJF

UC

	Can. Cor	R sq.	Wilk's	DF	Sig.
1	0.553	0.306	0.544	48.000	0.000
2	0.381	0.145	0.784	30.000	0.000
3	0.289	0.084	0.916	14.000	0.032

UC2

	Can. Cor	R sq.	Wilk's	DF	Sig.
1	0.547	0.299	0.578	48.000	0.000
2	0.336	0.113	0.825	30.000	0.003
3	0.265	0.070	0.930	14.000	0.099

Canonical Loadings for Dependent Data

DJF

UC

	1	2	3
s6mUCs1	0.219	-0.543	0.811
maxUCs1	0.793	-0.432	-0.430
minUCs1	0.994	0.053	-0.099

UC2

	1	2	3
s6mUC2s1	0.256	0.902	0.348
maxUC2s1	0.876	-0.349	0.334
minUC2s1	0.991	-0.051	-0.125

Cross Loadings for Dependent Data

DJF

UC

	1	2	3
s6mUCs1	0.121	-0.207	0.235
maxUCs1	0.439	-0.164	-0.124
minUCs1	0.550	0.020	-0.029

UC2

	1	2	3
s6mUC2s1	0.140	0.303	0.092
maxUC2s1	0.479	-0.117	0.089
minUC2s1	0.542	-0.017	-0.033

Table C.1 Continued

Canonical Loadings for Independent Data

DJF

UC

	1	2	3
amos1	0.417	0.528	0.113
naos1	0.516	-0.533	-0.238
pdos1	-0.505	0.009	-0.196
sois1	0.067	0.085	-0.362
amos2	0.211	0.433	0.113
naos2	0.021	0.101	-0.028
pdos2	-0.240	-0.271	-0.149
sois2	0.040	-0.072	-0.073
amos3	0.439	0.399	-0.031
naos3	0.120	-0.406	0.069
pdos3	-0.235	0.085	-0.033
sois3	0.065	-0.182	0.458
amos4	0.499	0.549	0.078
naos4	-0.056	-0.008	-0.542
pdos4	-0.113	-0.051	-0.109
sois4	0.104	-0.269	0.183

UC2

	1	2	3
amos1	0.134	-0.171	-0.107
naos1	0.715	0.074	0.011
pdos1	-0.438	0.062	-0.400
sois1	0.072	-0.587	-0.048
amos2	0.026	0.072	-0.088
naos2	0.104	0.024	-0.287
pdos2	-0.115	0.104	-0.216
sois2	0.006	-0.368	0.342
amos3	0.316	-0.074	-0.321
naos3	0.157	0.185	0.530
pdos3	-0.150	0.086	-0.379
sois3	0.067	0.048	0.142
amos4	0.281	-0.166	-0.230
naos4	-0.130	-0.603	0.349
pdos4	-0.044	0.132	-0.279
sois4	0.071	-0.169	0.268

Cross Loadings for Independent Data

DJF

UC

	1	2	3
amos1	0.231	0.201	0.033
naos1	0.285	-0.203	-0.069
pdos1	-0.279	0.003	-0.057
sois1	0.037	0.032	-0.105
amos2	0.117	0.165	0.033
naos2	0.011	0.039	-0.008
pdos2	-0.132	-0.103	-0.043
sois2	0.022	-0.027	-0.021
amos3	0.243	0.152	-0.009
naos3	0.066	-0.155	0.020
pdos3	-0.130	0.033	-0.010
sois3	0.036	-0.069	0.133
amos4	0.276	0.209	0.023
naos4	-0.031	-0.003	-0.157
pdos4	-0.063	-0.019	-0.032
sois4	0.057	-0.102	0.053

UC2

	1	2	3
amos1	0.073	-0.057	-0.028
naos1	0.391	0.025	0.003
pdos1	-0.240	0.021	-0.106
sois1	0.039	-0.197	-0.013
amos2	0.014	0.024	-0.023
naos2	0.057	0.008	-0.076
pdos2	-0.063	0.035	-0.057
sois2	0.003	-0.124	0.091
amos3	0.173	-0.025	-0.085
naos3	0.086	0.062	0.141
pdos3	-0.082	0.029	-0.101
sois3	0.036	0.016	0.038
amos4	0.154	-0.056	-0.061
naos4	-0.071	-0.202	0.092
pdos4	-0.024	0.044	-0.074
sois4	0.039	-0.057	0.071

Proportion of Variance in Dependent Set Explained by Opp. Can. Var.

DJF

UC

CV2-1	0.170
CV2-2	0.023
CV2-3	0.024

UC2

CV2-1	0.181
CV2-2	0.035
CV2-3	0.006

TABLE C.2: Results from the second sensitivity test investigating the different CCA results for SPI3, SPI6, SPI12, and SPI24.

Correlations for SPIs and Precip

DJF

SPI 6

	s6mUCs1	maxUCs1	minUCs1
s6mUCs1	1.000	0.059	0.108
maxUCs1	0.059	1.000	0.808
minUCs1	0.108	0.808	1.000

SPI 3

	s3mUCs1	maxUCs1	minUCs1
s3mUCs1	1.000	0.037	0.147
maxUCs1	0.037	1.000	0.808
minUCs1	0.147	0.808	1.000

SPI 12

	s12mUCs1	maxUCs1	minUCs1
s12mUCs1	1.000	0.058	0.025
maxUCs1	0.058	1.000	0.808
minUCs1	0.025	0.808	1.000

SPI 24

	s24mUCs1	maxUCs1	minUCs1
s24mUCs1	1.000	-0.009	-0.081
maxUCs1	-0.009	1.000	0.808
minUCs1	-0.081	0.808	1.000

Precip

	pUCs1	maxUCs1	minUCs1
pUCs1	1.000	0.004	0.193
maxUCs1	0.004	1.000	0.808
minUCs1	0.193	0.808	1.000

Canononical Correlations and P-values

DJF

SPI 6

	Can. Cor	R sq.	Wilk's	DF	Sig.
1	0.553	0.306	0.544	48.000	0.000
2	0.381	0.145	0.784	30.000	0.000
3	0.289	0.084	0.916	14.000	0.032

SPI 3

	Can. Cor	R sq.	Wilk's	DF	Sig.
1	0.551	0.304	0.538	48.000	0.000
2	0.383	0.147	0.772	30.000	0.000
3	0.309	0.095	0.905	14.000	0.010

SPI 12

	Can. Cor	R sq.	Wilk's	DF	Sig.
1	0.553	0.306	0.525	48.000	0.000
2	0.410	0.168	0.757	30.000	0.000
3	0.301	0.091	0.909	14.000	0.017

SPI 24

	Can. Cor	R sq.	Wilk's	DF	Sig.
1	0.578	0.334	0.472	48.000	0.000
2	0.464	0.215	0.709	30.000	0.000
3	0.311	0.097	0.903	14.000	0.009

Precip

	Can. Cor	R sq.	Wilk's	DF	Sig.
1	0.557	0.310	0.562	48.000	0.000
2	0.379	0.144	0.815	30.000	0.001
3	0.219	0.048	0.952	14.000	0.436

Redundancy Analysis

Proportion of Variance in Dependent Set Explained by Opp. Can. Var.

DJF

	SPI 6	SPI 3	SPI 12	SPI 24	Precip
CV2-1	0.170	0.168	0.161	0.160	0.159
CV2-2	0.023	0.024	0.050	0.089	0.023
CV2-3	0.024	0.027	0.016	0.011	0.016

TABLE C.3: Results from the sensitivity test comparing the use of maximum and minimum temperature as opposed to temperature range in conjunction with SPI6.

Correlations

DJF

Max&Min

	s6mUCs1	maxUCs1	minUCs1
s6mUCs1	1.000	0.059	0.108
maxUCs1	0.059	1.000	0.808
minUCs1	0.108	0.808	1.000

T Range

	s6mUCs1	rUCs1
s6mUCs1	1.000	-0.092
rUCs1	-0.092	1.000

Canononical Correlations and P-values

DJF

Max&Min

	Can. Cor	R sq.	Wilk's	DF	Sig.
1	0.553	0.306	0.544	48.000	0.000
2	0.381	0.145	0.784	30.000	0.000
3	0.289	0.084	0.916	14.000	0.032

T Range

	Can. Cor	R sq.	Wilk's	DF	Sig.
1	0.408	0.166	0.740	32.000	0.000
2	0.335	0.112	0.888	15.000	0.003

Redundancy Analysis

Proportion of Variance in Dependent Set Explained by Opp. Can. Var.

DJF

	Max&Min	T Range
CV2-1	0.170	0.081
CV2-2	0.023	0.057
CV2-3	0.024	

APPENDIX D

CANONICAL CORRELATION ANALYSIS RESULTS

Test One: Canonical correlation analysis results from the comprehensive meteorology variables across the ACF with the climate indices.

Table D.1: The CCA results for the Apalachicola sub-basin, station 89566. The first section, "Correlations for Apalachicola" represents the correlations between the input data. The second section, "Canonical Correlations and P-Values" gives the canonical correlations for each root and their significance levels, with the blue highlighted numbers indicating significant roots. The next section, "Redundancy Analysis" contains the information concerning the proportion of variance explained by the variates in the original data. We are only concerned with the proportion of variance explained by the independent variate to the dependent variables, which values for the examined roots are highlighted. Next the canonical coefficients are presented yet not examined. The "Canonical Loadings" and "Canonical Cross Loadings" for both the dependent and independent sets are presented and examined. The loadings describe the make up of the variates, while the cross loadings describe how the data from the original variables and their respective opposite variates are correlated. As mentioned in Chapter 3 we apply our analysis threshold values of 0.4 for the loadings, and 0.2 for the cross loadings. The values that meet the thresholds are highlighted. An example analysis of the data is presented in Chapter 3.

Correlations for Apalachicola

DJF

	s6mFLs1	maxFLs1	minFLs1
s6mFLs1	1.000	-0.170	-0.065
maxFLs1	-0.170	1.000	0.846
minFLs1	-0.065	0.846	1.000

MAM

	s6mFLs2	maxFLs2	minFLs2
s6mFLs2	1.000	-0.090	0.022
maxFLs2	-0.090	1.000	0.900
minFLs2	0.022	0.900	1.000

JJA

	s6mFLs3	maxFLs3	minFLs3
s6mFLs3	1.000	-0.328	0.004
maxFLs3	-0.328	1.000	0.190
minFLs3	0.004	0.190	1.000

SON

	s6mFLs4	maxFLs4	minFLs4
s6mFLs4	1.000	-0.042	0.053
maxFLs4	-0.042	1.000	0.940
minFLs4	0.053	0.940	1.000

Canononical Correlations and P-values

DJF

	Can. Cor	R Sq.	Wilk's	DF	Sig.
1	0.507	0.257	0.584	48.000	0.000
2	0.406	0.165	0.787	30.000	0.000
3	0.240	0.058	0.943	14.000	0.251

MAM

	Can. Cor	R Sq.	Wilk's	DF	Sig.
1	0.492	0.242	0.596	48.000	0.000
2	0.397	0.158	0.786	30.000	0.000
3	0.259	0.067	0.933	14.000	0.130

JJA

	Can. Cor	R Sq.	Wilk's	DF	Sig.
1	0.406	0.165	0.670	48.000	0.000
2	0.338	0.114	0.802	30.000	0.000
3	0.308	0.095	0.905	14.000	0.011

SON

	Can. Cor	R Sq.	Wilk's	DF	Sig.
1	0.397	0.158	0.698	48.000	0.000
2	0.320	0.102	0.828	30.000	0.004
3	0.278	0.077	0.923	14.000	0.056

TABLE D.1 Continued: Aplachicola

Redundancy Analysis

Proportion of Variance in Dependent Set Explained by Own Can. Var.

DJF

CV1-1	0.623
CV1-2	0.062

MAM

CV1-1	0.347
CV1-2	0.472

JJA

CV1-1	0.256
CV1-2	0.330
CV1-3	0.414

SON

CV1-1	0.647
CV1-2	0.029

Proportion of Variance in Dependent Set Explained by Opp. Can. Var.

DJF

CV2-1	0.160
CV2-2	0.010

MAM

CV2-1	0.084
CV2-2	0.074

JJA

CV2-1	0.042
CV2-2	0.038
CV2-3	0.039

SON

CV2-1	0.102
CV2-2	0.003

Proportion of Variance in Independent Set Explained by Own Can. Var.

DJF

CV2-1	0.074
CV2-2	0.099

MAM

CV2-1	0.072
CV2-2	0.073

JJA

CV2-1	0.145
CV2-2	0.086
CV2-3	0.064

SON

CV2-1	0.043
CV2-2	0.142

Proportion of Variance in Independent Set Explained by Opp. Can. Var.

DJF

CV1-1	0.019
CV1-2	0.016

MAM

CV1-1	0.017
CV1-2	0.012

JJA

CV1-1	0.024
CV1-2	0.010
CV1-3	0.006

SON

CV1-1	0.007
CV1-2	0.014

Standardized Canonical Coefficients Dependent Data

DJF

	1	2
s6mFLs1	-0.091	0.034
maxFLs1	0.636	1.766
minFLs1	0.385	-1.849

MAM

	1	2
s6mFLs2	0.966	0.067
maxFLs2	0.099	-1.604
minFLs2	0.182	0.747

JJA

	1	2	3
s6mFLs3	-0.652	0.356	-0.758
maxFLs3	-0.997	-0.380	0.173
minFLs3	-0.018	0.874	0.527

SON

	1	2
s6mFLs4	-0.025	0.484
maxFLs4	-0.560	2.940
minFLs4	-0.454	-2.964

Standardized Canonical Coefficients for Independent Data

DJF

	1	2
amos1	0.396	-0.434
naos1	0.560	-0.264
pdos1	-0.560	0.057
sois1	0.107	0.671
amos2	-0.761	0.500
naos2	-0.017	-0.054
pdos2	0.169	-0.193
sois2	0.110	0.013
amos3	0.632	-0.418
naos3	0.142	-0.144
pdos3	-0.233	0.099
sois3	-0.113	-0.193
amos4	0.066	0.433
naos4	0.066	0.344
pdos4	0.118	-0.387
sois4	-0.079	0.264

MAM

	1	2
amos1	-0.072	0.265
naos1	-0.166	0.111
pdos1	-0.039	0.192
sois1	-0.733	-0.249
amos2	0.292	-0.378
naos2	0.075	0.125
pdos2	0.052	-0.354
sois2	-0.309	-0.141
amos3	0.124	-0.400
naos3	0.197	-0.565
pdos3	-0.386	0.679
sois3	-0.146	0.080
amos4	-0.526	0.152
naos4	-0.087	-0.326
pdos4	0.003	0.016
sois4	0.060	0.209

JJA

	1	2	3
amos1	0.152	0.228	-0.767
naos1	0.173	0.338	0.194
pdos1	0.378	0.099	0.072
sois1	0.416	-0.454	0.502
amos2	-0.249	-0.503	0.447
naos2	0.148	-0.189	-0.028
pdos2	-0.091	0.446	0.283
sois2	0.186	-0.245	0.448
amos3	-0.504	0.400	0.542
naos3	0.052	0.306	0.067
pdos3	0.132	-0.398	0.197
sois3	0.024	0.320	0.263
amos4	-0.058	-0.354	0.165
naos4	0.068	-0.075	0.142
pdos4	0.285	0.119	0.015
sois4	-0.012	-0.416	-0.293

SON

	1	2
amos1	-0.286	0.424
naos1	0.138	-0.051
pdos1	-0.356	-0.140
sois1	0.078	0.121
amos2	0.473	-0.088
naos2	-0.208	-0.280
pdos2	0.412	-0.304
sois2	0.005	0.059
amos3	0.674	0.026
naos3	0.583	-0.137
pdos3	-0.446	-0.139
sois3	-0.062	0.433
amos4	-0.845	-0.373
naos4	0.192	-0.104
pdos4	0.133	-0.204
sois4	-0.155	-0.382

TABLE D.1 Continued: Apalachicola

Canonical Loadings for Dependent Data

DJF

	1	2
s6mFLs1	-0.224	-0.146
maxFLs1	0.977	0.195
minFLs1	0.929	-0.357

MAM

	1	2
s6mFLs2	0.961	0.228
maxFLs2	0.176	-0.938
minFLs2	0.293	-0.696

JJA

	1	2	3
s6mFLs3	-0.325	0.484	-0.813
maxFLs3	-0.787	-0.331	0.521
minFLs3	-0.210	0.804	0.557

SON

	1	2
s6mFLs4	-0.025	0.201
maxFLs4	-0.987	0.132
minFLs4	-0.983	-0.174

Cross Loadings for Dependent Data

DJF

	1	2
s6mFLs1	-0.114	-0.059
maxFLs1	0.496	0.079
minFLs1	0.472	-0.145

MAM

	1	2
s6mFLs2	0.473	0.090
maxFLs2	0.087	-0.372
minFLs2	0.144	-0.276

JJA

	1	2	3
s6mFLs3	-0.132	0.163	-0.250
maxFLs3	-0.319	-0.112	0.161
minFLs3	-0.085	0.271	0.172

SON

	1	2
s6mFLs4	-0.010	0.064
maxFLs4	-0.392	0.042
minFLs4	-0.390	-0.056

Canonical Loadings for Independent Data

DJF

	1	2
amos1	0.160	0.079
naos1	0.597	-0.276
pdos1	-0.567	-0.278
sois1	0.343	0.674
amos2	-0.080	0.035
naos2	-0.019	-0.168
pdos2	-0.296	-0.436
sois2	0.196	0.293
amos3	0.191	-0.028
naos3	0.178	-0.219
pdos3	-0.334	-0.362
sois3	0.044	0.165
amos4	0.174	0.116
naos4	0.059	0.317
pdos4	-0.108	-0.496
sois4	0.072	0.318

MAM

	1	2
amos1	-0.074	-0.264
naos1	-0.107	0.036
pdos1	0.140	0.191
sois1	-0.790	-0.285
amos2	0.144	-0.271
naos2	0.208	0.209
pdos2	0.184	0.108
sois2	-0.494	-0.250
amos3	-0.032	-0.224
naos3	0.189	-0.506
pdos3	-0.032	0.542
sois3	-0.241	-0.063
amos4	-0.199	-0.122
naos4	-0.053	-0.330
pdos4	0.044	0.251
sois4	-0.099	0.006

JJA

	1	2	3
amos1	-0.510	-0.155	0.020
naos1	0.136	0.407	0.199
pdos1	0.164	0.397	0.249
sois1	0.445	-0.509	0.289
amos2	-0.734	-0.079	0.264
naos2	0.111	-0.095	-0.219
pdos2	-0.027	0.500	0.369
sois2	0.306	-0.369	0.322
amos3	-0.750	-0.007	0.472
naos3	0.194	0.391	-0.018
pdos3	0.108	0.139	0.268
sois3	-0.076	-0.061	0.187
amos4	-0.640	-0.150	0.354
naos4	0.091	-0.094	0.067
pdos4	0.362	0.266	0.118
sois4	-0.096	-0.292	-0.049

SON

	1	2
amos1	-0.062	0.266
naos1	0.235	-0.106
pdos1	-0.146	-0.497
sois1	0.015	0.476
amos2	0.090	-0.014
naos2	-0.253	-0.230
pdos2	0.132	-0.711
sois2	0.008	0.412
amos3	0.047	-0.104
naos3	0.583	-0.092
pdos3	-0.195	-0.621
sois3	-0.078	0.509
amos4	-0.259	-0.115
naos4	0.239	-0.042
pdos4	0.080	-0.550
sois4	-0.059	0.073

Cross Loadings for Independent Data

DJF

	1	2
amos1	0.081	0.032
naos1	0.303	-0.112
pdos1	-0.288	-0.113
sois1	0.174	0.274
amos2	-0.040	0.014
naos2	-0.010	-0.068
pdos2	-0.150	-0.177
sois2	0.099	0.119
amos3	0.097	-0.012
naos3	0.091	-0.089
pdos3	-0.169	-0.147
sois3	0.022	0.067
amos4	0.088	0.047
naos4	0.030	0.129
pdos4	-0.055	-0.201
sois4	0.037	0.129

MAM

	1	2
amos1	-0.036	-0.105
naos1	-0.053	0.014
pdos1	0.069	0.076
sois1	-0.388	-0.113
amos2	0.071	-0.108
naos2	0.102	0.083
pdos2	0.090	0.043
sois2	-0.243	-0.099
amos3	-0.016	-0.089
naos3	0.093	-0.201
pdos3	-0.016	0.215
sois3	-0.119	-0.025
amos4	-0.098	-0.048
naos4	-0.026	-0.131
pdos4	0.022	0.100
sois4	-0.049	0.002

JJA

	1	2	3
amos1	-0.207	-0.052	0.006
naos1	0.055	0.137	0.061
pdos1	0.067	0.134	0.077
sois1	0.181	-0.172	0.089
amos2	-0.298	-0.027	0.081
naos2	0.045	-0.032	-0.067
pdos2	-0.011	0.169	0.114
sois2	0.124	-0.124	0.099
amos3	-0.304	-0.002	0.145
naos3	0.079	0.132	-0.005
pdos3	0.044	0.047	0.083
sois3	-0.031	-0.021	0.058
amos4	-0.260	-0.051	0.109
naos4	0.037	-0.032	0.021
pdos4	0.147	0.090	0.036
sois4	-0.039	-0.099	-0.015

SON

	1	2
amos1	-0.024	0.085
naos1	0.093	-0.034
pdos1	-0.058	-0.159
sois1	0.006	0.152
amos2	0.036	-0.005
naos2	-0.100	-0.074
pdos2	0.052	-0.227
sois2	0.003	0.132
amos3	0.018	-0.033
naos3	0.231	-0.029
pdos3	-0.077	-0.198
sois3	-0.031	0.163
amos4	-0.103	-0.037
naos4	0.095	-0.013
pdos4	0.032	-0.176
sois4	-0.023	0.023

TABLE D.2: Canonical correlation analysis results as described in Table D.1, for the Lower Flint sub-basin.

Correlations for Lower Flint

DJF

	s6mLFs1	maxLFs1	minLFs1
s6mLFs1	1.000	-0.210	-0.071
maxLFs1	-0.210	1.000	0.797
minLFs1	-0.071	0.797	1.000

MAM

	s6mLFs2	maxLFs2	minLFs2
s6mLFs2	1.000	-0.107	-0.006
maxLFs2	-0.107	1.000	0.882
minLFs2	-0.006	0.882	1.000

JJA

	s6mLFs3	maxLFs3	minLFs3
s6mLFs3	1.000	-0.375	-0.110
maxLFs3	-0.375	1.000	0.405
minLFs3	-0.110	0.405	1.000

SON

	s6mLFs4	maxLFs4	minLFs4
s6mLFs4	1.000	-0.082	0.055
maxLFs4	-0.082	1.000	0.916
minLFs4	0.055	0.916	1.000

Canononical Correlations and P-values

DJF

	Can. Cor	R sq.	Wilk's	DF	Sig.
1	0.571	0.326	0.524	48.000	0.000
2	0.380	0.144	0.778	30.000	0.000
3	0.300	0.090	0.910	14.000	0.017

MAM

	Can. Cor	R sq.	Wilk's	DF	Sig.
1	0.446	0.199	0.661	48.000	0.000
2	0.372	0.138	0.825	30.000	0.003
3	0.204	0.042	0.958	14.000	0.580

JJA

	Can. Cor	R sq.	Wilk's	DF	Sig.
1	0.467	0.218	0.659	48.000	0.000
2	0.323	0.104	0.843	30.000	0.015
3	0.243	0.059	0.941	14.000	0.229

SON

	Can. Cor	R sq.	Wilk's	DF	Sig.
1	0.411	0.169	0.740	48.000	0.000
2	0.301	0.091	0.890	30.000	0.299
3	0.144	0.021	0.979	14.000	0.965

TABLE D.2 Continued: Lower Flint

Redundancy Analysis

Proportion of Variance in Dependent Set Explained by Own Can. Var.

DJF

CV1-1	0.530
CV1-2	0.165
CV1-3	0.305

MAM

CV1-1	0.270
CV1-2	0.568

JJA

CV1-1	0.501
CV1-2	0.178

SON

CV1-1	0.621

Proportion of Variance in Dependent Set Explained by Opp. Can. Var.

DJF

CV2-1	0.173
CV2-2	0.024
CV2-3	0.027

MAM

CV2-1	0.054
CV2-2	0.079

JJA

CV2-1	0.109
CV2-2	0.018

SON

CV2-1	0.105

Proportion of Variance in Independent Set Explained by Own Can. Var.

DJF

CV2-1	0.093
CV2-2	0.121
CV2-3	0.108

MAM

CV2-1	0.090
CV2-2	0.061

JJA

CV2-1	0.187
CV2-2	0.069

SON

CV2-1	0.045

Proportion of Variance in Independent Set Explained by Opp. Can. Var.

DJF

CV1-1	0.031
CV1-2	0.018
CV1-3	0.010

MAM

CV1-1	0.018
CV1-2	0.008

JJA

CV1-1	0.041
CV1-2	0.007

SON

CV1-1	0.008

Standardized Canonical Coefficients Dependent Data

DJF

	1	2	3
s6mLFs1	-0.040	0.028	1.036
maxLFs1	-0.100	-1.641	0.478
minLFs1	1.075	1.261	-0.267

MAM

	1	2
s6mLFs2	-0.946	0.343
maxLFs2	-1.161	-0.927
minLFs2	0.849	0.028

JJA

	1	2
s6mLFs3	-0.028	-0.787
maxLFs3	0.588	-0.949
minLFs3	0.595	0.658

SON

	1
s6mLFs4	0.059
maxLFs4	-0.064
minLFs4	-0.942

Standardized Canonical Coefficients for Independent Data

DJF

	1	2	3
amos1	0.638	0.591	-0.101
naos1	0.492	-0.190	0.460
pdos1	-0.461	0.535	-0.222
sois1	-0.042	-0.405	-0.360
amos2	-0.656	-0.250	0.147
naos2	0.030	0.077	-0.004
pdos2	0.089	-0.331	0.435
sois2	0.105	-0.054	-0.229
amos3	0.457	-0.115	0.273
naos3	0.143	-0.173	-0.152
pdos3	-0.188	0.007	-0.244
sois3	-0.099	0.148	-0.038
amos4	0.298	0.329	-0.503
naos4	-0.031	-0.279	0.075
pdos4	0.133	0.227	0.175
sois4	-0.087	-0.202	-0.343

MAM

	1	2
amos1	0.212	0.358
naos1	0.207	0.150
pdos1	0.104	0.221
sois1	0.663	-0.378
amos2	-0.163	-0.448
naos2	0.154	-0.029
pdos2	-0.197	-0.449
sois2	0.192	-0.138
amos3	-0.311	-0.338
naos3	-0.297	-0.628
pdos3	0.289	0.584
sois3	0.232	-0.033
amos4	0.610	0.150
naos4	0.094	-0.345
pdos4	-0.066	-0.007
sois4	-0.041	0.249

JJA

	1	2
amos1	0.105	-0.193
naos1	0.026	0.445
pdos1	-0.102	0.115
sois1	-0.010	0.618
amos2	0.013	0.169
naos2	-0.138	0.117
pdos2	0.288	0.296
sois2	0.104	0.220
amos3	0.486	-0.354
naos3	0.083	0.096
pdos3	0.171	-0.307
sois3	0.107	0.512
amos4	0.348	0.414
naos4	0.039	0.029
pdos4	-0.108	0.126
sois4	-0.152	-0.385

SON

	1
amos1	-0.326
naos1	0.085
pdos1	-0.372
sois1	-0.003
amos2	0.544
naos2	-0.229
pdos2	0.386
sois2	0.032
amos3	0.598
naos3	0.553
pdos3	-0.429
sois3	0.000
amos4	-0.950
naos4	0.142
pdos4	0.081
sois4	-0.183

TABLE D.2 Continued: Lower Flint

Canonical Loadings for Dependent Data

DJF

	1	2	3
s6mLFs1	-0.095	0.284	0.954
maxLFs1	0.765	-0.642	0.047
minLFs1	0.998	-0.049	0.040

MAM

	1	2
s6mLFs2	-0.827	0.442
maxLFs2	-0.311	-0.939
minLFs2	-0.169	-0.791

JJA

	1	2
s6mLFs3	-0.314	-0.503
maxLFs3	0.840	-0.387
minLFs3	0.836	0.360

SON

	1
s6mLFs4	0.012
maxLFs4	-0.932
minLFs4	-0.997

Cross Loadings for Dependent Data

DJF

	1	2	3
s6mLFs1	-0.054	0.108	0.287
maxLFs1	0.437	-0.244	0.014
minLFs1	0.570	-0.019	0.012

MAM

	1	2
s6mLFs2	-0.369	0.165
maxLFs2	-0.139	-0.350
minLFs2	-0.075	-0.294

JJA

	1	2
s6mLFs3	-0.147	-0.162
maxLFs3	0.392	-0.125
minLFs3	0.390	0.116

SON

	1
s6mLFs4	0.005
maxLFs4	-0.383
minLFs4	-0.410

Canonical Loadings for Independent Data

DJF

	1	2	3
amos1	0.528	0.529	-0.238
naos1	0.487	-0.301	0.438
pdos1	-0.443	0.509	0.162
sois1	0.146	-0.466	-0.548
amos2	0.284	0.477	0.022
naos2	0.022	0.134	0.101
pdos2	-0.231	0.199	0.522
sois2	0.117	-0.225	-0.524
amos3	0.467	0.422	0.007
naos3	0.158	-0.181	-0.075
pdos3	-0.268	0.237	0.292
sois3	0.042	-0.064	-0.383
amos4	0.524	0.524	-0.186
naos4	-0.053	-0.317	0.045
pdos4	-0.139	0.161	0.403
sois4	0.018	-0.293	-0.406

MAM

	1	2
amos1	0.276	-0.175
naos1	0.111	0.067
pdos1	-0.211	0.172
sois1	0.724	-0.344
amos2	0.016	-0.192
naos2	0.033	0.082
pdos2	-0.357	0.034
sois2	0.437	-0.254
amos3	0.110	-0.143
naos3	-0.298	-0.552
pdos3	-0.169	0.450
sois3	0.365	-0.084
amos4	0.325	-0.047
naos4	0.049	-0.338
pdos4	-0.260	0.170
sois4	0.162	0.048

JJA

	1	2
amos1	0.669	-0.024
naos1	0.008	0.435
pdos1	0.210	-0.041
sois1	-0.185	0.625
amos2	0.787	-0.130
naos2	-0.230	-0.012
pdos2	0.397	-0.081
sois2	-0.063	0.413
amos3	0.899	-0.113
naos3	-0.032	0.163
pdos3	0.272	-0.325
sois3	0.079	0.409
amos4	0.858	0.043
naos4	-0.021	-0.021
pdos4	-0.047	-0.094
sois4	-0.053	-0.018

SON

	1
amos1	-0.134
naos1	0.183
pdos1	-0.172
sois1	-0.023
amos2	0.028
naos2	-0.252
pdos2	0.085
sois2	0.043
amos3	-0.060
naos3	0.563
pdos3	-0.221
sois3	-0.026
amos4	-0.377
naos4	0.208
pdos4	0.039
sois4	-0.047

Cross Loadings for Independent Data

DJF

	1	2	3
amos1	0.302	0.201	-0.071
naos1	0.278	-0.115	0.132
pdos1	-0.253	0.194	0.049
sois1	0.084	-0.177	-0.164
amos2	0.162	0.181	0.007
naos2	0.013	0.051	0.030
pdos2	-0.132	0.076	0.157
sois2	0.067	-0.085	-0.157
amos3	0.267	0.161	0.002
naos3	0.090	-0.069	-0.022
pdos3	-0.153	0.090	0.088
sois3	0.024	-0.024	-0.115
amos4	0.299	0.199	-0.056
naos4	-0.030	-0.121	0.014
pdos4	-0.079	0.061	0.121
sois4	0.010	-0.112	-0.122

MAM

	1	2
amos1	0.123	-0.065
naos1	0.050	0.025
pdos1	-0.094	0.064
sois1	0.323	-0.128
amos2	0.007	-0.072
naos2	0.015	0.030
pdos2	-0.159	0.013
sois2	0.195	-0.095
amos3	0.049	-0.053
naos3	-0.133	-0.206
pdos3	-0.075	0.167
sois3	0.163	-0.031
amos4	0.145	-0.017
naos4	0.022	-0.126
pdos4	-0.116	0.063
sois4	0.072	0.018

JJA

	1	2
amos1	0.312	-0.008
naos1	0.004	0.140
pdos1	0.098	-0.013
sois1	-0.086	0.202
amos2	0.367	-0.042
naos2	-0.107	-0.004
pdos2	0.185	-0.026
sois2	-0.030	0.133
amos3	0.420	-0.037
naos3	-0.015	0.053
pdos3	0.127	-0.105
sois3	0.037	0.132
amos4	0.400	0.014
naos4	-0.010	-0.007
pdos4	-0.022	-0.030
sois4	-0.025	-0.006

SON

	1
amos1	-0.055
naos1	0.075
pdos1	-0.071
sois1	-0.010
amos2	0.011
naos2	-0.103
pdos2	0.035
sois2	0.018
amos3	-0.025
naos3	0.231
pdos3	-0.091
sois3	-0.011
amos4	-0.155
naos4	0.085
pdos4	0.016
sois4	-0.019

TABLE D.3: Canonical correlation analysis results as described in Table D.1, for the Lower Chattahoochee sub-basin.

Correlations for LF

DJF

	s6mLCs1	maxLCs1	minLCs1
s6mLCs1	1.000	-0.112	0.008
maxLCs1	-0.112	1.000	0.818
minLCs1	0.008	0.818	1.000

MAM

	s6mLCs2	maxLCs2	minLCs2
s6mLCs2	1.000	-0.130	0.005
maxLCs2	-0.130	1.000	0.923
minLCs2	0.005	0.923	1.000

JJA

	s6mLCs3	maxLCs3	minLCs3
s6mLCs3	1.000	-0.452	0.051
maxLCs3	-0.452	1.000	0.244
minLCs3	0.051	0.244	1.000

SON

	s6mLCs4	maxLCs4	minLCs4
s6mLCs4	1.000	-0.095	0.012
maxLCs4	-0.095	1.000	0.924
minLCs4	0.012	0.924	1.000

Canononical Correlations and P-values

DJF

	Can. Cor	R sq	Wilk's	DF	Sig.
1	0.522	0.272	0.577	48.000	0.000
2	0.422	0.178	0.792	30.000	0.000
3	0.191	0.036	0.963	14.000	0.704

MAM

	Can. Cor	R sq	Wilk's	DF	Sig.
1	0.433	0.187	0.658	48.000	0.000
2	0.356	0.127	0.809	30.000	0.001
3	0.271	0.073	0.927	14.000	0.078

JJA

	Can. Cor	R sq	Wilk's	DF	Sig.
1	0.366	0.134	0.701	48.000	0.000
2	0.329	0.108	0.810	30.000	0.001
3	0.304	0.092	0.908	14.000	0.014

SON

	Can. Cor	R sq	Wilk's	DF	Sig.
1	0.412	0.170	0.689	48.000	0.000
2	0.362	0.131	0.830	30.000	0.005
3	0.212	0.045	0.955	14.000	0.503

TABLE D.3 Continued: Lower Chattahoochee

Redundancy Analysis

Proportion of Variance in Dependent Set Explained by Own Can. Var.

DJF

CV1-1	0.594
CV1-2	0.093

MAM

CV1-1	0.425
CV1-2	0.414

JJA

CV1-1	0.311
CV1-2	0.401
CV1-3	0.288

SON

CV1-1	0.563
CV1-2	0.205

Proportion of Variance in Dependent Set Explained by Opp. Can. Var.

DJF

CV2-1	0.162
CV2-2	0.017

MAM

CV2-1	0.080
CV2-2	0.052

JJA

CV2-1	0.042
CV2-2	0.043
CV2-3	0.027

SON

CV2-1	0.095
CV2-2	0.027

Proportion of Variance in Independent Set Explained by Own Can. Var.

DJF

CV2-1	0.070
CV2-2	0.094

MAM

CV2-1	0.057
CV2-2	0.056

JJA

CV2-1	0.134
CV2-2	0.057
CV2-3	0.076

SON

CV2-1	0.055
CV2-2	0.126

Proportion of Variance in Independent Set Explained by Opp. Can. Var.

DJF

CV1-1	0.019
CV1-2	0.017

MAM

CV1-1	0.011
CV1-2	0.007

JJA

CV1-1	0.018
CV1-2	0.006
CV1-3	0.007

SON

CV1-1	0.009
CV1-2	0.016

Standardized Canonical Coefficients Dependent Data

DJF

	1	2
s6mLCs1	0.147	0.092
maxLCs1	0.447	-1.656
minLCs1	0.596	1.570

MAM

	1	2
s6mLCs2	-0.818	-0.361
maxLCs2	-0.488	1.696
minLCs2	-0.181	-1.036

JJA

	1	2	3
s6mLCs3	-0.556	0.994	0.072
maxLCs3	-1.004	0.041	0.609
minLCs3	-0.240	-0.287	-0.981

SON

	1	2
s6mLCs4	0.244	-0.788
maxLCs4	1.361	-1.796
minLCs4	-0.400	2.123

Standardized Canonical Coefficients for Independent Data

DJF

	1	2
amos1	0.335	0.223
naos1	0.612	0.273
pdos1	-0.609	0.058
sois1	-0.007	-0.566
amos2	-0.616	-0.247
naos2	0.037	0.044
pdos2	0.189	-0.277
sois2	0.126	-0.297
amos3	0.645	0.232
naos3	0.180	-0.164
pdos3	-0.251	-0.009
sois3	-0.097	0.144
amos4	-0.078	-0.572
naos4	0.014	-0.450
pdos4	0.119	0.305
sois4	-0.121	-0.209

MAM

	1	2
amos1	0.138	-0.396
naos1	0.059	-0.155
pdos1	0.050	-0.085
sois1	0.598	0.535
amos2	-0.194	0.148
naos2	0.096	-0.009
pdos2	-0.032	0.675
sois2	0.176	0.212
amos3	-0.451	0.251
naos3	-0.555	0.411
pdos3	0.516	-0.609
sois3	0.139	0.070
amos4	0.635	0.237
naos4	0.001	0.378
pdos4	-0.145	-0.010
sois4	0.002	-0.191

JJA

	1	2	3
amos1	-0.070	0.690	-0.032
naos1	-0.075	-0.011	-0.274
pdos1	0.091	0.173	-0.029
sois1	0.287	-0.451	0.483
amos2	0.577	-0.557	0.090
naos2	0.184	-0.158	0.319
pdos2	-0.260	-0.354	-0.277
sois2	0.143	-0.445	-0.047
amos3	-0.835	0.404	-0.235
naos3	0.199	0.208	-0.249
pdos3	-0.140	-0.332	0.347
sois3	-0.265	-0.321	-0.378
amos4	-0.220	-0.518	0.546
naos4	-0.119	0.050	0.171
pdos4	0.277	-0.200	-0.208
sois4	0.198	0.462	0.637

SON

	1	2
amos1	0.488	-0.450
naos1	-0.031	-0.286
pdos1	0.384	-0.062
sois1	-0.019	-0.150
amos2	-0.677	0.395
naos2	0.188	0.103
pdos2	-0.420	0.092
sois2	-0.061	0.223
amos3	-0.372	-0.823
naos3	-0.519	-0.297
pdos3	0.464	0.171
sois3	0.180	-0.212
amos4	0.834	0.168
naos4	-0.090	-0.239
pdos4	-0.168	0.210
sois4	0.068	0.114

TABLE D.3 Continued: Lower Chattahoochee

Canonical Loadings for Dependent Data

DJF

	1	2
s6mLCs1	0.102	0.291
maxLCs1	0.918	-0.383
minLCs1	0.963	0.216

MAM

	1	2
s6mLCs2	-0.755	-0.587
maxLCs2	-0.549	0.787
minLCs2	-0.635	0.528

JJA

	1	2	3
s6mLCs3	-0.114	0.961	-0.253
maxLCs3	-0.811	-0.478	0.338
minLCs3	-0.512	-0.226	-0.829

SON

	1	2
s6mLCs4	0.110	-0.591
maxLCs4	0.968	0.240
minLCs4	0.860	0.455

Cross Loadings for Dependent Data

DJF

	1	2
s6mLCs1	0.053	0.123
maxLCs1	0.479	-0.162
minLCs1	0.502	0.091

MAM

	1	2
s6mLCs2	-0.327	-0.209
maxLCs2	-0.238	0.280
minLCs2	-0.275	0.188

JJA

	1	2	3
s6mLCs3	-0.042	0.316	-0.077
maxLCs3	-0.297	-0.157	0.103
minLCs3	-0.187	-0.074	-0.252

SON

	1	2
s6mLCs4	0.045	-0.214
maxLCs4	0.398	0.087
minLCs4	0.354	0.164

Canonical Loadings for Independent Data

DJF

	1	2
amos1	0.122	-0.299
naos1	0.653	0.257
pdos1	-0.571	0.125
sois1	0.218	-0.556
amos2	-0.064	-0.210
naos2	0.049	0.217
pdos2	-0.265	0.096
sois2	0.155	-0.477
amos3	0.166	-0.197
naos3	0.226	-0.064
pdos3	-0.319	0.249
sois3	0.022	-0.209
amos4	0.109	-0.326
naos4	0.013	-0.449
pdos4	-0.090	0.361
sois4	0.030	-0.320

MAM

	1	2
amos1	0.103	0.113
naos1	-0.054	-0.079
pdos1	-0.084	-0.005
sois1	0.583	0.477
amos2	-0.067	0.107
naos2	0.015	-0.150
pdos2	-0.107	0.138
sois2	0.293	0.342
amos3	0.030	0.178
naos3	-0.559	0.331
pdos3	0.151	-0.380
sois3	0.192	0.151
amos4	0.254	0.163
naos4	-0.036	0.363
pdos4	-0.092	-0.131
sois4	0.070	0.034

JJA

	1	2	3
amos1	-0.371	0.229	0.248
naos1	-0.087	0.045	-0.303
pdos1	-0.213	-0.078	-0.276
sois1	0.380	-0.283	0.424
amos2	-0.505	0.050	0.139
naos2	0.170	-0.060	0.211
pdos2	-0.384	-0.350	-0.341
sois2	0.268	-0.235	0.124
amos3	-0.803	0.043	0.189
naos3	0.316	0.235	-0.371
pdos3	-0.259	-0.447	-0.106
sois3	-0.166	0.014	0.044
amos4	-0.670	-0.094	0.342
naos4	-0.050	0.129	0.161
pdos4	0.129	-0.415	-0.317
sois4	-0.015	0.366	0.422

SON

	1	2
amos1	0.294	-0.606
naos1	-0.136	-0.307
pdos1	0.164	0.087
sois1	0.026	-0.167
amos2	0.087	-0.459
naos2	0.205	0.170
pdos2	-0.130	0.206
sois2	-0.010	-0.014
amos3	0.212	-0.627
naos3	-0.542	-0.243
pdos3	0.167	0.370
sois3	0.188	-0.342
amos4	0.472	-0.484
naos4	-0.158	-0.201
pdos4	-0.167	0.467
sois4	0.076	-0.184

Cross Loadings for Independent Data

DJF

	1	2
amos1	0.063	-0.126
naos1	0.341	0.109
pdos1	-0.298	0.053
sois1	0.114	-0.235
amos2	-0.033	-0.089
naos2	0.026	0.092
pdos2	-0.138	0.041
sois2	0.081	-0.201
amos3	0.087	-0.083
naos3	0.118	-0.027
pdos3	-0.166	0.105
sois3	0.011	-0.088
amos4	0.057	-0.137
naos4	0.007	-0.190
pdos4	-0.047	0.152
sois4	0.016	-0.135

MAM

	1	2
amos1	0.045	0.040
naos1	-0.023	-0.028
pdos1	-0.037	-0.002
sois1	0.252	0.170
amos2	-0.029	0.038
naos2	0.006	-0.053
pdos2	-0.046	0.049
sois2	0.127	0.121
amos3	0.013	0.063
naos3	-0.242	0.118
pdos3	0.065	-0.135
sois3	0.083	0.054
amos4	0.110	0.058
naos4	-0.016	0.129
pdos4	-0.040	-0.047
sois4	0.030	0.012

JJA

	1	2	3
amos1	-0.136	0.075	0.075
naos1	-0.032	0.015	-0.092
pdos1	-0.078	-0.026	-0.084
sois1	0.139	-0.093	0.129
amos2	-0.185	0.017	0.042
naos2	0.062	-0.020	0.064
pdos2	-0.140	-0.115	-0.103
sois2	0.098	-0.077	0.038
amos3	-0.294	0.014	0.057
naos3	0.116	0.077	-0.113
pdos3	-0.095	-0.147	-0.032
sois3	-0.061	0.004	0.013
amos4	-0.245	-0.031	0.104
naos4	-0.018	0.042	0.049
pdos4	0.047	-0.136	-0.096
sois4	-0.006	0.120	0.128

SON

	1	2
amos1	0.121	-0.219
naos1	-0.056	-0.111
pdos1	0.067	0.032
sois1	0.011	-0.060
amos2	0.036	-0.166
naos2	0.084	0.061
pdos2	-0.053	0.075
sois2	-0.004	-0.005
amos3	0.087	-0.227
naos3	-0.223	-0.088
pdos3	0.069	0.134
sois3	0.077	-0.124
amos4	0.194	-0.175
naos4	-0.065	-0.073
pdos4	-0.069	0.169
sois4	0.031	-0.066

TABLE D.4: Canonical correlation analysis results as described in Table D.1, for the Upper Flint sub-basin.

Correlations for Upper Flint

DJF

	s6mUFs1	maxUFs1	minUFs1
s6mUFs1	1.000	-0.067	0.041
maxUFs1	-0.067	1.000	0.768
minUFs1	0.041	0.768	1.000

MAM

	s6mUFs2	maxUFs2	minUFs2
s6mUFs2	1.000	-0.076	-0.035
maxUFs2	-0.076	1.000	0.928
minUFs2	-0.035	0.928	1.000

JJA

	s6mUFs3	maxUFs3	minUFs3
s6mUFs3	1.000	-0.334	-0.112
maxUFs3	-0.334	1.000	0.336
minUFs3	-0.112	0.336	1.000

SON

	s6mUFs4	maxUFs4	minUFs4
s6mUFs4	1.000	-0.078	0.030
maxUFs4	-0.078	1.000	0.934
minUFs4	0.030	0.934	1.000

Canononical Correlations and P-values

DJF

	Can. Cor	R sq	Wilk's	DF	Sig.
1	0.516	0.266	0.618	48.000	0.000
2	0.326	0.106	0.842	30.000	0.013
3	0.242	0.059	0.942	14.000	0.235

MAM

	Can. Cor	R sq	Wilk's	DF	Sig.
1	0.417	0.174	0.724	48.000	0.000
2	0.288	0.083	0.876	30.000	0.146
3	0.211	0.045	0.956	14.000	0.517

JJA

	Can. Cor	R sq	Wilk's	DF	Sig.
1	0.420	0.176	0.739	48.000	0.000
2	0.251	0.063	0.898	30.000	0.410
3	0.205	0.042	0.958	14.000	0.578

SON

	Can. Cor	R sq	Wilk's	DF	Sig.
1	0.399	0.159	0.713	48.000	0.000
2	0.327	0.107	0.848	30.000	0.021
3	0.225	0.051	0.950	14.000	0.381

TABLE D.4 Continued: Upper Flint

Redundancy Analysis

Proportion of Variance in Dependent Set Explained by Own Can. Var.

DJF		MAM		JJA		SON	
CV1-1	0.555	CV1-1	0.497	CV1-1	0.379	CV1-1	0.641
CV1-2	0.198					CV1-2	0.156

Proportion of Variance in Dependent Set Explained by Opp. Can. Var.

DJF		MAM		JJA		SON	
CV2-1	0.148	CV2-1	0.086	CV2-1	0.067	CV2-1	0.102
CV2-2	0.021					CV2-2	0.017

Proportion of Variance in Independent Set Explained by Own Can. Var.

DJF		MAM		JJA		SON	
CV2-1	0.059	CV2-1	0.046	CV2-1	0.095	CV2-1	0.043
CV2-2	0.098					CV2-2	0.088

Proportion of Variance in Independent Set Explained by Opp. Can. Var.

DJF		MAM		JJA		SON	
CV1-1	0.016	CV1-1	0.008	CV1-1	0.017	CV1-1	0.007
CV1-2	0.010					CV1-2	0.009

Standardized Canonical Coefficients Dependent Data

DJF

	1	2
s6mUFs1	0.184	0.380
maxUFs1	0.200	-1.355
minUFs1	0.817	1.050

MAM

	1
s6mUFs2	0.486
maxUFs2	1.320
minUFs2	-0.448

JJA

	1
s6mUFs3	0.378
maxUFs3	0.161
minUFs3	-0.945

SON

	1	2
s6mUFs4	0.092	0.895
maxUFs4	0.537	2.129
minUFs4	0.478	-2.175

Standardized Canonical Coefficients for Independent Data

DJF

	1	2
amos1	0.286	-0.027
naos1	0.673	0.153
pdos1	-0.580	0.369
sois1	-0.125	-0.437
amos2	-0.717	-0.007
naos2	0.038	0.102
pdos2	0.223	-0.368
sois2	0.026	-0.209
amos3	0.630	0.033
naos3	0.097	-0.280
pdos3	-0.252	0.048
sois3	0.041	0.331
amos4	0.019	0.169
naos4	-0.065	-0.469
pdos4	0.217	0.460
sois4	-0.077	-0.051

MAM

	1
amos1	-0.288
naos1	-0.203
pdos1	-0.071
sois1	-0.341
amos2	0.506
naos2	-0.021
pdos2	0.176
sois2	0.061
amos3	0.324
naos3	0.609
pdos3	-0.703
sois3	-0.073
amos4	-0.614
naos4	0.145
pdos4	0.204
sois4	-0.110

JJA

	1
amos1	0.284
naos1	-0.288
pdos1	0.157
sois1	0.026
amos2	0.138
naos2	0.217
pdos2	-0.740
sois2	-0.209
amos3	-0.522
naos3	-0.095
pdos3	-0.018
sois3	-0.316
amos4	-0.040
naos4	0.114
pdos4	0.040
sois4	0.538

SON

	1	2
amos1	0.297	0.660
naos1	-0.108	-0.166
pdos1	0.380	0.134
sois1	-0.041	-0.129
amos2	-0.545	-0.233
naos2	0.202	-0.082
pdos2	-0.410	-0.462
sois2	-0.074	-0.560
amos3	-0.593	0.049
naos3	-0.605	0.022
pdos3	0.491	-0.182
sois3	0.104	0.369
amos4	0.751	-0.505
naos4	-0.166	0.153
pdos4	-0.152	-0.259
sois4	0.131	-0.098

TABLE D.4 Continued: Upper Flint

Canonical Loadings for Dependent Data

DJF

	1	2
s6mUFs1	0.204	0.515
maxUFs1	0.815	-0.574
minUFs1	0.978	0.025

MAM

	1
s6mUFs2	0.402
maxUFs2	0.867
minUFs2	0.759

JJA

	1
s6mUFs3	0.431
maxUFs3	-0.283
minUFs3	-0.934

SON

	1	2
s6mUFs4	0.065	0.665
maxUFs4	0.976	0.027
minUFs4	0.983	-0.159

Cross Loadings for Dependent Data

DJF

	1	2
s6mUFs1	0.105	0.168
maxUFs1	0.421	-0.187
minUFs1	0.505	0.008

MAM

	1
s6mUFs2	0.167
maxUFs2	0.361
minUFs2	0.316

JJA

	1
s6mUFs3	0.181
maxUFs3	-0.119
minUFs3	-0.393

SON

	1	2
s6mUFs4	0.026	0.218
maxUFs4	0.390	0.009
minUFs4	0.392	-0.052

Canonical Loadings for Independent Data

DJF

	1	2
amos1	0.032	0.005
naos1	0.730	0.118
pdos1	-0.481	0.407
sois1	0.067	-0.563
amos2	-0.096	0.196
naos2	0.064	0.159
pdos2	-0.145	0.252
sois2	0.030	-0.411
amos3	0.179	0.251
naos3	0.145	-0.268
pdos3	-0.215	0.365
sois3	0.081	0.023
amos4	0.131	0.263
naos4	-0.072	-0.516
pdos4	0.017	0.382
sois4	0.075	-0.139

MAM

	1
amos1	-0.040
naos1	-0.111
pdos1	0.009
sois1	-0.306
amos2	0.093
naos2	-0.004
pdos2	0.033
sois2	0.013
amos3	-0.077
naos3	0.594
pdos3	-0.351
sois3	-0.075
amos4	-0.286
naos4	0.206
pdos4	0.037
sois4	-0.064

JJA

	1
amos1	0.043
naos1	-0.326
pdos1	-0.359
sois1	0.195
amos2	-0.185
naos2	0.247
pdos2	-0.712
sois2	0.073
amos3	-0.376
naos3	-0.088
pdos3	-0.440
sois3	0.026
amos4	-0.261
naos4	0.177
pdos4	-0.282
sois4	0.339

SON

	1	2
amos1	0.002	0.319
naos1	-0.204	-0.189
pdos1	0.173	-0.248
sois1	-0.004	0.038
amos2	-0.148	0.070
naos2	0.252	0.011
pdos2	-0.105	-0.580
sois2	-0.058	-0.144
amos3	-0.075	-0.070
naos3	-0.602	0.025
pdos3	0.237	-0.551
sois3	0.078	0.384
amos4	0.198	-0.135
naos4	-0.217	0.188
pdos4	-0.060	-0.553
sois4	0.044	0.154

Cross Loadings for Independent Data

DJF

	1	2
amos1	0.016	0.001
naos1	0.377	0.038
pdos1	-0.248	0.133
sois1	0.035	-0.183
amos2	-0.049	0.064
naos2	0.033	0.052
pdos2	-0.075	0.082
sois2	0.015	-0.134
amos3	0.093	0.082
naos3	0.075	-0.087
pdos3	-0.111	0.119
sois3	0.042	0.007
amos4	0.068	0.085
naos4	-0.037	-0.168
pdos4	0.009	0.124
sois4	0.039	-0.045

MAM

	1
amos1	-0.017
naos1	-0.046
pdos1	0.004
sois1	-0.128
amos2	0.039
naos2	-0.002
pdos2	0.014
sois2	0.005
amos3	-0.032
naos3	0.247
pdos3	-0.146
sois3	-0.031
amos4	-0.119
naos4	0.086
pdos4	0.015
sois4	-0.027

JJA

	1
amos1	0.018
naos1	-0.137
pdos1	-0.151
sois1	0.082
amos2	-0.078
naos2	0.104
pdos2	-0.299
sois2	0.031
amos3	-0.158
naos3	-0.037
pdos3	-0.185
sois3	0.011
amos4	-0.110
naos4	0.074
pdos4	-0.119
sois4	0.143

SON

	1	2
amos1	0.001	0.104
naos1	-0.081	-0.062
pdos1	0.069	-0.081
sois1	-0.001	0.012
amos2	-0.059	0.023
naos2	0.101	0.004
pdos2	-0.042	-0.190
sois2	-0.023	-0.047
amos3	-0.030	-0.023
naos3	-0.240	0.008
pdos3	0.095	-0.180
sois3	0.031	0.126
amos4	0.079	-0.044
naos4	-0.087	0.062
pdos4	-0.024	-0.181
sois4	0.017	0.050

TABLE D.5: Canonical correlation analysis results as described in Table D.1, for the Middle Chattahoochee sub-basin.

Station 94949

Correlations for LF

DJF

	s6mMCs1	maxMCs1	minMCs1
s6mMCs1	1.000	0.003	0.112
maxMCs1	0.003	1.000	0.801
minMCs1	0.112	0.801	1.000

MAM

	s6mMCs2	maxMCs2	minMCs2
s6mMCs2	1.000	-0.071	-0.003
maxMCs2	-0.071	1.000	0.924
minMCs2	-0.003	0.924	1.000

JJA

	s6mMCs3	maxMCs3	minMCs3
s6mMCs3	1.000	-0.342	-0.091
maxMCs3	-0.342	1.000	0.482
minMCs3	-0.091	0.482	1.000

SON

	s6mMCs4	maxMCs4	minMCs4
s6mMCs4	1.000	-0.071	0.022
maxMCs4	-0.071	1.000	0.930
minMCs4	0.022	0.930	1.000

Canononical Correlations and P-values

DJF

	Can. Cor	R sq.	Wilk's	DF	Sig.
1	0.528	0.279	0.581	48.000	0.000
2	0.352	0.124	0.805	30.000	0.000
3	0.285	0.081	0.919	14.000	0.040

MAM

	Can. Cor	R sq.	Wilk's	DF	Sig.
1	0.407	0.166	0.728	48.000	0.000
2	0.302	0.091	0.872	30.000	0.115
3	0.200	0.040	0.960	14.000	0.622

JJA

	Can. Cor	R sq.	Wilk's	DF	Sig.
1	0.422	0.178	0.706	48.000	0.000

SON

	Can. Cor	R sq.	Wilk's	DF	Sig.
1	0.439	0.193	0.683	48.000	0.000

TABLE D.5 Continued: Middle Chattahoochee

Redundancy Analysis

Proportion of Variance in Dependent Set Explained by Own Can. Var.

DJF

CV1-1	0.595
CV1-2	0.159
CV1-3	0.246

MAM

CV1-1	0.482

JJA

CV1-1	0.477
CV1-2	0.309

SON

CV1-1	0.541
CV1-2	0.247

Proportion of Variance in Dependent Set Explained by Opp. Can. Var.

DJF

CV2-1	0.166
CV2-2	0.020
CV2-3	0.020

MAM

CV2-1	0.080

JJA

CV2-1	0.085
CV2-2	0.025

SON

CV2-1	0.104
CV2-2	0.023

Proportion of Variance in Independent Set Explained by Own Can. Var.

DJF

CV2-1	0.064
CV2-2	0.118
CV2-3	0.039

MAM

CV2-1	0.054

JJA

CV2-1	0.115
CV2-2	0.069

SON

CV2-1	0.048
CV2-2	0.097

Proportion of Variance in Independent Set Explained by Opp. Can. Var.

DJF

CV1-1	0.018
CV1-2	0.015
CV1-3	0.003

MAM

CV1-1	0.009

JJA

CV1-1	0.020
CV1-2	0.005

SON

CV1-1	0.009
CV1-2	0.009

Standardized Canonical Coefficients Dependent Data

DJF

	1	2	3
s6mMCs1	-0.229	0.377	0.917
maxMCs1	-0.429	-1.446	0.761
minMCs1	-0.579	1.246	-1.002

MAM

	1
s6mMCs2	-0.543
maxMCs2	-1.347
minMCs2	0.508

JJA

	1	2
s6mMCs3	0.453	0.842
maxMCs3	-0.042	-0.135
minMCs3	-0.824	0.606

SON

	1	2
s6mMCs4	-0.392	-0.739
maxMCs4	-1.365	-1.685
minMCs4	0.447	2.125

Standardized Canonical Coefficients for Independent Data

DJF

	1	2	3
amos1	-0.372	0.108	0.040
naos1	-0.624	0.208	-0.174
pdos1	0.683	0.110	-0.636
sois1	0.059	-0.402	-0.500
amos2	0.581	-0.130	0.793
naos2	-0.032	0.142	-0.085
pdos2	-0.273	0.019	-0.030
sois2	-0.055	-0.105	0.282
amos3	-0.533	0.083	-0.665
naos3	-0.211	-0.115	0.252
pdos3	0.192	0.056	0.402
sois3	-0.004	0.266	-0.004
amos4	0.028	-0.077	-0.286
naos4	0.021	-0.562	-0.060
pdos4	-0.162	0.445	-0.081
sois4	0.072	-0.214	-0.031

MAM

	1
amos1	0.249
naos1	0.166
pdos1	0.100
sois1	0.283
amos2	-0.637
naos2	0.004
pdos2	-0.018
sois2	-0.049
amos3	-0.225
naos3	-0.667
pdos3	0.556
sois3	0.017
amos4	0.636
naos4	-0.122
pdos4	-0.081
sois4	0.037

JJA

	1	2
amos1	0.278	0.163
naos1	-0.257	0.181
pdos1	0.041	0.327
sois1	0.007	-0.494
amos2	0.042	-0.278
naos2	0.173	-0.066
pdos2	-0.732	-0.226
sois2	-0.191	-0.379
amos3	-0.262	0.327
naos3	0.004	0.346
pdos3	0.023	-0.113
sois3	-0.308	0.608
amos4	-0.192	-0.170
naos4	0.097	0.150
pdos4	-0.123	-0.275
sois4	0.483	-0.142

SON

	1	2
amos1	-0.442	-0.399
naos1	0.091	0.001
pdos1	-0.472	-0.050
sois1	0.062	0.122
amos2	0.517	0.043
naos2	-0.177	0.181
pdos2	0.569	0.382
sois2	0.166	0.422
amos3	0.462	-0.588
naos3	0.544	-0.223
pdos3	-0.483	0.079
sois3	-0.238	-0.448
amos4	-0.606	0.682
naos4	0.117	-0.211
pdos4	0.231	0.321
sois4	-0.108	0.158

TABLE D.5 Continued: Middle Chattahoochee

Canonical Loadings for Dependent Data

DJF

	1	2	3
s6mMCs1	-0.295	0.512	0.807
maxMCs1	-0.894	-0.447	-0.040
minMCs1	-0.948	0.129	-0.290

MAM

	1
s6mMCs2	-0.449
maxMCs2	-0.839
minMCs2	-0.735

JJA

	1	2
s6mMCs3	0.543	0.832
maxMCs3	-0.594	-0.130
minMCs3	-0.885	0.465

SON

	1	2
s6mMCs4	-0.286	-0.574
maxMCs4	-0.922	0.342
minMCs4	-0.831	0.542

Cross Loadings for Dependent Data

DJF

	1	2	3
s6mMCs1	-0.156	0.180	0.230
maxMCs1	-0.472	-0.157	-0.011
minMCs1	-0.500	0.045	-0.083

MAM

	1
s6mMCs2	-0.183
maxMCs2	-0.341
minMCs2	-0.299

JJA

	1	2
s6mMCs3	0.229	0.235
maxMCs3	-0.250	-0.037
minMCs3	-0.373	0.131

SON

	1	2
s6mMCs4	-0.125	-0.175
maxMCs4	-0.405	0.104
minMCs4	-0.365	0.165

Canonical Loadings for Independent Data

DJF

	1	2	3
amos1	-0.137	-0.121	0.075
naos1	-0.677	0.190	-0.185
pdos1	0.561	0.359	-0.404
sois1	-0.129	-0.537	-0.360
amos2	0.024	0.032	0.135
naos2	-0.038	0.220	-0.036
pdos2	0.176	0.431	-0.124
sois2	-0.082	-0.394	0.132
amos3	-0.176	0.076	-0.278
naos3	-0.254	-0.065	0.277
pdos3	0.234	0.483	0.134
sois3	-0.074	-0.155	-0.024
amos4	-0.139	0.052	-0.244
naos4	0.016	-0.589	0.024
pdos4	0.030	0.539	0.020
sois4	-0.072	-0.350	-0.044

MAM

	1
amos1	-0.041
naos1	0.072
pdos1	0.118
sois1	0.216
amos2	-0.135
naos2	0.010
pdos2	0.152
sois2	-0.085
amos3	0.084
naos3	-0.649
pdos3	0.436
sois3	-0.059
amos4	0.273
naos4	-0.187
pdos4	0.141
sois4	-0.057

JJA

	1	2
amos1	0.058	0.173
naos1	-0.266	0.257
pdos1	-0.467	0.227
sois1	0.227	-0.458
amos2	-0.182	0.190
naos2	0.211	-0.034
pdos2	-0.794	-0.048
sois2	0.110	-0.217
amos3	-0.321	0.212
naos3	-0.003	0.327
pdos3	-0.506	-0.203
sois3	0.070	0.496
amos4	-0.268	0.098
naos4	0.158	0.116
pdos4	-0.426	-0.383
sois4	0.359	0.218

SON

	1	2
amos1	-0.194	-0.433
naos1	0.195	-0.014
pdos1	-0.163	0.196
sois1	0.009	0.029
amos2	-0.007	-0.331
naos2	-0.217	0.160
pdos2	0.232	0.432
sois2	0.052	0.082
amos3	-0.058	-0.290
naos3	0.553	-0.177
pdos3	-0.107	0.452
sois3	-0.244	-0.487
amos4	-0.282	-0.068
naos4	0.166	-0.229
pdos4	0.243	0.585
sois4	-0.127	-0.217

Cross Loadings for Independent Data

DJF

	1	2	3
amos1	-0.072	-0.043	0.021
naos1	-0.357	0.067	-0.053
pdos1	0.296	0.126	-0.115
sois1	-0.068	-0.189	-0.103
amos2	0.013	0.011	0.039
naos2	-0.020	0.077	-0.010
pdos2	0.093	0.152	-0.035
sois2	-0.043	-0.139	0.038
amos3	-0.093	0.027	-0.079
naos3	-0.134	-0.023	0.079
pdos3	0.123	0.170	0.038
sois3	-0.039	-0.054	-0.007
amos4	-0.073	0.018	-0.069
naos4	0.009	-0.207	0.007
pdos4	0.016	0.190	0.006
sois4	-0.038	-0.123	-0.012

MAM

	1
amos1	-0.017
naos1	0.029
pdos1	0.048
sois1	0.088
amos2	-0.055
naos2	0.004
pdos2	0.062
sois2	-0.035
amos3	0.034
naos3	-0.264
pdos3	0.178
sois3	-0.024
amos4	0.111
naos4	-0.076
pdos4	0.058
sois4	-0.023

JJA

	1	2
amos1	0.024	0.049
naos1	-0.112	0.073
pdos1	-0.197	0.064
sois1	0.096	-0.130
amos2	-0.077	0.054
naos2	0.089	-0.010
pdos2	-0.335	-0.014
sois2	0.046	-0.061
amos3	-0.135	0.060
naos3	-0.001	0.092
pdos3	-0.213	-0.057
sois3	0.030	0.140
amos4	-0.113	0.028
naos4	0.067	0.033
pdos4	-0.180	-0.108
sois4	0.151	0.062

SON

	1	2
amos1	-0.085	-0.132
naos1	0.086	-0.004
pdos1	-0.071	0.060
sois1	0.004	0.009
amos2	-0.003	-0.101
naos2	-0.095	0.049
pdos2	0.102	0.132
sois2	0.023	0.025
amos3	-0.026	-0.088
naos3	0.243	-0.054
pdos3	-0.047	0.138
sois3	-0.107	-0.148
amos4	-0.124	-0.021
naos4	0.073	-0.070
pdos4	0.107	0.178
sois4	-0.056	-0.066

TABLE D.6: Canonical correlation analysis results as described in Table D.1, for the Upper Chattahoochee sub-basin.

Correlations for LF

DJF

	s6mUCs1	maxUCs1	minUCs1
s6mUCs1	1.000	0.059	0.108
maxUCs1	0.059	1.000	0.808
minUCs1	0.108	0.808	1.000

MAM

	s6mUCs2	maxUCs2	minUCs2
s6mUCs2	1.000	-0.096	-0.026
maxUCs2	-0.096	1.000	0.933
minUCs2	-0.026	0.933	1.000

JJA

	s6mUCs3	maxUCs3	minUCs3
s6mUCs3	1.000	-0.376	-0.060
maxUCs3	-0.376	1.000	0.543
minUCs3	-0.060	0.543	1.000

SON

	s6mUCs4	maxUCs4	minUCs4
s6mUCs4	1.000	-0.056	-0.004
maxUCs4	-0.056	1.000	0.908
minUCs4	-0.004	0.908	1.000

Canononical Correlations and P-values

DJF

	Can. Cor	R sq.	Wilk's	DF	Sig.
1	0.553	0.306	0.544	48.000	0.000
2	0.381	0.145	0.784	30.000	0.000
3	0.289	0.084	0.916	14.000	0.032

MAM

	Can. Cor	R sq.	Wilk's	DF	Sig.
1	0.406	0.165	0.716	48.000	0.000
2	0.302	0.091	0.858	30.000	0.044
3	0.237	0.056	0.944	14.000	0.272

JJA

	Can. Cor	R sq.	Wilk's	DF	Sig.
1	0.405	0.164	0.707	48.000	0.000
2	0.338	0.114	0.846	30.000	0.018
3	0.211	0.045	0.955	14.000	0.510

SON

	Can. Cor	R sq.	Wilk's	DF	Sig.
1	0.434	0.188	0.669	48.000	0.000
2	0.380	0.144	0.824	30.000	0.003
3	0.190	0.036	0.964	14.000	0.714

TABLE D.6 Continued: Upper Chattahoochee

Redundancy Analysis

Proportion of Variance in Dependent Set Explained by Own Can. Var.

DJF

CV1-1	0.555
CV1-2	0.161
CV1-3	0.284

MAM

CV1-1	0.486
CV1-2	0.435

JJA

CV1-1	0.529
CV1-2	0.322

SON

CV1-1	0.518
CV1-2	0.268

Proportion of Variance in Dependent Set Explained by Opp. Can. Var.

DJF

CV2-1	0.170
CV2-2	0.023
CV2-3	0.024

MAM

CV2-1	0.080
CV2-2	0.040

JJA

CV2-1	0.087
CV2-2	0.037

SON

CV2-1	0.098
CV2-2	0.039

Proportion of Variance in Independent Set Explained by Own Can. Var.

DJF

CV2-1	0.084
CV2-2	0.099
CV2-3	0.053

MAM

CV2-1	0.051
CV2-2	0.064

JJA

CV2-1	0.147
CV2-2	0.096

SON

CV2-1	0.064
CV2-2	0.068

Proportion of Variance in Independent Set Explained by Opp. Can. Var.

DJF

CV1-1	0.026
CV1-2	0.014
CV1-3	0.004

MAM

CV1-1	0.008
CV1-2	0.006

JJA

CV1-1	0.024
CV1-2	0.011

SON

CV1-1	0.012
CV1-2	0.010

Standardized Canonical Coefficients Dependent Data

DJF

	1	2	3
s6mUCs1	0.112	-0.596	0.804
maxUCs1	-0.018	-1.413	-0.941
minUCs1	0.996	1.259	0.574

MAM

	1	2
s6mUCs2	-0.648	0.745
maxUCs2	-0.948	-0.922
minUCs2	0.125	0.394

JJA

	1	2
s6mUCs3	0.603	0.811
maxUCs3	-0.204	0.199
minUCs3	-0.577	0.595

SON

	1	2
s6mUCs4	0.448	0.590
maxUCs4	0.398	1.878
minUCs4	-1.248	-1.320

Standardized Canonical Coefficients for Independent Data

DJF

	1	2	3
amos1	0.530	0.235	0.184
naos1	0.488	-0.390	-0.310
pdos1	-0.554	0.253	-0.303
sois1	-0.140	0.104	-0.537
amos2	-0.742	0.057	-0.006
naos2	0.011	0.088	-0.106
pdos2	0.068	-0.672	-0.063
sois2	0.027	-0.036	-0.135
amos3	0.485	-0.114	-0.381
naos3	0.119	-0.317	0.098
pdos3	-0.155	0.287	0.092
sois3	-0.081	-0.163	0.597
amos4	0.369	0.483	0.132
naos4	-0.032	0.079	-0.606
pdos4	0.150	0.045	0.044
sois4	0.013	-0.144	0.035

MAM

	1	2
amos1	-0.023	0.403
naos1	0.114	0.129
pdos1	0.266	-0.060
sois1	0.264	-0.485
amos2	-0.240	-0.190
naos2	0.084	-0.085
pdos2	-0.078	-0.709
sois2	0.123	-0.288
amos3	-0.736	-0.117
naos3	-0.651	-0.317
pdos3	0.573	0.215
sois3	0.012	0.055
amos4	0.810	-0.349
naos4	0.039	-0.433
pdos4	-0.115	-0.028
sois4	0.067	0.331

JJA

	1	2
amos1	0.331	0.348
naos1	-0.114	0.040
pdos1	0.091	-0.016
sois1	0.018	-0.385
amos2	-0.237	-0.383
naos2	0.112	-0.349
pdos2	-0.368	-0.282
sois2	-0.332	-0.188
amos3	-0.136	0.696
naos3	-0.025	0.286
pdos3	-0.149	-0.371
sois3	-0.026	0.526
amos4	-0.679	-0.260
naos4	-0.009	0.209
pdos4	-0.029	0.024
sois4	0.355	-0.309

SON

	1	2
amos1	-0.186	0.334
naos1	0.262	0.263
pdos1	-0.179	0.536
sois1	0.073	0.029
amos2	0.268	-0.579
naos2	-0.171	0.113
pdos2	0.344	-0.311
sois2	-0.242	-0.391
amos3	0.567	-0.105
naos3	0.406	-0.447
pdos3	-0.538	0.070
sois3	0.195	0.535
amos4	-1.019	-0.127
naos4	0.068	-0.137
pdos4	0.043	-0.209
sois4	-0.067	0.077

TABLE D.6 Continued: Upper Chattahoochee

Canonical Loadings for Dependent Data

DJF

	1	2	3
s6mUCs1	0.219	-0.543	0.811
maxUCs1	0.793	-0.432	-0.430
minUCs1	0.994	0.053	-0.099

MAM

	1	2
s6mUCs2	-0.560	0.824
maxUCs2	-0.770	-0.626
minUCs2	-0.743	-0.485

JJA

	1	2
s6mUCs3	0.714	0.700
maxUCs3	-0.744	0.218
minUCs3	-0.724	0.654

SON

	1	2
s6mUCs4	0.431	0.491
maxUCs4	-0.760	0.647
minUCs4	-0.889	0.382

Cross Loadings for Dependent Data

DJF

	1	2	3
s6mUCs1	0.121	-0.207	0.235
maxUCs1	0.439	-0.164	-0.124
minUCs1	0.550	0.020	-0.029

MAM

	1	2
s6mUCs2	-0.227	0.249
maxUCs2	-0.313	-0.189
minUCs2	-0.302	-0.147

JJA

	1	2
s6mUCs3	0.289	0.237
maxUCs3	-0.301	0.074
minUCs3	-0.294	0.221

SON

	1	2
s6mUCs4	0.187	0.187
maxUCs4	-0.330	0.246
minUCs4	-0.386	0.145

Canonical Loadings for Independent Data

DJF

	1	2	3
amos1	0.417	0.528	0.113
naos1	0.516	-0.533	-0.238
pdos1	-0.505	0.009	-0.196
sois1	0.067	0.085	-0.362
amos2	0.211	0.433	0.113
naos2	0.021	0.101	-0.028
pdos2	-0.240	-0.271	-0.149
sois2	0.040	-0.072	-0.073
amos3	0.439	0.399	-0.031
naos3	0.120	-0.406	0.069
pdos3	-0.235	0.085	-0.033
sois3	0.065	-0.182	0.458
amos4	0.499	0.549	0.078
naos4	-0.056	-0.008	-0.542
pdos4	-0.113	-0.051	-0.109
sois4	0.104	-0.269	0.183

MAM

	1	2
amos1	-0.185	-0.053
naos1	0.004	0.115
pdos1	0.211	-0.342
sois1	0.196	-0.238
amos2	-0.235	-0.143
naos2	0.063	0.051
pdos2	0.144	-0.549
sois2	0.067	-0.160
amos3	-0.164	-0.204
naos3	-0.611	-0.248
pdos3	0.417	-0.171
sois3	-0.033	0.192
amos4	0.110	-0.213
naos4	-0.025	-0.362
pdos4	0.136	-0.238
sois4	-0.017	0.298

JJA

	1	2
amos1	-0.360	0.444
naos1	-0.088	0.080
pdos1	-0.301	-0.164
sois1	0.208	-0.150
amos2	-0.593	0.334
naos2	0.192	-0.311
pdos2	-0.550	-0.334
sois2	0.029	0.047
amos3	-0.679	0.405
naos3	0.047	0.249
pdos3	-0.441	-0.465
sois3	0.145	0.508
amos4	-0.749	0.253
naos4	0.101	0.220
pdos4	-0.222	-0.353
sois4	0.311	0.158

SON

	1	2
amos1	-0.268	-0.209
naos1	0.373	0.233
pdos1	-0.134	0.176
sois1	0.056	0.082
amos2	-0.173	-0.363
naos2	-0.178	0.161
pdos2	-0.005	-0.220
sois2	-0.056	-0.081
amos3	-0.199	-0.253
naos3	0.456	-0.374
pdos3	-0.372	-0.177
sois3	0.174	0.496
amos4	-0.515	-0.247
naos4	0.141	-0.129
pdos4	-0.087	-0.310
sois4	0.131	0.299

Cross Loadings for Independent Data

DJF

	1	2	3
amos1	0.231	0.201	0.033
naos1	0.285	-0.203	-0.069
pdos1	-0.279	0.003	-0.057
sois1	0.037	0.032	-0.105
amos2	0.117	0.165	0.033
naos2	0.011	0.039	-0.008
pdos2	-0.132	-0.103	-0.043
sois2	0.022	-0.027	-0.021
amos3	0.243	0.152	-0.009
naos3	0.066	-0.155	0.020
pdos3	-0.130	0.033	-0.010
sois3	0.036	-0.069	0.133
amos4	0.276	0.209	0.023
naos4	-0.031	-0.003	-0.157
pdos4	-0.063	-0.019	-0.032
sois4	0.057	-0.102	0.053

MAM

	1	2
amos1	-0.075	-0.016
naos1	0.002	0.035
pdos1	0.086	-0.103
sois1	0.080	-0.072
amos2	-0.096	-0.043
naos2	0.026	0.016
pdos2	0.058	-0.166
sois2	0.027	-0.048
amos3	-0.067	-0.062
naos3	-0.248	-0.075
pdos3	0.169	-0.052
sois3	-0.014	0.058
amos4	0.045	-0.064
naos4	-0.010	-0.109
pdos4	0.055	-0.072
sois4	-0.007	0.090

JJA

	1	2
amos1	-0.146	0.150
naos1	-0.035	0.027
pdos1	-0.122	-0.055
sois1	0.084	-0.051
amos2	-0.240	0.113
naos2	0.078	-0.105
pdos2	-0.223	-0.113
sois2	0.012	0.016
amos3	-0.275	0.137
naos3	0.019	0.084
pdos3	-0.179	-0.157
sois3	0.059	0.172
amos4	-0.303	0.085
naos4	0.041	0.074
pdos4	-0.090	-0.119
sois4	0.126	0.053

SON

	1	2
amos1	-0.116	-0.080
naos1	0.162	0.089
pdos1	-0.058	0.067
sois1	0.024	0.031
amos2	-0.075	-0.138
naos2	-0.077	0.061
pdos2	-0.002	-0.084
sois2	-0.024	-0.031
amos3	-0.086	-0.096
naos3	0.198	-0.142
pdos3	-0.162	-0.068
sois3	0.076	0.189
amos4	-0.224	-0.094
naos4	0.061	-0.049
pdos4	-0.038	-0.118
sois4	0.057	0.114

Test Two Results: Various SPI values and climate oscillations for the northernmost and southernmost regions of the ACF.

TABLE D.7: Test two results from the canonical correlation analysis. Interpretation and description is the same from Table D.1, however there are only two dependent variables in this case with UC representing the Upper Chattahoochee and the FL representing the Apalachicola sub-basins. The data is broken up by the SPI value used, labeled SPI 3, SPI 6, SPI 12, and SPI 24. Each table represents results from a single season, with this first table for DJF. All significant canonical roots are examined in this case.

DJF

Correlations

SPI 3

	s3mFLs1	s3mUCs1
s3mFLs1	1.000	0.336
s3mUCs1	0.336	1.000

SPI 6

	s6mFLs1	s6mUCs1
s6mFLs1	1.000	0.271
s6mUCs1	0.271	1.000

SPI 12

	s12mFLs1	s12mUCs1
s12mFLs1	1.000	0.288
s12mUCs1	0.288	1.000

SPI 24

	s24mFLs1	s24mUCs1
s24mFLs1	1.000	0.309
s24mUCs1	0.309	1.000

Canononical Correlations and P-values

SPI 3

	Can. Cor	R sq.	Wilk's	DF	Sig.
1	0.403	0.162	0.738	32.000	0.000
2	0.345	0.119	0.881	15.000	0.001

SPI 6

	Can. Cor	R sq.	Wilk's	DF	Sig.
1	0.371	0.138	0.810	32.000	0.001
2	0.248	0.062	0.939	15.000	0.244

SPI 12

	Can. Cor	R sq.	Wilk's	DF	Sig.
1	0.377	0.142	0.806	32.000	0.001
2	0.247	0.061	0.939	15.000	0.252

SPI 24

	Can. Cor	R sq.	Wilk's	DF	Sig.
1	0.489	0.239	0.714	32.000	0.000
2	0.248	0.062	0.939	15.000	0.244

TABLE D.7 Continued: Test two DJF.

Redundancy Analysis

Proportion of Variance in Dependent Set Explained by Own Can. Var.

SPI 3		SPI 6		SPI 12		SPI 24	
CV1-1	0.445	CV1-1	0.390	CV1-1	0.525	CV1-1	0.541
CV1-2	0.555						

Proportion of Variance in Dependent Set Explained by Opp. Can. Var.

SPI 3		SPI 6		SPI 12		SPI 24	
CV2-1	0.072	CV2-1	0.054	CV2-1	0.075	CV2-1	0.129
CV2-2	0.066						

Proportion of Variance in Independent Set Explained by Own Can. Var.

SPI 3		SPI 6		SPI 12		SPI 24	
CV2-1	0.098	CV2-1	0.058	CV2-1	0.144	CV2-1	0.166
CV2-2	0.059						

Proportion of Variance in Independent Set Explained by Opp. Can. Var.

SPI 3		SPI 6		SPI 12		SPI 24	
CV1-1	0.016	CV1-1	0.008	CV1-1	0.020	CV1-1	0.040
CV1-2	0.007						

Standardized Canonical Coefficients Dependent Data

SPI 3			SPI 6		SPI 12		SPI 24	
	1	2		1		1		1
s3mFLs1	-1.062	-0.004	s6mFLs1	-0.596	s12mFLs1	0.060	s24mFLs1	0.023
s3mUCs1	0.353	1.001	s6mUCs1	0.980	s12mUCs1	-1.016	s24mUCs1	-1.007

Standardized Canonical Coefficients for Independent Data

SPI 3			SPI 6		SPI 12		SPI 24	
	1	2		1		1		1
amos1	0.353	0.230	amos1	0.324	amos1	0.243	amos1	0.288
naos1	0.373	0.232	naos1	0.153	naos1	-0.080	naos1	0.133
pdos1	-0.337	-0.348	pdos1	-0.573	pdos1	0.516	pdos1	0.364
sois1	0.476	-0.496	sois1	-0.287	sois1	0.024	sois1	-0.131
amos2	-0.542	-0.108	amos2	-0.777	amos2	-0.028	amos2	0.123
naos2	-0.211	-0.095	naos2	-0.313	naos2	0.109	naos2	0.064
pdos2	0.270	0.016	pdos2	0.499	pdos2	-0.231	pdos2	-0.374
sois2	0.175	-0.218	sois2	-0.142	sois2	-0.069	sois2	0.027
amos3	0.181	0.311	amos3	0.284	amos3	0.445	amos3	0.517
naos3	0.006	0.286	naos3	0.316	naos3	-0.211	naos3	-0.125
pdos3	0.063	-0.119	pdos3	-0.134	pdos3	0.096	pdos3	0.237
sois3	0.109	0.128	sois3	0.424	sois3	-0.535	sois3	-0.400
amos4	0.390	-0.483	amos4	0.093	amos4	0.071	amos4	0.019
naos4	-0.075	-0.663	naos4	-0.448	naos4	0.210	naos4	0.015
pdos4	-0.023	0.031	pdos4	0.015	pdos4	-0.035	pdos4	0.102
sois4	0.146	0.212	sois4	0.183	sois4	0.092	sois4	0.226

TABLE D.7 Continued: Test two DJF.

Canonical Loadings for Dependent Data

SPI 3

	1	2
s3mFLs1	-0.943	0.332
s3mUCs1	-0.004	1.000

SPI 6

	1
s6mFLs1	-0.331
s6mUCs1	0.819

SPI 12

	1
s12mFLs1	-0.233
s12mUCs1	-0.998

SPI 24

	1
s24mFLs1	-0.288
s24mUCs1	-1.000

Cross Loadings for Dependent Data

SPI 3

	1	2
s3mFLs1	-0.380	0.115
s3mUCs1	-0.001	0.345

SPI 6

	1
s6mFLs1	-0.123
s6mUCs1	0.303

SPI 12

	1
s12mFLs1	-0.088
s12mUCs1	-0.376

SPI 24

	1
s24mFLs1	-0.141
s24mUCs1	-0.489

Canonical Loadings for Independent Data

SPI 3

	1	2
amos1	0.267	0.002
naos1	0.399	0.350
pdos1	-0.367	-0.226
sois1	0.620	-0.383
amos2	0.029	0.057
naos2	-0.323	-0.019
pdos2	-0.187	-0.100
sois2	0.399	-0.232
amos3	0.248	0.047
naos3	0.022	0.325
pdos3	-0.207	-0.118
sois3	0.360	0.154
amos4	0.348	-0.068
naos4	-0.053	-0.592
pdos4	-0.215	-0.108
sois4	0.346	0.200

SPI 6

	1
amos1	-0.012
naos1	0.327
pdos1	-0.305
sois1	-0.080
amos2	-0.106
naos2	-0.286
pdos2	0.028
sois2	0.003
amos3	0.070
naos3	0.321
pdos3	-0.120
sois3	0.447
amos4	0.081
naos4	-0.373
pdos4	-0.095
sois4	0.384

SPI 12

	1
amos1	0.497
naos1	-0.194
pdos1	0.509
sois1	-0.247
amos2	0.570
naos2	0.082
pdos2	0.313
sois2	-0.291
amos3	0.651
naos3	-0.279
pdos3	0.296
sois3	-0.453
amos4	0.568
naos4	0.140
pdos4	0.080
sois4	-0.213

SPI 24

	1
amos1	0.627
naos1	0.036
pdos1	0.380
sois1	-0.352
amos2	0.735
naos2	0.003
pdos2	0.235
sois2	-0.209
amos3	0.807
naos3	-0.184
pdos3	0.320
sois3	-0.254
amos4	0.699
naos4	-0.026
pdos4	0.081
sois4	-0.023

Cross Loadings for Independent Data

SPI 3

	1	2
amos1	0.108	0.001
naos1	0.161	0.121
pdos1	-0.148	-0.078
sois1	0.250	-0.132
amos2	0.012	0.020
naos2	-0.130	-0.006
pdos2	-0.075	-0.034
sois2	0.161	-0.080
amos3	0.100	0.016
naos3	0.009	0.112
pdos3	-0.083	-0.041
sois3	0.145	0.053
amos4	0.140	-0.023
naos4	-0.021	-0.204
pdos4	-0.086	-0.037
sois4	0.139	0.069

SPI 6

	1
amos1	-0.005
naos1	0.121
pdos1	-0.113
sois1	-0.030
amos2	-0.039
naos2	-0.106
pdos2	0.010
sois2	0.001
amos3	0.026
naos3	0.119
pdos3	-0.045
sois3	0.166
amos4	0.030
naos4	-0.138
pdos4	-0.035
sois4	0.142

SPI 12

	1
amos1	0.187
naos1	-0.073
pdos1	0.192
sois1	-0.093
amos2	0.215
naos2	0.031
pdos2	0.118
sois2	-0.110
amos3	0.245
naos3	-0.105
pdos3	0.112
sois3	-0.171
amos4	0.214
naos4	0.053
pdos4	0.030
sois4	-0.080

SPI 24

	1
amos1	0.307
naos1	0.017
pdos1	0.186
sois1	-0.172
amos2	0.359
naos2	0.002
pdos2	0.115
sois2	-0.102
amos3	0.395
naos3	-0.090
pdos3	0.157
sois3	-0.124
amos4	0.342
naos4	-0.013
pdos4	0.040
sois4	-0.011

TABLE D.8: Canonical correlation results for test two as described for Table D.7, for the MAM season.

MAM

Correlations

SPI 3

	s3mFLs2	s3mUCs2
s3mFLs2	1.000	0.324
s3mUCs2	0.324	1.000

SPI 6

	s6mFLs2	s6mUCs2
s6mFLs2	1.000	0.410
s6mUCs2	0.410	1.000

SPI 12

	s12mFLs2	s12mUCs2
s12mFLs2	1.000	0.280
s12mUCs2	0.280	1.000

SPI 24

	s24mFLs2	s24mUCs2
s24mFLs2	1.000	0.265
s24mUCs2	0.265	1.000

Canononical Correlations and P-values

SPI 3

	Can. Corr	R sq.	Wilk's	DF	Sig.
1	0.424	0.180	0.744	32.000	0.000
2	0.304	0.092	0.907	15.000	0.021

SPI 6

	Can. Corr	R sq.	Wilk's	DF	Sig.
1	0.483	0.233	0.697	32.000	0.000
2	0.302	0.091	0.909	15.000	0.023

SPI 12

	Can. Corr	R sq.	Wilk's	DF	Sig.
1	0.349	0.122	0.803	32.000	0.001
2	0.293	0.086	0.914	15.000	0.037

SPI 24

	Can. Corr	R sq.	Wilk's	DF	Sig.
1	0.442	0.195	0.748	32.000	0.000
2	0.264	0.070	0.930	15.000	0.141

TABLE D.8 Continued: Test two MAM.

Redundancy Analysis

Proportion of Variance in Dependent Set Explained by Own Can. Var.

SPI 3		SPI 6		SPI 12		SPI 24	
CV1-1	0.467	CV1-1	0.580	CV1-1	0.455	CV1-1	0.534
CV1-2	0.533	CV1-2	0.420	CV1-2	0.545		

Proportion of Variance in Dependent Set Explained by Opp. Can. Var.

SPI 3		SPI 6		SPI 12		SPI 24	
CV2-1	0.084	CV2-1	0.135	CV2-1	0.055	CV2-1	0.105
CV2-2	0.049	CV2-2	0.038	CV2-2	0.047		

Proportion of Variance in Independent Set Explained by Own Can. Var.

SPI 3		SPI 6		SPI 12		SPI 24	
CV2-1	0.087	CV2-1	0.080	CV2-1	0.141	CV2-1	0.180
CV2-2	0.088	CV2-2	0.111	CV2-2	0.070		

Proportion of Variance in Independent Set Explained by Opp. Can. Var.

SPI 3		SPI 6		SPI 12		SPI 24	
CV1-1	0.016	CV1-1	0.019	CV1-1	0.017	CV1-1	0.035
CV1-2	0.008	CV1-2	0.010	CV1-2	0.006		

Standardized Canonical Coefficients Dependent Data

SPI 3			SPI 6			SPI 12			SPI 24	
	1	2		1	2		1	2		1
s3mFLs2	-1.055	-0.065	s6mFLs2	1.005	0.439	s12mFLs2	-0.313	-0.993	s24mFLs2	0.004
s3mUCs2	0.280	1.019	s6mUCs2	-0.012	-1.096	s12mUCs2	1.041	-0.023	s24mUCs2	-1.001

Standardized Canonical Coefficients for Independent Data

SPI 3			SPI 6			SPI 12			SPI 24	
	1	2		1	2		1	2		1
amos1	-0.110	0.229	amos1	-0.010	-0.384	amos1	0.043	0.313	amos1	0.356
naos1	-0.069	-0.269	naos1	-0.160	-0.126	naos1	0.007	0.101	naos1	0.132
pdos1	0.182	0.003	pdos1	-0.028	0.276	pdos1	-0.439	-0.054	pdos1	0.384
sois1	0.757	-0.281	sois1	-0.790	0.108	sois1	-0.168	0.726	sois1	-0.110
amos2	-0.063	0.026	amos2	0.201	0.144	amos2	-0.493	-0.594	amos2	0.057
naos2	-0.011	-0.085	naos2	0.088	0.222	naos2	-0.337	-0.368	naos2	0.080
pdos2	-0.349	-0.811	pdos2	0.004	0.514	pdos2	0.068	0.297	pdos2	-0.166
sois2	0.311	-0.230	sois2	-0.343	0.137	sois2	0.010	-0.019	sois2	0.011
amos3	-0.004	0.377	amos3	0.017	-0.519	amos3	0.183	0.567	amos3	0.330
naos3	-0.043	0.013	naos3	0.064	-0.211	naos3	0.221	-0.016	naos3	-0.138
pdos3	0.331	-0.149	pdos3	-0.258	0.094	pdos3	-0.254	0.015	pdos3	0.268
sois3	0.171	-0.010	sois3	-0.103	-0.140	sois3	0.478	-0.073	sois3	-0.360
amos4	0.137	-0.766	amos4	-0.408	0.705	amos4	-0.268	0.132	amos4	0.116
naos4	0.227	0.191	naos4	-0.135	0.375	naos4	-0.208	0.088	naos4	0.070
pdos4	0.100	0.089	pdos4	-0.014	-0.075	pdos4	0.025	-0.127	pdos4	-0.023
sois4	-0.242	0.107	sois4	0.088	-0.181	sois4	0.026	-0.132	sois4	0.036

TABLE D.8 Continued: Test two MAM.

Canonical Loadings for Dependent Data

SPI 3

	1	2
s3mFLs2	-0.964	0.265
s3mUCs2	-0.062	0.998

SPI 6

	1	2
s6mFLs2	1.000	-0.011
s6mUCs2	0.400	-0.916

SPI 12

	1	2
s12mFLs2	-0.022	-1.000
s12mUCs2	0.954	-0.301

SPI 24

	1
s24mFLs2	-0.261
s24mUCs2	-1.000

Cross Loadings for Dependent Data

SPI 3

	1	2
s3mFLs2	-0.409	0.081
s3mUCs2	-0.026	0.304

SPI 6

	1	2
s6mFLs2	0.483	-0.003
s6mUCs2	0.193	-0.277

SPI 12

	1	2
s12mFLs2	-0.008	-0.293
s12mUCs2	0.333	-0.088

SPI 24

	1
s24mFLs2	-0.116
s24mUCs2	-0.442

Canonical Loadings for Independent Data

SPI 3

	1	2
amos1	-0.092	0.051
naos1	-0.134	-0.283
pdos1	-0.142	-0.419
sois1	0.836	-0.015
amos2	-0.307	-0.089
naos2	-0.122	0.010
pdos2	-0.351	-0.728
sois2	0.536	0.038
amos3	-0.200	-0.177
naos3	-0.046	-0.001
pdos3	-0.043	-0.489
sois3	0.165	0.157
amos4	-0.126	-0.364
naos4	0.193	0.271
pdos4	0.030	-0.273
sois4	-0.071	0.197

SPI 6

	1	2
amos1	-0.076	-0.144
naos1	-0.118	-0.185
pdos1	0.160	0.574
sois1	-0.848	-0.197
amos2	0.136	0.031
naos2	0.236	0.184
pdos2	0.202	0.704
sois2	-0.544	-0.156
amos3	-0.029	0.015
naos3	0.058	-0.241
pdos3	0.061	0.508
sois3	-0.224	-0.365
amos4	-0.155	0.167
naos4	-0.108	0.276
pdos4	0.063	0.354
sois4	-0.088	-0.343

SPI 12

	1	2
amos1	-0.308	0.285
naos1	0.146	0.095
pdos1	-0.529	-0.058
sois1	0.232	0.698
amos2	-0.474	0.100
naos2	-0.285	-0.457
pdos2	-0.458	0.023
sois2	0.331	0.166
amos3	-0.389	0.370
naos3	0.261	-0.036
pdos3	-0.480	-0.053
sois3	0.564	0.019
amos4	-0.429	0.359
naos4	-0.099	0.054
pdos4	-0.240	-0.116
sois4	0.398	-0.031

SPI 24

	1
amos1	0.607
naos1	0.017
pdos1	0.496
sois1	-0.381
amos2	0.704
naos2	0.039
pdos2	0.400
sois2	-0.275
amos3	0.739
naos3	-0.179
pdos3	0.424
sois3	-0.342
amos4	0.681
naos4	0.001
pdos4	0.111
sois4	-0.204

Cross Loadings for Independent Data

SPI 3

	1	2
amos1	-0.039	0.015
naos1	-0.057	-0.086
pdos1	-0.060	-0.127
sois1	0.355	-0.004
amos2	-0.130	-0.027
naos2	-0.052	0.003
pdos2	-0.149	-0.221
sois2	0.227	0.012
amos3	-0.085	-0.054
naos3	-0.020	0.000
pdos3	-0.018	-0.149
sois3	0.070	0.048
amos4	-0.054	-0.111
naos4	0.082	0.083
pdos4	0.013	-0.083
sois4	-0.030	0.060

SPI 6

	1	2
amos1	-0.037	-0.044
naos1	-0.057	-0.056
pdos1	0.078	0.174
sois1	-0.410	-0.060
amos2	0.066	0.009
naos2	0.114	0.056
pdos2	0.097	0.213
sois2	-0.263	-0.047
amos3	-0.014	0.004
naos3	0.028	-0.073
pdos3	0.029	0.153
sois3	-0.108	-0.110
amos4	-0.075	0.050
naos4	-0.052	0.083
pdos4	0.030	0.107
sois4	-0.043	-0.104

SPI 12

	1	2
amos1	-0.107	0.084
naos1	0.051	0.028
pdos1	-0.184	-0.017
sois1	0.081	0.205
amos2	-0.165	0.029
naos2	-0.099	-0.134
pdos2	-0.160	0.007
sois2	0.115	0.049
amos3	-0.136	0.109
naos3	0.091	-0.011
pdos3	-0.168	-0.016
sois3	0.197	0.006
amos4	-0.150	0.105
naos4	-0.035	0.016
pdos4	-0.084	-0.034
sois4	0.139	-0.009

SPI 24

	1
amos1	0.269
naos1	0.007
pdos1	0.219
sois1	-0.169
amos2	0.311
naos2	0.017
pdos2	0.177
sois2	-0.122
amos3	0.327
naos3	-0.079
pdos3	0.187
sois3	-0.151
amos4	0.301
naos4	0.001
pdos4	0.049
sois4	-0.090

TABLE D.9: Canonical correlation analysis results for test two as described in Table D.7, for JJA season.

JJA

Correlations

SPI 3

	s3mFLs3	s3mUCs3
s3mFLs3	1.000	0.430
s3mUCs3	0.430	1.000

SPI6

	s6mFLs3	s6mUCs3
s6mFLs3	1.000	0.408
s6mUCs3	0.408	1.000

SPI 12

	s12mFLs3	s12mUCs3
s12mFLs3	1.000	0.334
s12mUCs3	0.334	1.000

SPI 24

	s24mFLs3	s24mUCs3
s24mFLs3	1.000	0.294
s24mUCs3	0.294	1.000

Canononical Correlations and P-values

SPI 3

	Can. Corr	R Sq.	Wilk's	DF	Sig.
1	0.359	0.129	0.820	32.000	0.004
2	0.241	0.058	0.942	15.000	0.299

SPI 6

	Can. Corr	R Sq.	Wilk's	DF	Sig.
1	0.374	0.140	0.772	32.000	0.000
2	0.320	0.102	0.897	15.000	0.008

SPI 12

	Can. Corr	R Sq.	Wilk's	DF	Sig.
1	0.381	0.145	0.784	32.000	0.000
2	0.287	0.082	0.917	15.000	0.051

SPI 24

	Can. Corr	R Sq.	Wilk's	DF	Sig.
1	0.478	0.228	0.719	32.000	0.000
2	0.262	0.069	0.932	15.000	0.152

TABLE D.9 Continued: Test two JJA.

Redundancy Analysis

Proportion of Variance in Dependent Set Explained by Own Can. Var.

SPI 3		SPI 6		SPI 12		SPI 24	
CV1-1	0.494	CV1-1	0.551	CV1-1	0.553	CV1-1	0.536
		CV1-2	0.449				

Proportion of Variance in Dependent Set Explained by Opp. Can. Var.

SPI 3		SPI 6		SPI 12		SPI 24	
CV2-1	0.064	CV2-1	0.077	CV2-1	0.080	CV2-1	0.122
		CV2-2	0.046				

Proportion of Variance in Independent Set Explained by Own Can. Var.

SPI 3		SPI 6		SPI 12		SPI 24	
CV2-1	0.113	CV2-1	0.119	CV2-1	0.100	CV2-1	0.174
		CV2-2	0.084				

Proportion of Variance in Independent Set Explained by Opp. Can. Var.

SPI 3		SPI 6		SPI 12		SPI 24	
CV1-1	0.015	CV1-1	0.017	CV1-1	0.015	CV1-1	0.040
		CV1-2	0.009				

SPI 3		SPI 6			SPI 12		SPI 24	
	1		1	2		1		1
s3mFLs3	0.259	s6mFLs3	-0.093	-1.092	s12mFLs3	0.010	s24mFLs3	0.026
s3mUCs3	-1.084	s6mUCs3	1.034	0.361	s12mUCs3	-1.003	s24mUCs3	-1.007

Standardized Canonical Coefficients for Independent Data

SPI 3		SPI 6			SPI 12		SPI 24	
	1		1	2		1		1
amos1	-0.382	amos1	0.441	-0.511	amos1	-0.401	amos1	0.162
naos1	-0.114	naos1	-0.060	0.029	naos1	-0.078	naos1	0.078
pdos1	-0.084	pdos1	0.077	0.202	pdos1	0.277	pdos1	0.287
sois1	-0.044	sois1	-0.174	0.771	sois1	0.432	sois1	-0.049
amos2	0.538	amos2	-0.401	0.369	amos2	0.451	amos2	0.232
naos2	0.029	naos2	-0.128	0.092	naos2	0.155	naos2	0.116
pdos2	-0.033	pdos2	-0.484	-0.243	pdos2	0.065	pdos2	-0.086
sois2	0.385	sois2	-0.345	0.444	sois2	0.286	sois2	0.053
amos3	-0.305	amos3	0.349	0.154	amos3	-0.174	amos3	0.134
naos3	-0.338	naos3	0.160	-0.023	naos3	-0.282	naos3	-0.241
pdos3	0.384	pdos3	-0.329	0.301	pdos3	0.341	pdos3	0.335
sois3	-0.490	sois3	0.327	0.188	sois3	-0.496	sois3	-0.480
amos4	0.504	amos4	-0.690	0.021	amos4	0.458	amos4	0.175
naos4	-0.067	naos4	0.143	0.246	naos4	0.204	naos4	0.050
pdos4	0.123	pdos4	-0.002	0.072	pdos4	-0.011	pdos4	0.031
sois4	-0.159	sois4	0.081	0.010	sois4	-0.112	sois4	0.012

TABLE D.9 Continued: Test two JJA.

Canonical Loadings for Dependent Data

SPI 3

	1
s3mFLs3	-0.206
s3mUCs3	-0.972

SPI 6

	1	2
s6mFLs3	0.329	-0.944
s6mUCs3	0.996	-0.085

SPI 12

	1
s12mFLs3	-0.325
s12mUCs3	-1.000

SPI 24

	1
s24mFLs3	-0.271
s24mUCs3	-1.000

Cross Loadings for Dependent Data

SPI 3

	1
s3mFLs3	-0.074
s3mUCs3	-0.349

SPI 6

	1	2
s6mFLs3	0.123	-0.303
s6mUCs3	0.373	-0.027

SPI 12

	1
s12mFLs3	-0.124
s12mUCs3	-0.381

SPI 24

	1
s24mFLs3	-0.129
s24mUCs3	-0.478

Canonical Loadings for Independent Data

SPI 3

	1
amos1	0.079
naos1	-0.227
pdos1	0.172
sois1	-0.206
amos2	0.310
naos2	0.031
pdos2	0.350
sois2	-0.090
amos3	0.245
naos3	-0.366
pdos3	0.582
sois3	-0.598
amos4	0.367
naos4	-0.148
pdos4	0.421
sois4	-0.478

SPI 6

	1	2
amos1	-0.006	-0.125
naos1	-0.016	-0.002
pdos1	-0.342	-0.076
sois1	0.121	0.757
amos2	-0.259	-0.164
naos2	-0.056	-0.104
pdos2	-0.657	-0.244
sois2	0.098	0.639
amos3	-0.272	-0.044
naos3	0.189	-0.065
pdos3	-0.642	-0.068
sois3	0.461	0.342
amos4	-0.425	-0.079
naos4	0.235	0.241
pdos4	-0.401	-0.051
sois4	0.359	0.222

SPI 12

	1
amos1	0.055
naos1	-0.195
pdos1	0.401
sois1	0.118
amos2	0.227
naos2	0.070
pdos2	0.431
sois2	-0.036
amos3	0.244
naos3	-0.325
pdos3	0.522
sois3	-0.555
amos4	0.327
naos4	0.096
pdos4	0.326
sois4	-0.413

SPI 24

	1
amos1	0.433
naos1	-0.050
pdos1	0.476
sois1	-0.366
amos2	0.594
naos2	0.087
pdos2	0.485
sois2	-0.322
amos3	0.594
naos3	-0.275
pdos3	0.563
sois3	-0.525
amos4	0.573
naos4	-0.028
pdos4	0.276
sois4	-0.335

Cross Loadings for Independent Data

SPI 3

	1
amos1	0.028
naos1	-0.081
pdos1	0.062
sois1	-0.074
amos2	0.111
naos2	0.011
pdos2	0.126
sois2	-0.032
amos3	0.088
naos3	-0.132
pdos3	0.209
sois3	-0.215
amos4	0.132
naos4	-0.053
pdos4	0.151
sois4	-0.172

SPI 6

	1	2
amos1	-0.002	-0.040
naos1	-0.006	-0.001
pdos1	-0.128	-0.024
sois1	0.045	0.243
amos2	-0.097	-0.053
naos2	-0.021	-0.033
pdos2	-0.246	-0.078
sois2	0.037	0.205
amos3	-0.102	-0.014
naos3	0.071	-0.021
pdos3	-0.240	-0.022
sois3	0.172	0.110
amos4	-0.159	-0.025
naos4	0.088	0.077
pdos4	-0.150	-0.016
sois4	0.134	0.071

SPI 12

	1
amos1	0.021
naos1	-0.074
pdos1	0.153
sois1	0.045
amos2	0.086
naos2	0.027
pdos2	0.164
sois2	-0.014
amos3	0.093
naos3	-0.124
pdos3	0.199
sois3	-0.211
amos4	0.124
naos4	0.037
pdos4	0.124
sois4	-0.157

SPI 24

	1
amos1	0.207
naos1	-0.024
pdos1	0.227
sois1	-0.175
amos2	0.284
naos2	0.042
pdos2	0.232
sois2	-0.154
amos3	0.284
naos3	-0.131
pdos3	0.269
sois3	-0.251
amos4	0.274
naos4	-0.013
pdos4	0.132
sois4	-0.160

TABLE D.10: Canonical correlation analysis results for test two as described in Table D.7, for the SON season.

SON

Correlations

SPI 3

	s3mFLs4	s3mUCs4
s3mFLs4	1.000	0.401
s3mUCs4	0.401	1.000

SPI 6

	s6mFLs4	s6mUCs4
s6mFLs4	1.000	0.391
s6mUCs4	0.391	1.000

SPI 12

	s12mFLs4	s12mUCs4
s12mFLs4	1.000	0.411
s12mUCs4	0.411	1.000

SPI 24

	s24mFLs4	s24mUCs4
s24mFLs4	1.000	0.364
s24mUCs4	0.364	1.000

Canononical Correlations and P-values

SPI 3

	Can. Corr	R Sq.	Wilk's	DF	Sig.
1	0.274	0.075	0.901	32.000	0.555
2	0.162	0.026	0.974	15.000	0.934

SPI 6

	Can. Corr	R Sq.	Wilk's	DF	Sig.
1	0.309	0.095	0.849	32.000	0.040
2	0.247	0.061	0.939	15.000	0.248

SPI 12

	Can. Corr	R Sq.	Wilk's	DF	Sig.
1	0.431	0.186	0.732	32.000	0.000
2	0.318	0.101	0.899	15.000	0.009

SPI 24

	Can. Corr	R Sq.	Wilk's	DF	Sig.
1	0.455	0.207	0.737	32.000	0.000
2	0.266	0.071	0.929	15.000	0.131

TABLE D.10 Continued: Test two SON. The First root is italicized because neither root passed the significance test and will not be analyzed.

Redundancy Analysis

Proportion of Variance in Dependent Set Explained by Own Can. Var.

SPI 3	
CV1-1	*0.567*
CV1-2	*0.433*

SPI 6	
CV1-1	0.681

SPI 12	
CV1-1	0.698
CV1-2	0.302

SPI 24	
CV1-1	0.517

Proportion of Variance in Dependent Set Explained by Opp. Can. Var.

SPI 3	
CV2-1	*0.042*
CV2-2	*0.011*

SPI 6	
CV2-1	0.065

SPI 12	
CV2-1	0.129
CV2-2	0.031

SPI 24	
CV2-1	0.107

Proportion of Variance in Independent Set Explained by Own Can. Var.

SPI 3	
CV2-1	*0.048*
CV2-2	*0.054*

SPI 6	
CV2-1	0.078

SPI 12	
CV2-1	0.053
CV2-2	0.137

SPI 24	
CV2-1	0.168

Proportion of Variance in Independent Set Explained by Opp. Can. Var.

SPI 3	
CV1-1	*0.004*
CV1-2	*0.001*

SPI 6	
CV1-1	0.007

SPI 12	
CV1-1	0.010
CV1-2	0.014

SPI 24	
CV1-1	0.035

Standardized Canonical Coefficients Dependent Data

SPI 3	*1*	*2*
s3mFLs4	*1.015*	*-0.402*
s3mUCs4	*-0.039*	*1.091*

SPI 6	1
s6mFLs4	0.412
s6mUCs4	0.764

SPI 12	1	2
s12mFLs4	0.714	0.832
s12mUCs4	0.465	-0.994

SPI 24	1
s24mFLs4	0.149
s24mUCs4	-1.045

Standardized Canonical Coefficients for Independent Data

SPI 3	*1*	*2*
amos1	*0.291*	*-0.104*
naos1	*-0.582*	*0.339*
pdos1	*-0.025*	*-0.041*
sois1	*-0.488*	*-0.095*
amos2	*-0.327*	*0.144*
naos2	*-0.037*	*-0.016*
pdos2	*-0.282*	*0.253*
sois2	*-0.340*	*-0.429*
amos3	*0.107*	*0.376*
naos3	*0.154*	*-0.487*
pdos3	*0.377*	*-0.363*
sois3	*-0.136*	*0.105*
amos4	*-0.329*	*-0.855*
naos4	*0.128*	*-0.298*
pdos4	*-0.425*	*-0.218*
sois4	*0.453*	*0.011*

SPI 6	1
amos1	0.614
naos1	-0.119
pdos1	0.057
sois1	-0.303
amos2	-0.692
naos2	-0.154
pdos2	-0.120
sois2	-0.602
amos3	0.218
naos3	0.122
pdos3	-0.243
sois3	0.275
amos4	-0.666
naos4	0.030
pdos4	-0.294
sois4	0.171

SPI 12	1	2
amos1	0.402	-0.242
naos1	-0.195	-0.444
pdos1	-0.066	0.081
sois1	-0.693	-0.316
amos2	-0.253	0.187
naos2	-0.078	0.132
pdos2	-0.233	0.158
sois2	-0.520	0.057
amos3	0.220	-0.352
naos3	0.169	-0.042
pdos3	-0.208	0.245
sois3	0.053	-0.376
amos4	-0.683	0.500
naos4	-0.146	0.199
pdos4	-0.126	-0.105
sois4	0.167	-0.097

SPI 24	1
amos1	-0.042
naos1	0.007
pdos1	0.297
sois1	0.023
amos2	0.309
naos2	0.045
pdos2	-0.097
sois2	0.138
amos3	0.122
naos3	-0.177
pdos3	0.324
sois3	-0.497
amos4	0.301
naos4	0.105
pdos4	0.021
sois4	-0.080

TABLE D.10 Continued: Test two SON.

Canonical Loadings for Dependent Data

SPI 3

	1	*2*
s3mFLs4	*0.999*	*0.036*
s3mUCs4	*0.368*	*0.930*

SPI 6

	1
s6mFLs4	0.711
s6mUCs4	0.925

SPI 12

	1	2
s12mFLs4	0.906	0.424
s12mUCs4	0.759	-0.651

SPI 24

	1
s24mFLs4	-0.231
s24mUCs4	-0.990

Cross Loadings for Dependent Data

SPI 3

	1	*2*
s3mFLs4	*0.273*	*0.006*
s3mUCs4	*0.101*	*0.151*

SPI 6

	1
s6mFLs4	0.220
s6mUCs4	0.286

SPI 12

	1	2
s12mFLs4	0.390	0.135
s12mUCs4	0.327	-0.207

SPI 24

	1
s24mFLs4	-0.105
s24mUCs4	-0.451

Canonical Loadings for Independent Data

SPI 3

	1	*2*
amos1	*0.013*	*-0.285*
naos1	*-0.515*	*0.344*
pdos1	*-0.020*	*-0.020*
sois1	*-0.429*	*-0.177*
amos2	*-0.033*	*-0.098*
naos2	*0.051*	*0.086*
pdos2	*-0.122*	*0.053*
sois2	*-0.247*	*-0.381*
amos3	*-0.091*	*-0.072*
naos3	*0.060*	*-0.421*
pdos3	*0.087*	*-0.215*
sois3	*0.015*	*0.082*
amos4	*-0.184*	*-0.334*
naos4	*0.192*	*-0.247*
pdos4	*-0.254*	*-0.229*
sois4	*0.300*	*0.090*

SPI 6

	1
amos1	-0.094
naos1	-0.040
pdos1	-0.151
sois1	-0.113
amos2	-0.315
naos2	-0.027
pdos2	-0.346
sois2	-0.214
amos3	-0.326
naos3	0.157
pdos3	-0.437
sois3	0.333
amos4	-0.459
naos4	0.119
pdos4	-0.420
sois4	0.327

SPI 12

	1	2
amos1	-0.025	0.019
naos1	-0.124	-0.483
pdos1	-0.098	0.413
sois1	-0.570	-0.530
amos2	-0.042	0.217
naos2	0.089	0.181
pdos2	-0.194	0.530
sois2	-0.427	-0.341
amos3	-0.154	0.118
naos3	0.178	-0.120
pdos3	-0.212	0.565
sois3	0.038	-0.571
amos4	-0.314	0.227
naos4	-0.073	0.116
pdos4	-0.200	0.330
sois4	0.126	-0.426

SPI 24

	1
amos1	0.380
naos1	-0.109
pdos1	0.481
sois1	-0.282
amos2	0.570
naos2	0.003
pdos2	0.475
sois2	-0.254
amos3	0.579
naos3	-0.224
pdos3	0.562
sois3	-0.559
amos4	0.584
naos4	0.003
pdos4	0.291
sois4	-0.401

Cross Loadings for Independent Data

SPI 3

	1	*2*
amos1	*0.004*	*-0.046*
naos1	*-0.141*	*0.056*
pdos1	*-0.006*	*-0.003*
sois1	*-0.117*	*-0.029*
amos2	*-0.009*	*-0.016*
naos2	*0.014*	*0.014*
pdos2	*-0.033*	*0.009*
sois2	*-0.067*	*-0.062*
amos3	*-0.025*	*-0.012*
naos3	*0.017*	*-0.068*
pdos3	*0.024*	*-0.035*
sois3	*0.004*	*0.013*
amos4	*-0.050*	*-0.054*
naos4	*0.052*	*-0.040*
pdos4	*-0.069*	*-0.037*
sois4	*0.082*	*0.015*

SPI 6

	1
amos1	-0.029
naos1	-0.012
pdos1	-0.046
sois1	-0.035
amos2	-0.097
naos2	-0.008
pdos2	-0.107
sois2	-0.066
amos3	-0.101
naos3	0.049
pdos3	-0.135
sois3	0.103
amos4	-0.142
naos4	0.037
pdos4	-0.130
sois4	0.101

SPI 12

	1	2
amos1	-0.011	0.006
naos1	-0.053	-0.154
pdos1	-0.042	0.131
sois1	-0.246	-0.169
amos2	-0.018	0.069
naos2	0.038	0.058
pdos2	-0.084	0.168
sois2	-0.184	-0.109
amos3	-0.066	0.038
naos3	0.076	-0.038
pdos3	-0.091	0.180
sois3	0.016	-0.182
amos4	-0.135	0.072
naos4	-0.031	0.037
pdos4	-0.086	0.105
sois4	0.054	-0.136

SPI 24

	1
amos1	0.173
naos1	-0.050
pdos1	0.219
sois1	-0.128
amos2	0.259
naos2	0.001
pdos2	0.216
sois2	-0.116
amos3	0.264
naos3	-0.102
pdos3	0.256
sois3	-0.254
amos4	0.266
naos4	0.001
pdos4	0.133
sois4	-0.182

APPENDIX E

GRAPHICAL CANONICAL CORRELATION RESULTS

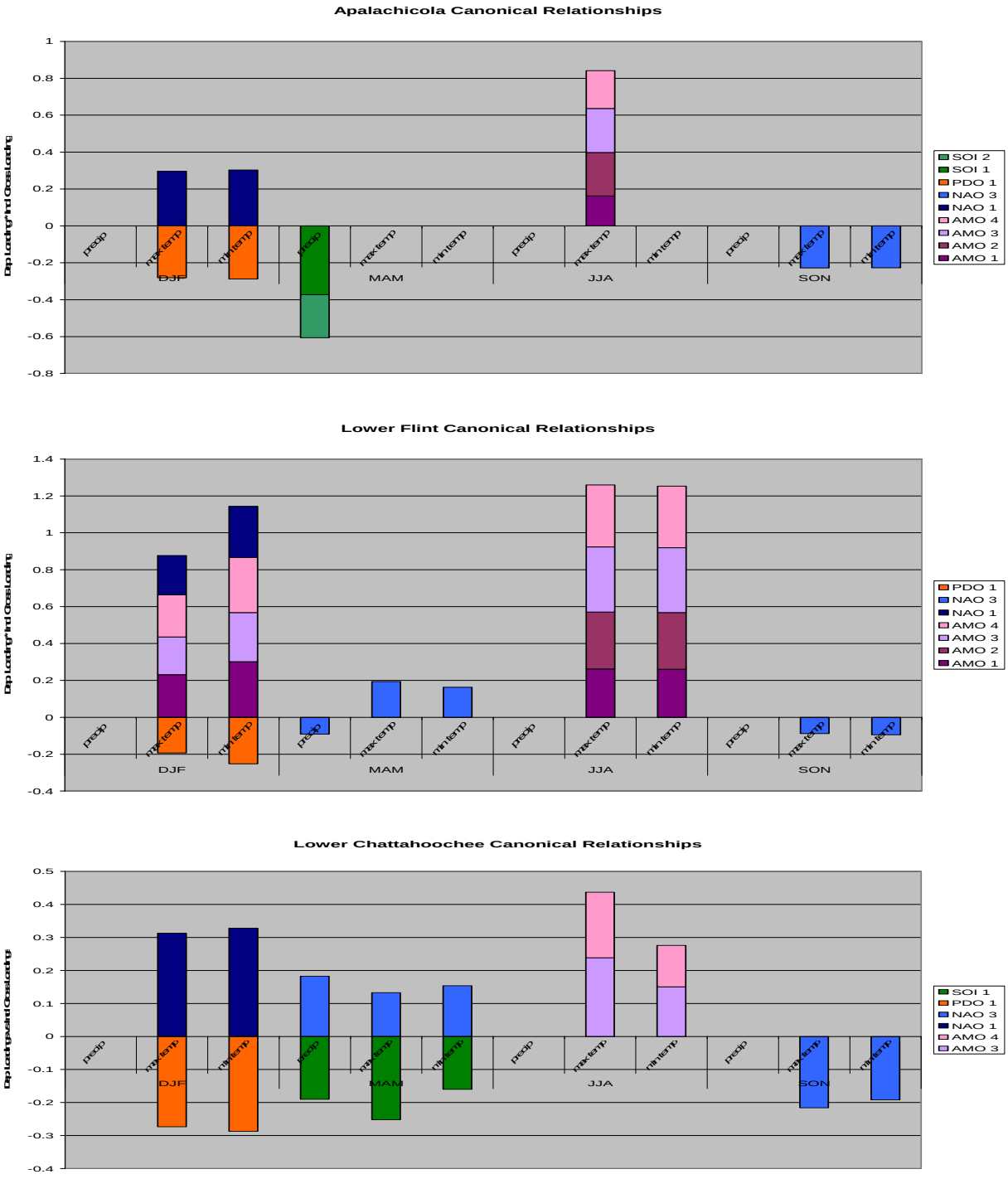

FIG. E.1: Results from test one by basin, represented as described in Figure 5.1.

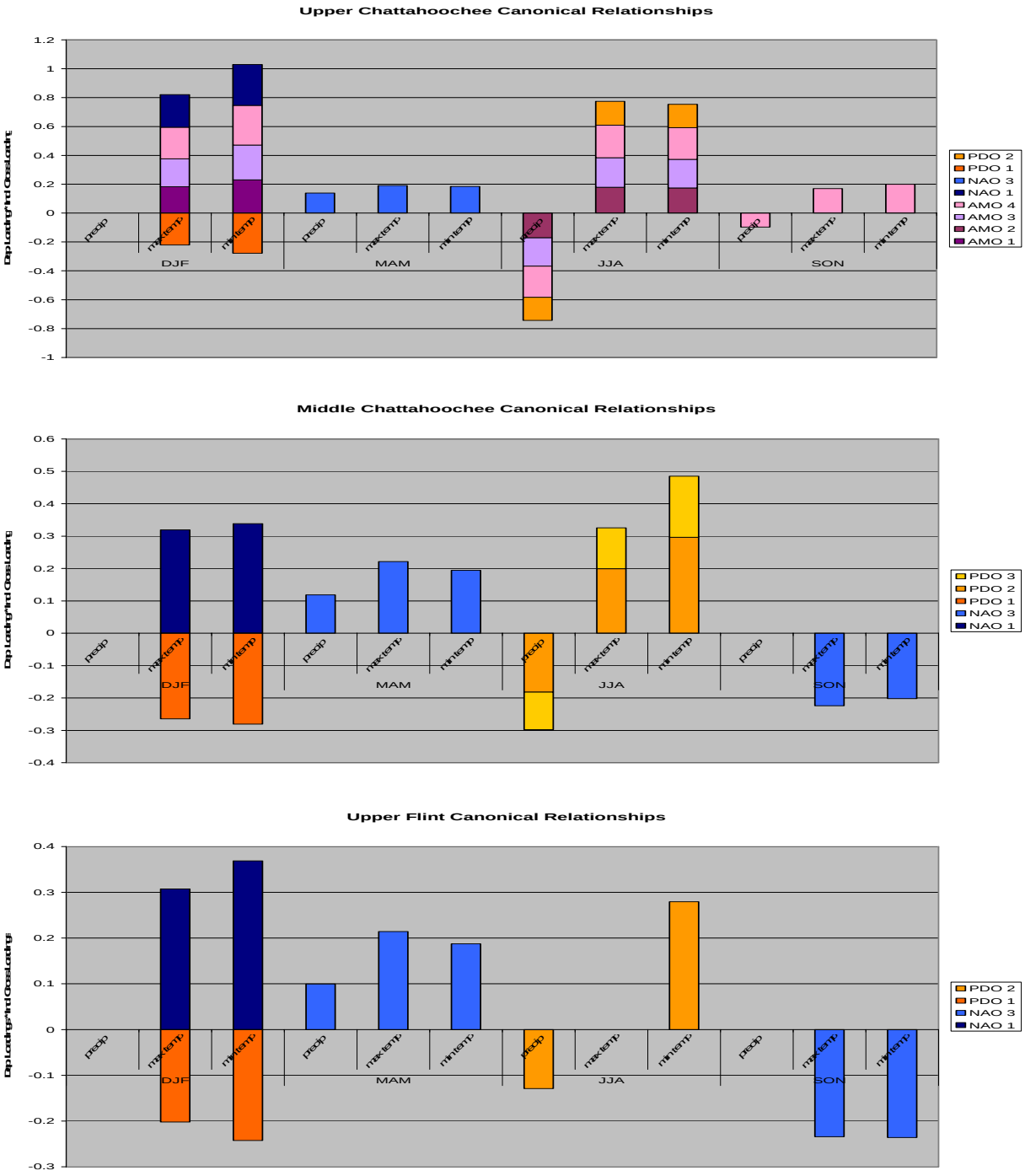

FIG. E.1 Continued

REFERENCES

Arrocha, G. and P. Ruscher, 2005: Analysis of precipitation variability and meteorological drought in the Aplachicola-Chattahoochee-Flint River Basin. J7.3, *The 85th Annual AMS Meeting*, San Diego, CA, American Meteorological Society.

Barnston, A., and R. Livezey, 1986: Classification, seasonality and persistence of low-frequency atmospheric circulation patterns. *Mon. Wea. Rev.*, **115,** 1083-1126.

_____, and C.F. Ropelewski, 1991: Prediction of ENSO episodes using canonical correlation analysis. *J. Climate*. **5**, 1316-1345

Barlow, M., S.Nigam, and E.H. Berbery, 2000: ENSO, Pacific decadal variability, and U.S. summertime precipitation, drought, and stream flow. *J. Climate,* **14**, 2105-2128.

Bretherton, C.S., C.M. Smith, and J.M. Wallace, 1991: An intercomparison of methods for finding coupled patterns in climate data. *J. Climate*, **5**, 541-998.

Carriker, R.R., 2000: Water wars: Water allocation law and the Apalachicola-Chattahoochee-Flint River Basin. Department of Food and Resource Economics, Florida Cooperative Extension Service, Institute of Food and Agricultural Sciences, University of Florida. [Available online at http://edis.ifas.ufl.edu.]

Cartwright, T.J., 2004: Warm season mesoscale superensemble precipitation forecasts. Ph.D. dissertation, Florida State University, 105 pp.

Cusick, Daniel, 2007. "Ga. has 'no choice' but to sue Army Corps—Gov. Perdue." *Greenwire*. 18 Oct. 2007 (electronic newsletter).

Daly, C., Gibson, G.H. Taylor, G.L. Johnson, P.Pasteris. 2002. A knowledge-based approach to the statistical mapping of climate. *Climate Research*, **22,** 99-113.

_____, W. Gibson, M. Doggett, J. Smith, and G. Taylor, 2004: Up-to-date monthly climate maps for the conterminous United States. *14th AMS Conference on Applied Climatology*, Seattle, WA, Amer. Meteor. Soc., P5.1.

Enfield, D.B.,A.M.Mestas-Nuñez, and P.J. Trimble, 2001: The Atlantic multidecadal oscillation and its relation to rainfall and river flows in the continental U.S., *Geophys. Res. Lett.,* **28,** 2077-2080.

Gershunov, A., and T.P. Barnett, 1998: Interdecadal modulation of ENSO teleconnections. *Bull. Am. Meteorol. Soc.*, **79**, 2715-2725.

Gilbert, Debbie, 2007. "Corps wants a drought summit." *The Times, Gainesville*. 15 June 2007.

Glahn, H.R., 1968: Canonical correlation and its relationship to discriminant analysis and multiple regression. *J. Atmos. Sci.* **25**, 23-31.

Green, P.M., D.M. Legler, C.J. Miranda V., and J.J. O'Brien, 1997: The North American climate patterns associated with the El Niño-Southern Oscillation. Unpublished manuscript, COAPS Report Series 97-1, Center for Ocean-Atmosphere Prediction Studies, Florida State University, Tallahassee. [Available online at http://www.coaps.fsu.edu/lib/booklet/.]

Griffin, Melissa, 2007. Personal communication.

Hair, J.F., R.E. Anderson, R.L. Tatham and W.C. Black, 1998: Canonical Correlation Analysis. *Multivariate Data Analysis,* 5th ed. Prentice Hall, Inc., 500 pp.

Hayes, M.J., M.D. Svoboda, D.A. Wilhite, O.V. Vanyarkho, 1999: Monitoring the 1996 drought using the standardized precipitation index. *Bull. Am. Meteorol. Soc.,* **80,** Mar 1999.

Hornberger, G.M., J.P. Raffensperger, P.L. Wiberg, and K.N. Eshleman, 1998: *Elements of Physical Hydrology*. The Johns Hopkins University Press, 302 pp.

Hurrell, J.W., Y. Kushnir, M. Visbeck, and G. Ottersen, 2003: An Overview of the North Atlantic Oscillation. *The North Atlantic Oscillation: Climate Significance and Environmental Impact,* J.W. Hurrell, Y. Kushnir, G. Ottersen, and M. Visbeck, Eds., *Geophysical Monograph,* **134**, American Geophysical Union, 35 pp.

Kelly, Martin, 2004: Florida river flow patterns and the Atlantic Multidecadal Oscillation. Southwest Florida Water Management District. Unpublished manuscript available from SWFWMD, 10 Aug. 2004.

Kerr, R.A., 2000: A North Atlantic climate pacemaker for the centuries. *Science*, **288**, 2000.

_____, 2005: Atlantic climate pacemaker for millennia past, decades hence? *Science,* **309**, 1 July 2005.

Keyantash, J., and J.A. Dracup, 2002: The quantification of drought: An evaluation of drought indices. *Bull. Am. Meterolo. Soc.,* Aug. 2002, 1167-1180.

Light, H.M., K.R. Vincent, M.R. Darst, and F.D. Price, 2006: Water-level decline in the Apalachicola River, Florida, from 1954 to 2004, and effects on floodplain habitats: U.S. Geological Survey Scientific Investigations Report 2006-5173, 83 pp.

Mann, M.E. and K.A. Emanuel, 2006: Atlantic hurricane trends linked to climate change. *EOS,* **87,** June 2006.

Mantua, N., cited 2007: The Pacific decadal oscillation and climate forecasting for North America. Unpublished manuscript, Joint Institute for the Study of the Atmosphere and Oceans, University of Washington, Seattle, Washington, USA. [Available online at http://www.atmos.washington.edu/~mantua/REPORTS/PDO/PDO_cs.htm]

_____, N. J. and S.R. Hare, 2002: The Pacific Decadal Oscillation. *J. Oceanogr.,* **58**, 5835-44.

McCabe, G. J., M. Palecki, and J.L. Betancourt, 2004: Pacific and Atlantic Ocean influences on multidecadal drought frequency in the United States. *Proc. Nat. Acad. Sci.,* **101**, 4136-4141.

McKee, T.B., N.J. Doesken and J. Kleist, 1993: The relationship of drought frequency and duration to time scale. *Eighth Conference on Applied Climatology*, Anaheim, CA, Amer. Meteor. Soc., 179-184.

Minobe, S., 2000: Spatio-temporal structure of the pentadecadal variability over the north Pacific. *Progress in Oceanography*, **47**, 381-408.

NOAA, cited 2007: North Atlantic Oscillation. [Available online at http://www.cpc.noaa.gov/data/teledoc/nao.shtml.]

Rajagopalan B., E. Cook, U. Lall and B. K. Ray. 2000: Spatiotemporal variability of ENSO and SST teleconnections to summer drought over the United States during the Twentieth Century**.** *J. Clim.*, **13**, 4244–4255.

RSI, cited 2007: FFT. IDL Reference Guide. [Available online at http://idlastro.gsfc.nasa.gov/idl_html_help/FFT.html.]

Ruhl, J.B., 2005: Water wars, Eastern style: Divvying up the Apalachicola-Chattahoochee-Flint River Basin. *J. Cont. Water Res. & Ed.*, **131,** 47-54.

Ropelewski C.F., and M.S. Halpert, 1986: North American precipitation and temperature patterns associated with the El Niño/Southern Oscillation (ENSO). *Mon. Weather Rev.*, **115**, 2352-2362.

Smith S.R., P. M.Green, A. P. Leonardi and J. J. O'Brien. 1998: Role of multiple-level tropospheric circulations in forcing ENSO winter precipitation Anomalies. *Mon. Weather Rev.*: **126**, No. 12, 3102–3116.

Stahle D.R., and M. K.Cleaveland. 1992: Reconstruction and analysis of spring rainfall over the southeastern U.S. for the past 1000 Years. *Bull. Am. Meteorol. Soc.*, **73**, No. 12, 1947–1961.

Steinemann, Anne, 2003: Drought indicators and triggers: A stochastic approach to evaluation. *J. Am. Water Resour. Assoc.,* **39**(5), 1217-1233.

Sutton, R.T., and D.L.R. Hodson, 2003: Influence of the ocean on North Atlantic climate variability 1871-1999. *J. Clim.,* **16**, 3296-3313.

_____, and D.L.R. Hodson, 2005: Atlantic Ocean forcing of North American and European summer climate. *Science*. **309**. 1 July 2005.

Trenberth, Kevin and D.J. Shea, 2006: Atlantic Hurricanes and natural variability in 2005. *Geophys. Res. Lett.,* **33,** L12704.

Tootle, G. A., T. C. Piechota, and A. Singh, 2005: Coupled oceanic-atmospheric variability and U.S. streamflow. *Water Resour. Res.,* **41**, W12408.

USACE (U.S. Army Corps of Engineers),1998: Draft Environmental Impact Statement on Water Allocation for the Apalachicola-Chattahoochee-Flint (ACF) River Basin. Alabama, Florida, and Georgia, Main Report, Mobile District, Mobile, Alabama.

Vicente-Serrano, S. M., 2005: El Niño and La Niña influence on droughts at different timescales in the Iberian Peninsula. *Water Resour. Res.,* **41**, W12415.

Wilks, D.S., 2006: *Statistical Methods in the Atmospheric Sciences*. 2nd ed. International Geophysics Series, Vol. 59, Academic Press, 464 pp.

Zorita, E., V. Kharin, and H.V. Storch, 1991: The atmospheric circulation and sea surface temperature in the North Atlantic area in winter: Their interaction and relevance for Iberian Precipitation. *J. Climate*. **5**, 1097, 1107.

BIOGRAPHICAL SKETCH

Kelly Ann Stevens was born in Rochester, NY on January 20th, 1982 to the parents of Thom and Sharon. She has a younger sister Jenna who currently resides in Utah working as a chemist. Science and math were always strong suits for Kelly allowing her to attend the State University College of New York at Oneonta on a presidential scholarship in 2000. Along with science, another passion of Kelly's is athletics. While attending Oneonta State she became an NCAA National Champion in women's soccer, was a two time All-American in indoor track, and was selected as Oneonta State's academic athlete of the year in 2002-2003 and female athlete of the year for 2003-2004. For her academic achievements and leadership involvement at Oneonta State, she was inducted into Chi Alpha Sigma, Phi Eta Sigma, and Omnicron Delta Kappa honor societies. She graduated with honors in 2004 with a Bachelor's of Science degree in meteorology with a minor in both earth science and mathematics.

Inspired by her professors at Oneonta State, Kelly decided to move to Tallahassee, Florida, to pursue a master's degree in meteorology at Florida State University. Kelly was funded as a teaching assistant for her first 2 years of graduate school, and also worked as the Program for Instructional Excellence Associate for the meteorology department during her second year. While taking classes and working on her research under Dr. Paul Ruscher, Kelly was inducted into the meteorology honor society Chi Epsilon Pi.

In the fall of 2006, Kelly accepted a meteorologist position working for the Department of Environmental Protection for the State of Florida in the Division of Air Resource Management. She is still happily involved with athletics as she plays soccer in several Tallahassee leagues, coaches for a local soccer club, and is currently training for her second marathon.